Environmental Science Nano

ROYAL SOCIETY OF CHEMISTRY

FRONTIER

View Article Online
View Journal | View Issue

Check for updates

Cite this: *Environ. Sci.: Nano*, 2026, **13**, 1255

# Graphitic carbon nitride (g-$C_3N_4$) nanomaterials for foliar applications and soil–water remediation in agriculture: a review

Rajasekaran Jayasoorya, [a]
Thangavel Pradeesh Kumar *[a] and Selvaraj Mohana Roopan [b]

Considering the serious issues of global warming and food security, novel technologies are required in agriculture to enhance productivity from the available arable land. Abiotic stresses, including salinity, drought, and pollution, have led to considerable agricultural losses. Nanotechnology offers potential solutions for cultivating crops under adverse conditions. This review examines the implications of metal-free graphitic carbon nitride (g-$C_3N_4$) nanomaterials in agriculture and their interaction with the plant systems. g-$C_3N_4$ is a rich source of carbon (C) and nitrogen (N) and has diverse applications. Elements like C and N are essential for plants to complete their life cycle. Additionally, they play key roles in the physicochemical and microbial dynamics of the soil. The fluorescence property of g-$C_3N_4$ has been reported to enhance photosynthesis in plants through artificial light harvesting. Photosynthesis influences carbohydrate synthesis and produces more biomass at harvest time. Additionally, g-$C_3N_4$ activates antioxidant enzymes under plant stress conditions. Owing to the intrinsic properties of g-$C_3N_4$, it has been identified as a potential candidate for pollutant degradation and associated stress mitigation. The biocompatibility, accumulation in the plant system, and industrial scalability of g-$C_3N_4$ are discussed in this review. Aligning with Sustainable Development Goals (SDG, 2030) 2, 3, 6, 12, and 13, this review explores the potential of g-$C_3N_4$ for yield enhancement in agriculture. Additionally, this review serves as a reference to encourage the use of biocompatible g-$C_3N_4$ in agroecosystems.

Received 5th May 2025,
Accepted 15th December 2025

DOI: 10.1039/d5en00446b

rsc.li/es-nano

Open Access Article. Published on 09 Nyenyankulu 2026. Downloaded on 2026-05-16 11:57:57.
This article is licensed under a Creative Commons Attribution 3.0 Unported Licence.

### Environmental significance

The increasing challenges of climate change and food insecurity necessitate sustainable strategies to improve crop productivity under environmental stress. This review highlights the potential of metal-free graphitic carbon nitride (g-$C_3N_4$) nanosheets as an eco-friendly nanomaterial in agriculture. Their biocompatibility, enrichment in essential elements (carbon and nitrogen), and ability to enhance photosynthesis, stress tolerance, and soil health underline their promise in reducing the reliance on agrochemicals. Furthermore, their unique photocatalytic and optoelectronic properties enable the light-driven degradation of contaminants and promote plant growth under stress conditions. These findings emphasise the transformative potential of nanotechnology in promoting eco-friendly, efficient, and scalable agricultural interventions. The strategies discussed here can be generalised to broader agro-environmental systems, supporting global efforts toward climate-resilient and low-impact food production and mitigating pollutant-related stress.

## 1. Introduction

In recent times, sustainable agriculture has emerged as a central global priority in response to the shortcomings of contemporary agriculture.[1] The challenges in agriculture include climate fluctuation, soil degradation, biodiversity extinction and soaring demand for food.[2] Globally, the population is projected to increase at a rate of 1.06% annually, rising from approximately 7.9 billion in 2022 to an anticipated 9.73 billion by 2064.[3] This significant demographic shift necessitates an augmentation in agricultural production.[4] The modern agricultural system must feed the growing population while maintaining ecological stability and sustainable productivity.[5] Since the green revolution, farming practices have been characterised by intensive chemical use, resulting in greenhouse gas emissions, soil nutrient imbalance, declining soil organic matter, hazards to living organisms and water contamination.[6,7] Similarly, chemical fertilisers play a crucial

[a] *Department of Agronomy, VIT School of Agricultural Innovations and Advanced Learning, Vellore Institute of Technology, Vellore, India.*
*E-mail: pradeeshkumar.t@vit.ac.in*
[b] *Chemistry of Heterocycles and Natural Product Research Laboratory, Department of Chemistry, School of Advanced Sciences, Vellore Institute of Technology, Vellore 632014, Tamil Nadu, India*

Open Access Article. Published on 09 Nyenyankulu 2026. Downloaded on 2026-05-16 11:57:57.
This article is licensed under a Creative Commons Attribution 3.0 Unported Licence.

role in adequate food production to support the growing global population.

Nevertheless, a substantial amount of applied nutrients is non-utilised due to limited efficiency in nutrient use, with more than half of the nutrients being transformed into unavailable forms.[8] These losses contribute to environmental hazards through precipitation, adsorption, leaching and volatilisation.[9] Collectively, these circumstances degrade the soil and water quality with long-term negative impacts on environmental sustainability. On the other hand, food production is the largest human use of land, accounting for 34% use of the available terrestrial land surface on Earth, excluding glaciers.[7] Under current consumption trends and policies, food production contributes approximately 21% of global greenhouse gas emissions,[10] accounts for 70% of freshwater consumption[11] and contribute to 80% of deforestation.[12] These environmental variabilities highlight a paradigm shift toward sustainable agricultural models that maximise efficacy while reducing ecological footprints. Agricultural sustainability depends on maintaining soil nutrient cycles and harmonious interactions between plants, microbes and the environment.[13,14]

Recent advancements in nanotechnology reveal its potential to address these pressing challenges in agriculture.[5,8,15] Nanotechnology has firmly established its presence in numerous sectors, including cosmetics, biomedicine, electronics, pharmaceuticals and agriculture.[6] Innovations in nanotechnology are critical in enhancing agricultural production through improved plant breeding, the targeted delivery of plant protection agents, and deployment of biosensors for precision agriculture.[16] The range of applications is extensive, encompassing the direct deployment of nanomaterials, nutrient biofortification, enhanced plant health, increased photosynthetic rate and higher nutrient cycling.[5,17] Nanoscale materials enhance crop resilience to combat biotic and abiotic stress caused by several factors.[18] Nanotechnology is providing solutions to address the limitations of contemporary agricultural activities.[19,20] It is noteworthy that agriculture is directly connected to human health. Therefore, minimising the application of chemicals is essential to achieve environmentally sustainable agrarian production.[21,22] Nanotechnology has an enormous application scope in agriculture, enhancing crop growth and productivity.[23]

Nanoparticles (NPs), sized between 1 to 100 nm, feature a high surface-to-volume ratio, leading to reduced chemical use in agriculture.[24] Materials such as zinc, zinc oxide, titanium dioxide, copper, copper oxide, cobalt, cesium, selenium, silver, iron oxide, calcium carbonate, silicon, silicon dioxide, manganese carbonate, magnesium carbonate, and carbon NPs are widely studied for their impact on plant growth.[25,26] Surface-functionalized catalytic metal NPs mimic the actions of enzyme in photosynthetic processes, especially $H_2$ evolution, $O_2$ evolution, and $CO_2$ reduction.[27] Conversely, metal NPs resist degradation and harm to living organisms and the environment.[28,29] For example, treating rice crop with ferric oxide ($Fe_3O_4$) at 500 mg $L^{-1}$ negatively influences its growth due to the high concentration required.[30] In addition to plants, soil species, such as microorganisms, nematodes, and earthworms, are also more vulnerable to $Fe_3O_4$ NPs at various levels.[31]

Apart from metal and metal oxide NPs, carbon-based nanomaterials, such as carbon dots (CD), carbon nanotubes (CNT), graphene sheets, and fullerenes, offer numerous benefits in agriculture.[32] Carbon-based nanomaterials are highly rated for their biocompatibility with living organisms.[33] Research findings explored the potential effect of CNTs[34] and CDs[35] on plant growth. Carbon-based nanomaterials enhance crop productivity by improving nutrient use efficiency and mitigating both biotic and abiotic stress factors.[36] A comparative study was conducted to evaluate three distinct carbon nanomaterials: 1) CD, 2) fullerene, and 3) graphene nanoplatelets at varying concentrations to assess their effectiveness in mitigating drought stress in bell pepper plants. This study found that all three carbon nanomaterials significantly enhanced the morpho-physiological and biochemical responses under water stress conditions compared to the control group. Among the three carbon nanomaterials, 200 mg $L^{-1}$ of graphene nanoplatelets increased the number of flowers and fruits.[37] For instance, under drought conditions, applying nitrogen-doped fluorescent carbon dots as a foliar spray significantly boosts the root length, root tip count, and fresh and dry weights of maize plants. This leads to a cumulative yield increase of 30% in maize.[38] Findings indicate that $C_{60}$ fullerene is resistant to mineralisation and remains in the soil environment for at least 1–2 years. $C_{60}$ fullerene exhibits high lipophilicity, suggesting the potential for biomagnification.[39] The long-term persistence of these nanomaterials poses risks to human health and may lead to unpredictable deformities in living organisms.[40] Similarly, Sharma *et al.* reported that engineered carbon nanomaterials exhibit a wide range of toxicity in living organisms.[32]

Alternatively, g-$C_3N_4$ offers advantages such as metal-free composition, cost-effective material production, and broader environmental applicability.[41] In contrast to the high-cost fabrication techniques associated with CNTs and fullerenes, g-$C_3N_4$ can be synthesised *via* simple thermal polymerisation with low-cost precursors.[42] Notably, the production of CNTs requires complex techniques, including chemical vapour deposition, arc discharge, and laser ablation.[43,44] Furthermore, these methods employ high temperatures ranging from 550 °C to 1400 °C.[45] The absence of intrinsic photocatalytic properties in carbon nanomaterials limits their light absorption and poor charge separation capacities. Often, surface modification with metal oxides and heteroatoms can enhance their catalytic activity.[46] In contrast, layered structures and tri-*s*-triazine composition ensure visible light-driven g-$C_3N_4$-mediated photocatalysis. The versatility of g-$C_3N_4$ is further highlighted by its tunable dimensions (0D, 1D, 2D, and 3D), as well as doping and heterojunction formation with other nanomaterials.[47,48]

 This journal is © The Royal Society of Chemistry 2026

Open Access Article. Published on 09 Nyenyankulu 2026. Downloaded on 2026-05-16 11:57:57.
This article is licensed under a Creative Commons Attribution 3.0 Unported Licence.

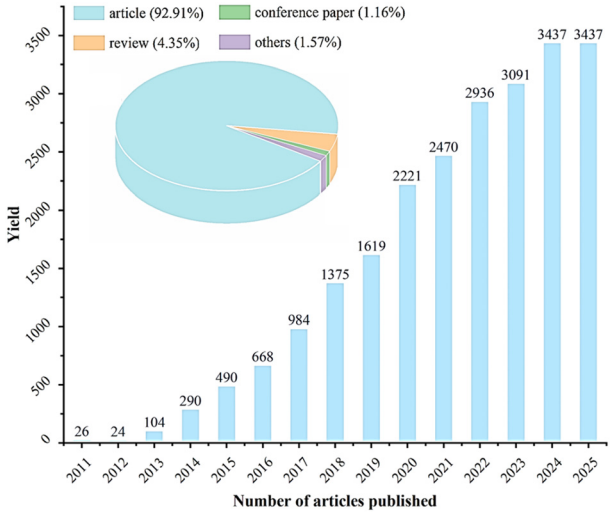


**Fig. 1** Number of reports in the literature on g-$C_3N_4$-related studies across various fields from 2011 to 2025.

These features position g-$C_3N_4$ as an alternative to other carbon nanomaterials.[49] Fig. 1 displays the Scopus data on the number of scientific documents focused on "g-$C_3N_4$" research across various fields from 2011 to 29th November, 2025, demonstrating a gradual increase over the years, accompanied by a constant rate after 2021.

g-$C_3N_4$ demonstrates deliverable outcomes in drug delivery, $H_2O_2$ production, $N_2$ fixation, and the development of nanosensors.[47] Due to its superior physiochemical properties, g-$C_3N_4$ is regarded as the "Holy Grail" and a promising next-generation photocatalyst.[48,50,51] At the same time, g-$C_3N_4$ is widely used in various fields but is less commonly employed in agriculture. In the search for metal-free, eco-friendly nanomaterials, g-$C_3N_4$ is an ideal candidate for achieving sustainability in agriculture.[52,53] NPs exhibit excellent photocatalytic properties owing to their photoluminescence property.[54] The photocatalytic properties of nanomaterials has been widely investigated to promote pollutant degradation using visible light from solar radiation. This phenomenon can be crucial for increasing the photosynthetic efficiency in plants through artificial light harvesting. Thus, graphene-based nanomaterials have been attracting interest among researchers due to their stability under various conditions.[55] The N content in g-$C_3N_4$ endows it with unique characteristics, including complexing ability, semiconducting properties, stability under a wide pH range (pH 1–14), and impressive thermal stability up to 600 °C.[56]

Determining the sustainability of g-$C_3N_4$ requires comparable benchmarked impacts with other existing photocatalysts. Globally, the photocatalyst market has been projected to attain a value of $5.07 billion by 2026, demonstrating an annual growth rate of 10.5% since 2020. Concurrently, titanium dioxide ($TiO_2$) dominates the photocatalyst industry, accounting for 98% of total applications across various sectors, including consumer products and construction.[52] A predominant advantage of g-$C_3N_4$ as a sustainable photocatalyst over other photocatalysts is the use of non-metal precursors for its synthesis. Most comparable photocatalysts to g-$C_3N_4$ are produced from metal precursors, which contributes to environmental toxicity.[57,58]

The traditional photocatalysts, such as $TiO_2$[59] and $Fe_2O_3$,[60] highly rely on extrinsic modifications like doping and adding nanostructures for their activation and to sustain their photocatalytic efficiency. The defect-related active sites in g-$C_3N_4$ nanostructures display reduced recombination and superior carrier lifetime, enabling high photocatalytic efficiency. Especially, the active role of nitrogen-based defects enhances charge localisation and molecular adsorption.[61] Aquino de Carvalho and Gilbertson emphasised that g-$C_3N_4$ activated with a visible light LED source offered 52% energy saving in its use phase compared to $TiO_2$.[52] Thus, the multitude of benefits exhibited by g-$C_3N_4$, including broad light utilisation, non-metallic nature, and biocompatibility, surpass that of comparable materials.

Although $TiO_2$ is comparable with g-$C_3N_4$, $TiO_2$ NPs are associated with toxicity concerns and are regarded as unsuitable for the enhancement of plant growth, particularly considering their long-term impacts on the ecosystem and food safety concerns. The direct application of $TiO_2$ NPs to plants at higher concentrations poses a toxicity risk and can potentially affect the food web adversely.[62,63] Notably, g-$C_3N_4$ is a nitrogen-rich source, presenting a viable alternative to metal-based photocatalysts. Carbon nitride was discovered in the early 19th century. Subsequent investigations have predicted the presence of carbon nitride in five distinct phases, namely, $C_3N_4$ (g-$C_3N_4$), α-$C_3N_4$, β-$C_3N_4$, cubic $C_3N_4$, and pseudocubic $C_3N_4$.[52,64,65] Among these phases, g-$C_3N_4$ has relatively higher chemical and thermal stability.[66] Additionally, 2D g-$C_3N_4$ nanosheets can stack into layers owing to the presence of weak van der Waals forces, forming a nanostructure with enhanced catalytic properties.[67]

The features of g-$C_3N_4$ nanomaterials such as chemical stability, eco-friendliness, modifiable electronic properties, and photocatalytic properties make them ideal options for applications in the environmental and energy-related sectors. The hetero-aggregation of biomolecules with g-$C_3N_4$ provides a way to explore a broader array of applications.[68] However, only a few studies have examined the use of g-$C_3N_4$ in promoting crop production and agricultural intervention.[69] Fig. 2 depicts the potential application of g-$C_3N_4$ in the agroecosystem. Accordingly, this review delves into the potential and prospects of novel g-$C_3N_4$ applications in agriculture. The following section describes the synthesis routes, available precursors, production process optimisation and stability of g-$C_3N_4$ materials.

## 2. Synthesis and properties of g-$C_3N_4$

g-$C_3N_4$ is an excellent nanomaterial widely applied in various research fields,[52] including the health sector, drug delivery, wound healing, artificial enzymes, and bioimaging.[70] Thus far, nitrogen-rich urea,[71] thiourea,[72] cyanamide,[67]

Open Access Article. Published on 09 Nyenyankulu 2026. Downloaded on 2026-05-16 11:57:57.
This article is licensed under a Creative Commons Attribution 3.0 Unported Licence.

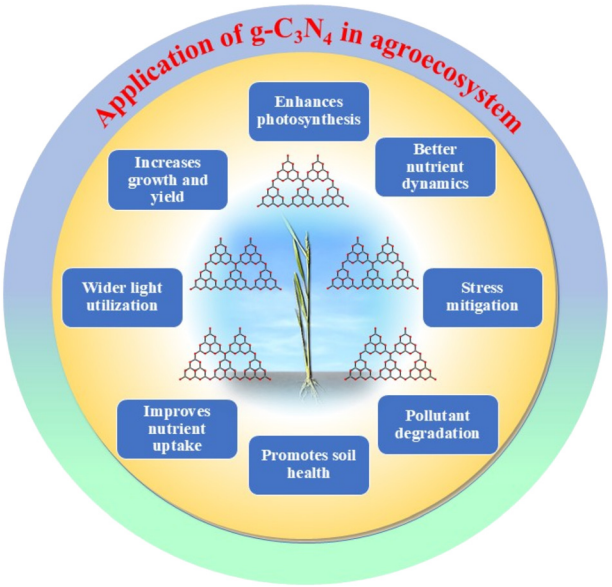


Fig. 2 Various applications of g-$C_3N_4$ in agriculture.

dicyandiamide,[73] and melamine,[55,74] have been reported as precursors for the synthesis of g-$C_3N_4$.[75,76] Generally, bulk g-$C_3N_4$ is prepared through various methods, including thermal polymerisation,[77] microwave-assisted synthesis,[78] direct pyrolysis,[79] hydrothermal/solvothermal synthesis,[80,81] vapour phase deposition,[82,83] and template-assisted synthesis.[84,85] Together, these synthesis methods underscore distinct advantages and unique characteristics that define the utility of each approach. Notably, thermal pyrolysis has been the predominant approach employed in reported studies for producing bulk g-$C_3N_4$.[86] Fig. 3 illustrates the precursors for synthesising g-$C_3N_4$ through thermal pyrolysis and the temperature they require. The merits of g-$C_3N_4$ firmly establish it as an outstanding material in photocatalytic applications. The synthesis parameters, including precursor type, temperature, time and heating rate, define the structure, morphology, and optoelectrical properties of g-$C_3N_4$.[78,87,88] Collectively, its photocatalytic characteristics are directly influenced by its porosity, surface area, crystallinity, composition, photoluminescence, and functional groups.[89,90] In this case, the procedure for the synthesis of g-$C_3N_4$ often determines its characteristics. For example, Safari *et al.* synthesised g-$C_3N_4$ using urea as the precursor at varying temperatures ranging from 400 °C to 600 °C.[91] The photocatalyst produced at a temperature of 450 °C exhibited superior photoreduction activity[91] and complete material disappearance at temperatures higher than 600 °C, indicating the decomposition of its precursor.[92] The material obtained at 600 °C demonstrated an almost stoichiometric C/N ratio, attaining a value of 0.72.[92] Capobianco *et al.* reported that polymerisation was complete around 575 °C, and beyond 600 °C, disruption of the structure occurs.[93] Wang *et al.* revealed that g-$C_3N_4$ prepared using melamine at 550 °C for 4 h was obtained in 31.5-times higher yield than g-$C_3N_4$ prepared using urea precursor under the same conditions. When the temperature was reduced to 500 °C and the calcination time was set to 1 h, the yield increased by up to 4.8%.[94] Moreover, the grafting of functional groups on the surface of g-$C_3N_4$ provides more active sites and functional defects. The commonly available functional groups in g-$C_3N_4$ are hydroxyl, aromatic, amino, urea, carboxyl, and cyano groups. The inherent defects of g-$C_3N_4$, when tailored through functional group modification, enable excellent performance and extended applicability in multiple fields.[95] Overall, the findings on the synthesis of g-$C_3N_4$ highlight how different parameters translate to varying outcomes.[96,97] Fabricating g-$C_3N_4$ with the desired dimensions (0D, 1D, 2D and 3D) is a key factor governing its performance across designated applications. Its size affects its active surface area, optical absorption, transition route, porosity and $e^-/h^+$ trasnsport.[98] Many researchers are focusing on modifying pristine g-$C_3N_4$ to enhance its photocatalytic efficiency through dimensional tuning, formation of g-$C_3N_4$-based heterojunction

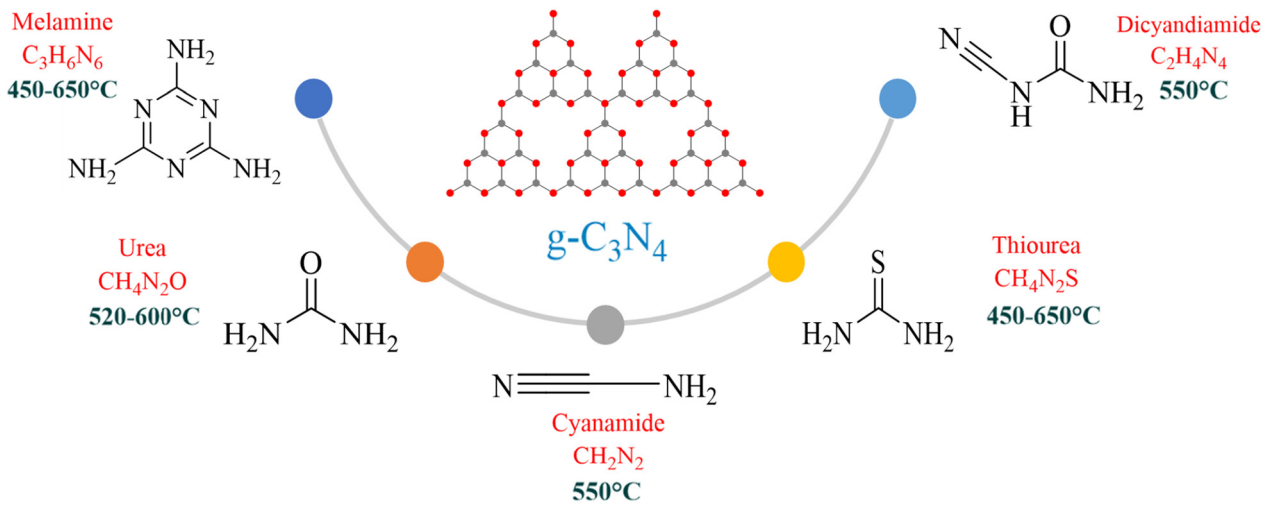


Fig. 3 Sources of g-$C_3N_4$ precursors and their required synthesis temperatures.


This journal is © The Royal Society of Chemistry 2026

Open Access Article. Published on 09 Nyenyankulu 2026. Downloaded on 2026-05-16 11:57:57.
This article is licensed under a Creative Commons Attribution 3.0 Unported Licence.

nanomaterials or elemental doping.[99,100] Distinctive approaches have been used to prepare 0D, 1D, 2D, and 3D nanomaterials. An extensive assessment of fabricating techniques to control their dimensions encourages their effective utilisation in renewable fields.[101] Table 1 lists the dimensions of g-$C_3N_4$ along with its key properties and applications. To increase its photocatalytic efficiency, g-$C_3N_4$ has been synthesised in tailored forms such as quantum dots, nanosheets, and mesoporous structures, which are designed to increase its surface area and enrich its active sites.

Beyond its well-established energy and environmental applications, research on g-$C_3N_4$ has expanded to explore its effects on plant growth and metabolism. A study has examined different structural modifications of g-$C_3N_4$, focusing on homogeneous lamellar (layered sheets) and irregular agglomerated forms, to understand how these variations influence plant physiological processes. Moreover, its structural, optical, and photocatalytic properties exerted a pronounced effect on pollutant degradation, modulating the physiological and metabolic pathways underlying lettuce plant growth.[102] The relevant results and implications are discussed in detail in the subsequent sections herein. Furthermore, a study highlights that the lamellar structure exhibits favourable XPS outcomes, with a nitrogen content of 30.76%. SEM images reveal sheet-like morphologies with uniform pores, whereas the heterogeneous structured nanoscale aggregates have irregular interfaces. The lamellar form also exhibited a uniform elemental distribution of C, N, and O. Moreover, BET analysis confirmed its higher surface area (53.4 $m^2\ g^{-1}$) and pore volume (0.18 $cm^3\ g^{-1}$) compared with the heterogeneous form (35.7 $m^2\ g^{-1}$ and 0.12 $cm^3\ g^{-1}$, respectively), supporting enhanced photocatalysis, plant growth, and cytotoxicity performance.[102]

It has been reported that g-$C_3N_4$ nanosheets are the most widely used and extensively studied form among the different forms of g-$C_3N_4$. Based on the literature prevalence, eight manufacturing procedures have been employed to synthesise g-$C_3N_4$ nanosheets,[52] including chemical exfoliation,[103] supramolecular assembly,[104] biological exfoliation,[105] boron doping with melamine,[106] boron doping with urea,[107] C-doping,[108] O-doping,[109] and thermal etching.[110] Overall, we discuss the sustainability of g-$C_3N_4$ production with respect to $TiO_2$ production. Compared with $TiO_2$, g-$C_3N_4$ has been reported to be an alternative in the field of photocatalysts. The sustainability of g-$C_3N_4$ relative to $TiO_2$ depends strongly on its synthesis route and precursors, which are instrumental in determining its environmental impacts. A comparison of the comprehensive life cycle assessment of the synthesis methods and precursor impacts of g-$C_3N_4$ with two nano-$TiO_2$ synthesis methods and precursors has been performed. Nano-$TiO_2$ is typically produced *via* the sol–gel (titanium isopropoxide – TTIP) and radio frequency thermal plasma methods (titanium tetrabutoxide – TTBO) with the respective precursors. According to the results, it was concluded that the eight methods for the synthesis of g-$C_3N_4$ generate higher global warming potential (GWP) impacts than the nano-$TiO_2$ sol–gel method, but have a substantially lower GWP impact than the radio frequency thermal plasma method.[52] However, this claim has been validated in terms of producing g-$C_3N_4$ nanosheets, not as a representation of all g-$C_3N_4$ nanomaterials.

## 3. Augmentation of photosynthesis and plant growth using g-$C_3N_4$

Engineered NPs demonstrate various plant growth-promoting characteristics, including enhancing photosynthetic pigments, mitigating environmental stresses through increased antioxidant enzyme activity, and improving nutrient absorption.[111,112] Photosynthesis is a vital physiological process in plants, directly affecting crop yield.[111] The complex photosynthesis reaction proposed occurs in the chloroplasts of cells, where solar optical energy is converted into chemical energy, thus producing food materials.[113] During the photo reaction, light-dependent reactions (water splitting) and light-independent reactions ($CO_2$ fixation) produce glucose as the product (Fig. 4).[54]

In the chloroplast, light reactions occur in photosystem I (PS I) and photosystem II (PSII), accompanied by energy transformation and electron transport. Fig. 4 illustrates the key components produced during the decomposition of water, as follows: 1) adenosine triphosphate (ATP), 2) oxygen ($O_2$), and 3) nicotinamide adenine dinucleotide phosphate (NADPH).[114] Improving the crop yield through artificial photosynthesis mediated by the intrinsic properties of NPs is an emerging research area. According to research findings, g-$C_3N_4$ was discovered to be a non-toxic material that enhances

**Table 1** Comparison of the dimensions and key properties of g-$C_3N_4$ (ref. 101)

| Dimension | Morphology | Synthesis method | Key properties | Applications |
|---|---|---|---|---|
| 0D | Quantum dots | Microwave, solid-state and acid exfoliation | Quantum confinement, strong PL | Sensing, bioimaging, $H_2$ evolution |
| 1D | Nanorods, nanotubes, nanowires | Soft and hard templates, chemical vapour deposition, and hydrothermal | Fast charge transport and separation | Photocatalysis, pollutant degradation |
| 2D | Nanosheets | Post calcination/liquid exfoliation | High surface area, increased electron transport | $H_2$ generation, sensing, degradation |
| 3D | Nanoporous, nanospheres, nanohydrogels | Thermal decomposition, porogens, self-assembly | High porosity, light scattering, strong adsorption | $CO_2$ reduction, ORR, OER, pollutant degradation |

Open Access Article. Published on 09 Nyenyankulu 2026. Downloaded on 2026-05-16 11:57:57.
This article is licensed under a Creative Commons Attribution 3.0 Unported Licence.

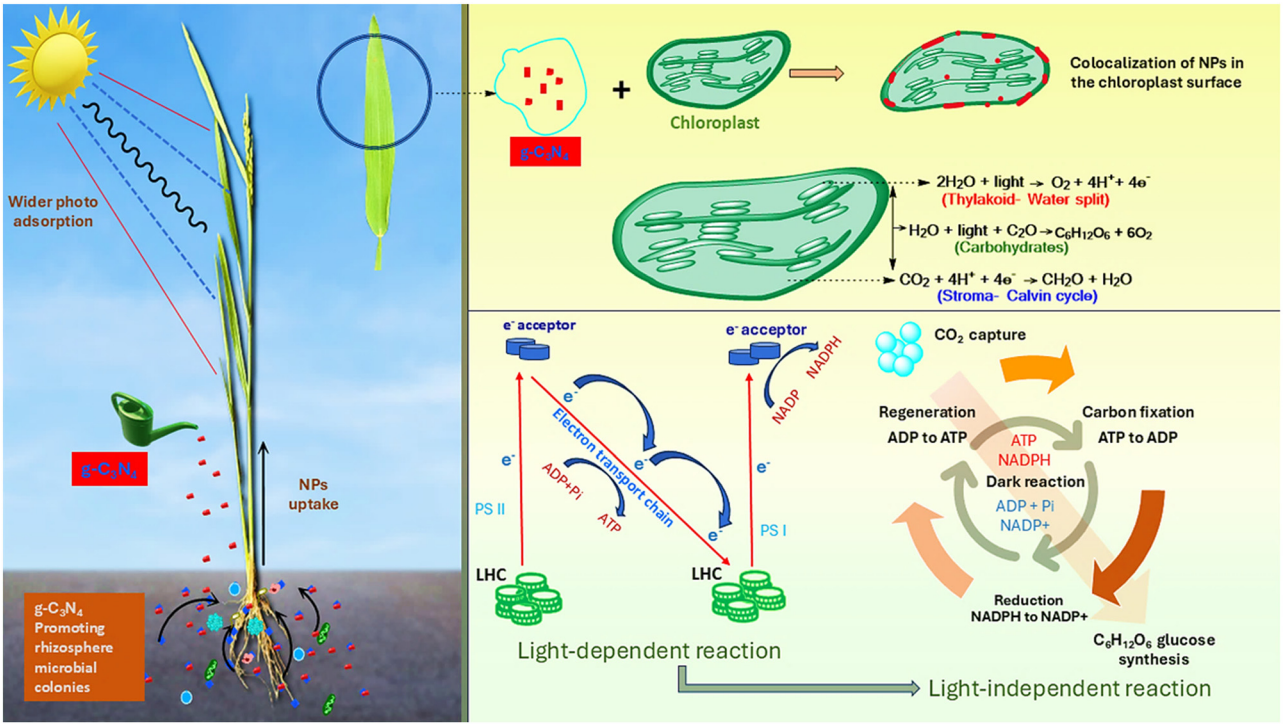


**Fig. 4** Function and mechanism of g-$C_3N_4$ in plant photoreaction (photosynthesis).

photosynthesis and physiological efficiency more than other NPs. Herein, the following sections will highlight the role played by g-$C_3N_4$ with different dimensions in plant physiology and its impact on the agroecosystem.

For instance, wheat growth has been influenced by different concentrations of g-$C_3N_4$ (0 to 50 mg $mL^{-1}$). This study concluded that hydroponic growth with g-$C_3N_4$ at concentrations of 10 mg $mL^{-1}$ and 20 mg $mL^{-1}$ improves the photosynthetic efficiency and morphological characteristics of wheat plants. Both concentrations (10 mg $mL^{-1}$ and 20 mg $mL^{-1}$) significantly increased the plant height by 11.7% and 11.45%, and increased root length by 8.29% and 2.56%, respectively. In addition, this study demonstrated that the concentration with the optimal promoting effect was 20 mg $mL^{-1}$, while higher concentrations inhibited overall growth.[115] A study demonstrated that two structural forms of g-$C_3N_4$, a homogeneous lamellar architecture and an aggregated heterogeneous structure, exhibited a distinct influence on lettuce plant growth applied through foliar spray. At 200 mg $L^{-1}$, the lamellar structure significantly enhanced the growth parameters of lettuce plant height, stem diameter, and leaf area up to 30%, 25%, and 40%, respectively. Although the heterogeneous form also improved growth relative to the control, its effects were consistently less pronounced. Biomass accumulation followed a similar pattern, with shoot and root fresh weights increasing by 40% and 30%, and dry weights by 30% and 25%, respectively, in both forms. Notable increases were also observed in chlorophyll a, chlorophyll b, and carotenoids by up to 32.1%, 26.9%, and 31.5%, respectively, and these values correlated with the SPAD values. In addition, there was an enhancement in photosynthetic rate, stomatal conductance, intercellular $CO_2$ and transpiration rate by up to 38.7%, 32.6%, 15.8% and 30.2%, respectively. In contrast, a higher concentration of 300 mg $L^{-1}$ of both forms inhibited growth, likely due to oxidative stress and metabolic imbalance.[102] Collectively, the findings underscore that the structural morphology of g-$C_3N_4$ strongly influences plant growth and development.

The chloroplasts house photoreactive components that capture incident visible light, facilitating the conversion of water and carbon dioxide into carbohydrates, which serve as essential energy sources for plants.[116] Wang *et al.* reported that hydroponic treatment with g-$C_3N_4$ at 10 mg $L^{-1}$ significantly influences the physiological activity of maize plants compared to control treatments. The enhanced light-harvesting efficiency of g-$C_3N_4$ is correlated with an increase in the electron transfer rate (ETR), net photosynthetic rate, and carbohydrate assimilation by 44.5%, 30.0%, and 32.3%, respectively. The notable increase in the magnesium (1.1%), phosphorus (51.8%), iron (44.6%), and manganese (121.8%) levels suggests that g-$C_3N_4$ positively impacts the nutrient use efficiency in maize.[69] The significant rise in manganese content was associated with the 12.1% increase in chlorophyll level,[69] which is critical for photosynthesis and biomass production.[117] Additionally, a parallel investigation revealed that exposing soil to g-$C_3N_4$ at 250 mg $kg^{-1}$ resulted in elevated levels of essential nutrients in the shoots of rice plants compared to the untreated control, which included potassium (65%), magnesium (24.4%), sulfur (40.9%), zinc (84%), and copper (136%). This study established a robust

 This journal is © The Royal Society of Chemistry 2026

Open Access Article. Published on 09 Nyenyankulu 2026. Downloaded on 2026-05-16 11:57:57.
This article is licensed under a Creative Commons Attribution 3.0 Unported Licence.

correlation between enhanced nutrient concentrations and the proliferation of beneficial bacterial species. There was a 3.30-fold increase in beneficial endophytic bacterial species, including *Saccharimonadales*, *Streptomyces*, and *Thermosporothrix*,[118] suggesting that g-$C_3N_4$ has the potential to augment soil microbial communities.

The soil application of g-$C_3N_4$ at 100 mg $kg^{-1}$ in cadmium (Cd)-exposed soil increased the plant height, root length, shoot and root dry weight by 25.3%, 44.5%, 49.5% and 63.4%, respectively. Meanwhile, g-$C_3N_4$ greatly amplifies the photosynthetic productivity and the nonphotochemical quenching coefficient of soybean plants under Cd-contaminated conditions. Owing to the effect of g-$C_3N_4$, chlorophyll fluorescence parameters like total chlorophyll content (52.7%), ETR (56.9%), quantum yield of PSII (56.9%), and energy conversion efficiency (58.1%) significantly increased. Moreover, g-$C_3N_4$ helps mitigate endogenous nitric oxide loss in nodules, thereby ensuring nitrogen availability and promoting the formation of more nodules with a 70.7% increase in nodule diameter in g-$C_3N_4$-treated plants.[119] In a soybean pot experiment, the g-$C_3N_4$-treated group significantly influenced Cd accumulation and the carbon-to-nitrogen-to-phosphorus (C/N/P) ratios in the root zone compared to the control group. There was a significant increase in nitrogen content in the g-$C_3N_4$-treated groups. The total nitrogen content increased by about fivefold in the g-$C_3N_4$-treated groups. Compared to the control and Cd-treated group, the SOM and TOC contents increased significantly by $0.2 \times 10^3$ mg $kg^{-1}$ in the g-$C_3N_4$ and Cd + g-$C_3N_4$ in the soil groups. Functional genes related to C/N/P modifications are associated with the microbial abundance in the treated group. Additionally, Cd detoxification and improved soil microbiota contribute to increased shoot and root lengths in the Cd + g-$C_3N_4$ group by up to 51%. The g-$C_3N_4$-enriched soil nitrogen content alters the rhizosphere microbial community and enzymatic activities in the Cd-exposed groups, impeding Cd uptake and associated stress factors.[120] Furthermore, we corroborate the g-$C_3N_4$-mediated heavy metal resistance and soil nutrient dynamics in the following section.

In a recent study, g-$C_3N_4$ and Fe-$C_3N_4$ were applied to rice plants in a column experiment, enhancing the agronomic traits, nutrient dynamics, and physicochemical parameters. The application of g-$C_3N_4$ did not significantly affect the plant height or tiller count throughout the entire growth cycle. However, treatment of the soil with Fe-$C_3N_4$ at a concentration of 2 g $kg^{-1}$ increased the five-hundred-grain weight and the organic matter of straw compared to the non-treated control group. The soil fractions, including total nitrogen content of ~5.5 g $kg^{-1}$ and soil organic matter levels up to 7.25%, have been significantly increased by g-$C_3N_4$ at a concentration of 2 g $kg^{-1}$ soil. Compared to the control group, the soil application of g-$C_3N_4$ and Fe-$C_3N_4$ at 0.5 g $kg^{-1}$ significantly increased the total phosphorus by 0.02 g $kg^{-1}$. Notably, the increased chlorophyll content and enzyme-mimicking activities due to Fe-$C_3N_4$ treatment at 0.5 g $kg^{-1}$ soil enhanced the ATPase (37%) and NADPH (28.35 U $L^{-1}$) activity, which was attributed to the improved light harvesting and ETR.[121]

Findings indicate that NPs activate antioxidant enzymes such as peroxidase (POD), catalase (CAT), and superoxide dismutase (SOD), which scavenge excess free radicals.[122] Under plant stress, the key antioxidant activity in maize leaves was assessed with subsequent exposure to nitrogen-doped carbon dots. The results indicate an increase in the key antioxidant activity of SOD (26.7%) and an 18.9% reduction in malondialdehyde (MDA) levels. The elevated SOD activity effectively scavenges free radicals. The decreased MDA concentration and reactive oxygen species (ROS) are mainly due to the application of nitrogen-doped CD.[38] MDA is a key indicator of plant lipid peroxidation and oxidative stress. The lipid peroxidation process generates MDA as a byproduct, making it a stress marker. The application of 100 ppm rGO per g-$C_3N_4$ nanocomposite in rice plants resulted in low MDA levels ($0.29 \pm 0.014$ μM $mg^{-1}$ protein), but a slight increase in MDA was observed at 250 ppm compared to the control. The variations in MDA level underscore the importance of dose and elicit increased stress rather than plant protection.[123]

Cheng *et al.* reported that the application of g-$C_3N_4$ at 2 g $kg^{-1}$ to soil resulted in an increase in POD level up to 57.58% compared to the control group. POD has a broader substrate (hydroxyl radical ($^{\bullet}OH$), superoxide ($^{\bullet}O_2^-$), and other peroxidases) affinity and is involved in multiple physiological activities, including photosynthesis and stress mitigation. Enabling the plant to cope with oxidative stress and the dominance of POD level lessens SOD and CAT, but eliminates superoxide radicals and hydrogen peroxide, respectively.[121] Thus, g-$C_3N_4$ can play a crucial role in photosynthesis and combating stress. Applying metal-based NPs at high concentration increases the ROS and reactive nitrogen species (RNS) in the plant system.[124] The ROS and RNS reactive species are produced in subcellular organelles, *viz.*, mitochondria, peroxisomes, chloroplasts, cytoplasm, and apoplast.[125] The elevation of ROS in the plant system causes cells to activate an oxidative stress state and is considered a well-developed defence mechanism in plants.[126,127] The excess production of RNS strengthens nitrosative signalling and alters the protein, nucleic acid, and lipid-related actions in plants.[128] RNS associates with ROS to form multiple linkages and provides nitro-oxidative signalling under stress conditions.[129] However, a higher concentration may induce oxidative stress, harming plants. At 200 mg $L^{-1}$, two different morphologies of g-$C_3N_4$ enhanced the quality traits of lettuce compared to the control group, with the homogeneous lamellar structure yielding higher soluble sugar, protein, and vitamin C contents (36.7%, 24.5%, and 33.1%, respectively). In contrast, higher concentrations reduced its overall performance, likely due to ROS-induced metabolic stress. The antioxidant activity was also greater in the homogeneous structural form, elevating SOD, POD, and CAT by 138.6%, 36.2% and 53.6%, respectively.[102]

Open Access Article. Published on 09 Nyenyankulu 2026. Downloaded on 2026-05-16 11:57:57.
This article is licensed under a Creative Commons Attribution 3.0 Unported Licence.

Analysis of the ground fractions revealed a significant increase in total nitrogen (TN), total phosphorus (TP), and soil organic matter (SOM) upon g-$C_3N_4$ exposure. The higher surface area of NPs facilitates the adsorption of free nitrogen and phosphorus ions, thereby inhibiting their mobilisation into water bodies. Moreover, the application of g-$C_3N_4$ and Fe-$C_3N_4$ was found to stimulate soil enzymes at three different growth stages of rice (basal, tiller and panicle fertilisation). Enzymes, including β-glucosidase (BG), dehydrogenase (DHA), and *N*-acetylglucosaminidase (NAG), are crucial for carbon cycling. They accelerate the decomposition of chitin, cellulose, and glucosamine polymers, respectively, ultimately increasing SOM.[121] The $Fe^{2+}$ moiety present in Fe-$C_3N_4$ promotes the Fenton reaction, generating hydrogen peroxide ($H_2O_2$).[130] The $H_2O_2$ decomposition produces free radicals,[130] which can degrade organic matter, such as lignocellulosic and livestock waste.[131] The Fenton-based reaction induces the decomposition of organic matter *via* the generation of ROS. Combining g-$C_3N_4$ with metal and metal oxide NPs increases soil fertility by increasing organic matter. However, applying metals and metal oxides to the ecosystem causes environmental pollution. Therefore, dose optimisation to ensure zero toxicity is necessary to explore nanocomposite materials for wider applications.

Applying g-$C_3N_4$ greatly influences plant photosynthesis and increases crop production. Thus, using g-$C_3N_4$ can greatly enhance crop yields in agriculture, while ensuring environmental safety. Alternatively, pristine metal NPs also provide similar benefits to plants as g-$C_3N_4$. However, metals and metal oxides are associated with toxicity concerns to living organisms. Herein, the next section critically reviews the benefits of NPs on plant growth, photosynthesis, and the related hazards posed by pristine metal NPs.

## 4. Role of NPs in plant growth and photosynthesis mechanism

Some engineered nanomaterials promote the photosynthetic efficiency artificially in the plant system.[69,121,132–134] For instance, silica NPs attach to PSII and split water, subsequently producing oxygen, and thereby increasing the transport of electrons to the quinone molecule, an electron acceptor.[135] Integrating fluorescent NPs into the photosynthesis machinery acts as an artificial antenna.[136] NPs convert ultraviolet light into visible light, which is essential for improving the photosynthetic efficiency in chloroplasts.[137]

Alternatively, enhanced artificial photosynthesis is a highly anticipated technique mediated by photocatalytic NPs. Materials such as titanium dioxide ($TiO_2$)[52,138] and platinum (Pt)[139] are explored in multiple ways to determine their catalytic properties to enhance photosynthesis. However, the results contradict the anticipated output because of their limited visible light absorption and large optical bandwidth.[67]

Exposure of algae (*Chlorella vulgaris*) to $CeO_2$ NPs at 10 mg $L^{-1}$ increased their photosynthesis performance. The exposure to $CeO_2$ NPs increases the photosynthesis-oriented pigments (*Chl a* and *Chl b*). Also, it upregulates photosynthesis-related genes such as *psaA*, *atpB*, *petA*, *petB*, and *rbcL*.[140] Similarly, applying iron dioxide ($FeO_2$) NPs in soybean under hydroponic conditions reduced Fe deficiency and increased the chlorophyll content.[141] In another study, mung bean plants were exposed to manganese (Mn) NPs in laboratory settings. The NPs were found to be located on the chloroplast perimeter, which was corroborated by transmission electron microscopy (TEM) and field emission scanning electron microscope (FESEM) analysis. NPs show promising results, even at higher doses than conventional Mn salts. To support this, Mn NP-treated plants showed enhanced chlorophyll-binding protein (CP43) binding at PS II.[142]

Apart from improving photosynthesis, NPs can enhance crop quality[143] and produce biofortified food products. Nanopriming with Fe NPs at a concentration of 150 ppm in rice seeds resulted in an increase in agronomic characteristics and Fe content in the rice seeds.[144] In another study, seed nanopriming with ZnO NPs at a concentration of 25 ppm mitigates drought stress and improves the agronomic profile of the rice crop.[145] A study observed that soil (50 mg $kg^{-1}$) and foliar (40 ppm) application of copper (Cu) NPs in cowpea plant significantly influences its physicochemical properties and morphological characters.[146] Li *et al.* demonstrated that the soil application of molybdenum disulfide ($MoS_2$) NPs in soybean plants improves their yield and boosts rhizosphere health mediated by N fixation and delayed nodule senescence.[147] The soil application of silver (Ag) NPs in wheat plants significantly increases the plant fresh weight, leaf area, number of grains, root length, and shoot length under heat stress conditions.[148] NPs can play a crucial role in activating antioxidant enzyme activities, assisting plants in avoiding abiotic stresses.[149,150] The application of silicon (Si) NPs enhanced the performance of blueberry and bamboo plants under hypoxia stress (waterlogged) and heavy metal (lead toxicity) stress conditions, respectively.[151,152]

The above-mentioned results have furnished the advantages of NPs in improving plant physiology. However, attention must be paid to the negative consequences of metal accumulation in the ecosystem to avoid undesirable outcomes.[124] For instance, the antimicrobial properties of NPs have been applied in preserving cultural heritage items such as stone, paper, textiles, and wood.[153] This clearly indicates that NPs have antimicrobial capacity, which could be hazardous to beneficial microbes as well. In another study, the plant application of silver, copper, copper oxide, zinc oxide, iron-based NPs, titanium dioxide, and other rare earth elements confirmed the antibacterial and antifungal properties of NPs. Nevertheless, agricultural applications are prone to NP accumulation in the food system.[154] Engineered NPs are an anthropogenic cause of pollution, but less

 This journal is © The Royal Society of Chemistry 2026

Open Access Article. Published on 09 Nyenyankulu 2026. Downloaded on 2026-05-16 11:57:57.
This article is licensed under a Creative Commons Attribution 3.0 Unported Licence.

prevalent. The rise in the use of NPs in the natural biota increases their bioaccumulation and creates toxicity. The stress associated with NPs affects living organisms due to the non-availability of a specialised defence mechanism.[155] Research findings indicate that applying NPs to increase the photosynthetic efficacy is worthwhile in agriculture. However, focusing on environmental safety, identifying NPs without toxic implications could circumvent detrimental effects. According to the reports of *in vitro* and *in vivo* toxicity studies, NPs cause problems in two ways in living organisms: 1) exposure to NPs at lower concentrations over a long period creates chronic toxicity and 2) exposure to NPs for a shorter

**Table 2** Examples of toxicity caused by metal/metal oxides and carbon-based NPs

| NP | Organism | Concentration | Impact | References |
|---|---|---|---|---|
| ZnO | Plant-dragon head | 0, 40, 80, 160, and 400 mg $L^{-1}$ | Foliar application of ZnO NPs resulted in a higher ZnO level in tissues compared to conventional Zn sources<br>The MDA and $H_2O_2$ levels are significantly higher in ZnO treatment, causing lipid peroxidation and leading to oxidative stress | 156 |
| ZnO | Algae-*Chlorella vulgaris* | 0.5, 10, 20, and 25 mg $L^{-1}$ | The sorption of ZnO with tire wire particles affects aquatic life<br>The combined effect enhances the bioavailability of ZnO, reduces chlorophyll, biomass, and antioxidant enzyme activity, and increases MDA and $H_2O_2$ contents | 157 |
| Cu | Algae-*Chlamydomonas reinhardtii* | 5, 10, 15, 25, 50, and 100 mg $L^{-1}$ | The concentration of 25 mg $L^{-1}$ of Cu NPs exhibits severe toxicity to the unicellular organism<br>The study confirms increased ROS levels and stress-responsive metabolites due to NP toxicity | 158 |
| Ag | Plant-*Lycopersicon esculentum* | 10, 20, and 30 mg $L^{-1}$ | Under hydroponic conditions, NP exposure exhibited a significantly lower growth rate (2–7 times) due to phytotoxicity | 159 |
| Ag | Plant-*Camelina sativa* | 0.5, 1, 2, 3, and 4 g $L^{-1}$ | Applying 4 g $L^{-1}$ Ag NPs drastically reduces the height and dry weight to 53% and 61%, respectively<br>Ag NPs at 2 g $L^{-1}$ increase stress signalling and antioxidant responses | 160 |
| Cu | Plant-*Bacopa monnieri* | 5, 10, 20, 30, 40, 50, 75, and 100 mg $L^{-1}$ | Cu NPs induce abiotic stress due to cellular permeability | 161 |
| ZnO | Soil microbiome (archaea, fungi, bacteria, and viruses) | 0, 50, and 500 g $kg^{-1}$ soil | A high dose of ZnO, 500 mg $kg^{-1}$ soil, affected the complexity and connectivity of the microbial network<br>The NPs impede the genes involved in C, N, P, and S cycling | 162 |
| $TiO_2$ | Plant-*Oryza sativa* | 20, 50, and 100 mg $kg^{-1}$ | Multi-omics studies reveal that anatase and rutile forms of $TiO_2$ NPs induce toxicity in rice | 116 |
| NiO | Rat | 1, 20, and 150 mg $kg^{-1}$ | NiO NPs cause antioxidant imbalance and result in increased testicular toxicity | 163 |
| CuO | *Moina macrocopa* | 0.013 to 0.039 mg $L^{-1}$ | Accumulation of NPs in the gut region of *M. macrocopa* severely inhibits the digestive and antioxidant enzyme activities | 164 |
| ZnO | *Capsicum annum* | 10, 20, 50, 100, and 200 mg $L^{-1}$ | Nano-priming of seeds leads to decreased plumule dry weight | 165 |
| Graphene oxide (GO) | Bacteria-5 *Bacillus* strains (*B. megaterium*, *B. cereus*, *B. subtilis*, *B. mycoides*, and *B. marisflavi*) | 0–100 μg $mL^{-1}$ GO | Based on the time and dose of GO, the biochemical and cell viability were significantly affected in the bacterial strains | 166 |
| Multi-walled carbon nanotube (MWCNT) | Plant-*Allium cepa* | *Allium cepa* roots-10, 20, and 50 ppm | Higher concentration of MWCNT causes DNA damage and apoptosis in plant and mammalian cells | 167 |
| | Human-lymphocytes | Lymphocyte treatment-1, 2, 5, and 10 μg $mL^{-1}$ | | |
| | Swiss albino male mice-bone marrow cells and Pbr322 plasmid DNA | Bone marrow assay-2, 5, and 10 mg per kg body weight | | |
| MWCNT | Plant-*Allium cepa* | 5 and 10 μg $mL^{-1}$ | The nanotubes induced cytotoxicity and genotoxicity in *Allium cepa* | 168 |
| Carbon quantum dots (CQD) | Human cells | ~0.1 mg $mL^{-1}$ | High doses of CQD cause a form of apoptosis, suggesting cytotoxicity at elevated concentrations | 169 |
| CQD | Mice | 0–10 μg $mL^{-1}$ | CQDs, as a drug delivery vehicle, accumulated in the tumour cells in mice, and may cause toxicity | 170 |

Open Access Article. Published on 09 Nyenyankulu 2026. Downloaded on 2026-05-16 11:57:57.
This article is licensed under a Creative Commons Attribution 3.0 Unported Licence.

period at high concentrations may cause acute toxicity.[124] Table 2 summarises the toxicity of NPs on various organisms susceptible to accumulation and exposure.

## 5. Mechanism of action of g-$C_3N_4$ in the plant system

Nanomaterials enhance the photosynthetic performance by modulating the charge separation efficiency and interfacial charge transfer dynamics. Owing to the auxiliary light-harvesting property of g-$C_3N_4$, it acts as a potential light-harvesting component in the photosystem of plants. Electron transfer is a complex aspect of the photosynthesis machinery, which demonstrates electron flow from photon absorption to the final production of photosynthates.[3] For instance, the application of fluorescent carbon dots (CD) increases carbohydrates in mung bean plants, possibly due to the influence of NPs on the photosynthesis mechanism. The photosynthetic indicators, such as ETR, chlorophyll content, and RuBisCO activity, were significantly influenced in the mung bean sprouts.[171] Duan *et al.* reported that g-$C_3N_4$ improves the chlorophyll content and photosynthetic efficiency in wheat seedlings. The results substantiate that g-$C_3N_4$ at concentrations of 10 mg $mL^{-1}$ and 20 mg $mL^{-1}$ upregulated the expression of chlorophyll a/b binding protein genes in wheat leaves. Gene induction in wheat leaves enhances chlorophyll accumulation and their photosynthetic performance, accompanied by efficient photon absorption and electron transfer.[115] Conversely, fluorescent nanomaterials absorb broader wavelengths of light, which can augment the artificial light-harvesting capacity of chloroplasts.[172] The fluorescent intensity was observed to estimate the electron transfer efficiency of g-$C_3N_4$ and the chloroplast complex. The water-dispersed g-$C_3N_4$ showed better UV absorption and emitted blue fluorescence in an aqueous solution. As shown in Fig. 5(a), the fluorescence emission from g-$C_3N_4$ is correlated with the absorption spectrum of chloroplasts.[69] The photoluminescent properties of NPs enhance photosynthesis through photon absorption and emission. Plants receive photons from sunlight and utilise only the visible spectrum in a short wavelength range. Chlorophyll is a natural antenna that absorbs and passes the captured energy to the reaction sites.[173] Conversely, the photons absorbed by artificial antennas enable higher electron transfer between PSI and PSII. NPs act as artificial antennas, absorbing more photons, leading to greater electron transport within photosystems.[136,173,174] The photosynthesis process in higher plants occurs based on cyclic and non-cyclic electron flow. The electrons generated from water splitting at PSII move through the linear electron transport chain to $NADP^+$, forming NADPH.[175] In this process, protons released into the thylakoid lumen contribute to the proton ($H^+$) gradient in the thylakoid layer, aiding adenosine triphosphate synthase to produce ATP molecules through electron-coupled proton translocation.[175,176] In contrast, cyclic electron flow around PSI returns the electron from ferredoxin back into the cytochrome protein complex (b6/f) instead of going to $NADP^+$. This process increases the proton motive force and supports additional ATP generation, thereby balancing the ATP/NADPH ratio required for carbon fixation.[177]

The photosynthetic machinery features photon-harvesting complexes, which transfer energy to its reaction sites. When NPs have the appropriate design and compatibility with the reaction centre, a massive amount of energy is absorbed and transferred to produce photosynthates. Regarding interfacial charge transfer, apart from light-absorbing capacity, NPs can donate electrons directly to chloroplasts.[178] For example, carbon quantum dots (CQD) exhibit similar photoluminescent properties to g-$C_3N_4$. For instance, electron charge transfer between the CD and chloroplasts has been reported in mung bean plants.[171,178] However, the overall pathway for interfacial charge transfer between g-$C_3N_4$ and chloroplasts is still unclear.

Fig. 6 depicts the possible electron transfer mechanism between g-$C_3N_4$ and the chloroplast. When the wavelength of light excites electrons in both chloroplasts and CD, accelerated electron transfer occurs from CD to the

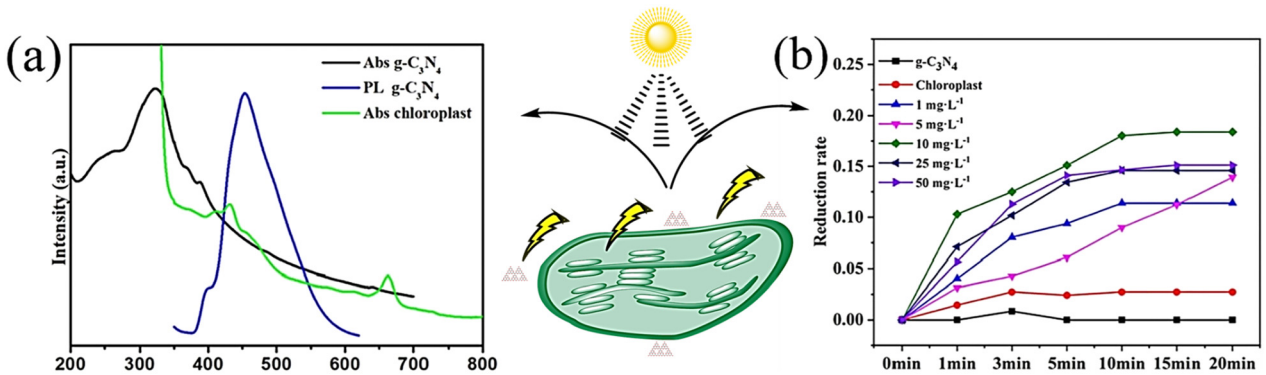


Fig. 5 (a) Absorption spectra of chloroplast and g-$C_3N_4$, and PL of aqueous g-$C_3N_4$ excited at 330 nm. (b) DCPIP reduction rate in the presence of g-$C_3N_4$, chloroplasts and g-$C_3N_4$/chloroplast complex (where g-$C_3N_4$ at 1, 5, 10, 25, and 50 mg $L^{-1}$) under a light intensity of 210 W[69] (adapted from ref. 69 with permission from Elsevier, Copyright 2021).

 This journal is © The Royal Society of Chemistry 2026

Open Access Article. Published on 09 Nyenyankulu 2026. Downloaded on 2026-05-16 11:57:57.
This article is licensed under a Creative Commons Attribution 3.0 Unported Licence.

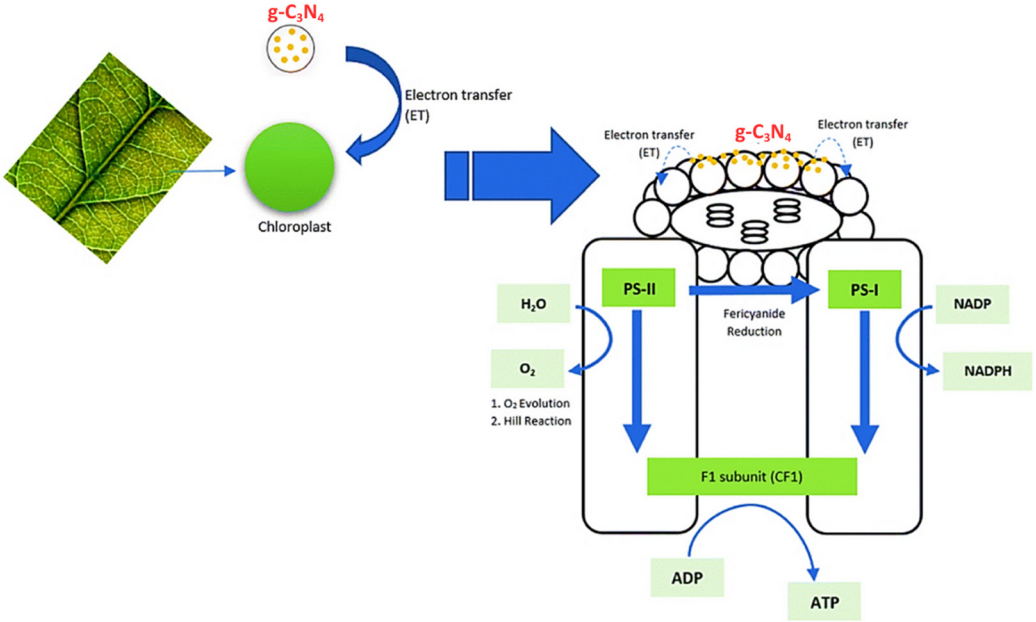


Fig. 6 Illustration of interfacial charge transfer between g-$C_3N_4$ and chloroplast[3] (adapted from ref. 3 © 2023, RSC. Published under the CC BY-NC 3.0 licence).

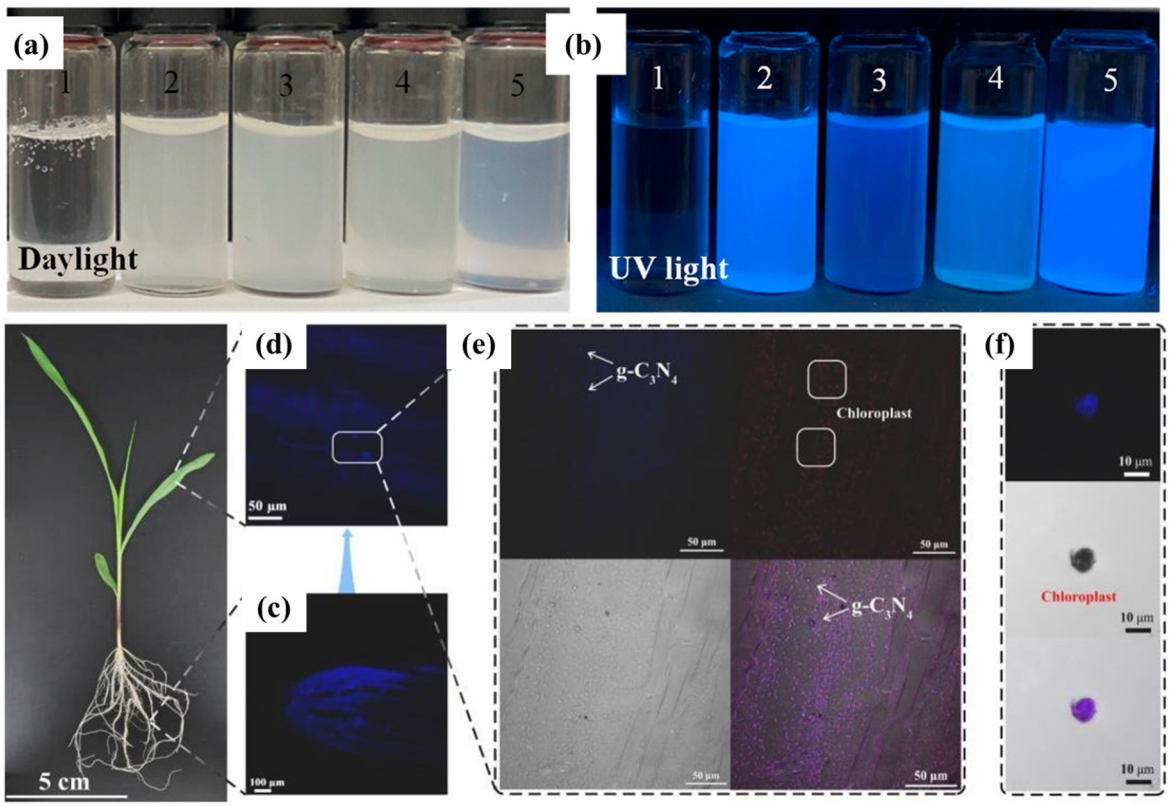


Fig. 7 (a and b) Digital camera images of g-$C_3N_4$ and hyaluronic acid composites under daylight and UV light ($\lambda$ = 365 nm), respectively. 1) HA microgel, 2) g-$C_3N_4$@HA microgel, 3) $^{B}$g-$C_3N_4$@HA microgel, 4) $^{P}$g-$C_3N_4$@HA microgel, and 5) $^{S}$g-$C_3N_4$@HA microgel[186] ((a) and (b) have been adapted from ref. 186, © 2024 MDPI. Published under the CC BY license). CLSM depicts the distribution of g-$C_3N_4$ fluorescent signal in maize at $\lambda$ = 405 nm. (c) CLSM image of blue fluorescence, indicating the presence of g-$C_3N_4$ in the root; (d) CLSM image of blue fluorescence, indicating the presence of g-$C_3N_4$ in the leaf; (e) high-resolution CLSM image, indicating isolated g-$C_3N_4$ present around the chloroplast; and (f) blue and red fluorescence in the CLSM image, indicating the presence of g-$C_3N_4$ and isolated chloroplast[69] (adapted from ref. 69 with permission from Elsevier, Copyright 2021) (please refer to the web version of this article to view the colour-coded elements described in the figure legend).

Open Access Article. Published on 09 Nyenyankulu 2026. Downloaded on 2026-05-16 11:57:57.
This article is licensed under a Creative Commons Attribution 3.0 Unported Licence.

chloroplast and from the chloroplast to the photosynthetic machinery.[171]

A higher electron transfer rate from the donor (CQD) to the acceptor (chloroplast) occurs in the light-harvesting mechanism, which encompasses both the NP and the chloroplast. The massive electron flow rate between PSII and PSI enhances the total electron transfer chain, resulting in increased NADP reduction, ATP production, and $O_2$ splitting.[3,179,180] Fluorescent NPs can generate light-excited electron and hole pairs that do not undergo recombination.

In an *in situ* characterisation, synthesised g-$C_3N_4$ was treated with isolated chloroplasts to confirm its light-harvesting properties. g-$C_3N_4$ emits a strong blue fluorescence peak at 440 nm when excited at a wavelength of 313 nm. Further investigation by confocal laser scanning microscopy (CLSM) and UV absorption spectroscopy confirmed that the g-$C_3N_4$ was complexed with the chloroplast perimeter. As shown in Fig. 7(e), the CLSM image presents blue fluorescence from g-$C_3N_4$ and red fluorescence from the chloroplasts.[69] Stokes-shifted photons may lead to the conversion of non-photosynthetically active luminescence into a photosynthetically active spectrum. For instance, exposure to green-synthesised fluorescent CDs improved the light-harvesting and photosynthetic rate in lettuce plants.[181] PSI inherently produces a fluorescence peak at a wavelength above 700 nm. Nonetheless, the PSII fluorescence peak is detected in the far-red to near-infrared region, ranging from 650–780 nm.[182]

Meanwhile, Chandra *et al.* tested excitation wavelengths of 390, 420, and 442 nm in three samples, *viz.*, CQD, plant-extracted chloroplasts, and the CQD–chloroplast mixture. The peaks were observed at different wavelengths, reportedly 440–450 nm for CQD, 650–780 nm for chloroplast, and at both ranges of 440–450 and 650–780 nm for CQD–chloroplast.[183] It was inferred that chloroplasts and PSII tend to emit the same level of electrons to a higher state at the wavelength of 650–780 nm. These equivalent values reveal insights into the near relation of the chloroplast-housed chlorophyll-embedded PSII system. The CQD–chloroplast complex is observed to have a lower peak intensity at 400–450 nm and higher at 650–780 nm. Subsequently, the CQDs are hypothesised to act as an electron donor to the chloroplast within the complex, resulting in lower fluorescence than pure CQDs but higher fluorescence than isolated chloroplasts at the respective wavelengths.[184,185] These results substantiate the functional interaction at the chloroplast and CQD interface with a spectral overlap-based charge transfer mechanism, as described in previous studies.

Upon excitation, electrons are transferred to the chloroplast, causing it to gain additional energy and exhibit enhanced fluorescence relative to its unexcited state. This mechanism confirms the efficient utilisation of electrons between the donor and acceptor. Fig. 4 reiterates the mechanism of action of g-$C_3N_4$ in the photosynthetic process. These phenomena reveal that g-$C_3N_4$ on the chloroplast surface absorbs non-photosynthetic wavelengths and emits blue fluorescence.

Fig. 7(a and b) illustrate the optical activity of doped and undoped g-$C_3N_4$@HA (HA – hyaluronic acid) microgels under daylight and UV light, respectively. Exposure to UV light resulted in the emission of strong fluorescence compared to the pure HA microgels at a wavelength of 365 nm.[186] Similarly, Fig. 7(c–f) indicate the blue fluorescence emission from g-$C_3N_4$ inside the plant system, including root, stem and leaf.[69] It facilitates the chloroplast to capture more light and enhance water splitting at PSII. As a result of $H_2O$ decomposition in PSII, more electrons will be produced and flow through the protein complexes. As a result of increased electron flow, the photosynthetic efficiency in maize plants was drastically improved.[69,172] Furthermore, Kopnov *et al.* confirmed that 2,6-dichlorophenolindophenol (DCPIP) reduction, ferricyanide reduction assay, and photoluminescence (PL) lifetime measurement are strategies to estimate electron transfer between fluorescent NPs and the chloroplast.[187] Furthermore, the reduction level of DCPIP confirms an increase in the ETR between the photosystems (PSII to PSI).[69,187] During photoreaction in the chloroplast, DCPIP exhibits a higher affinity to electrons, causing a diversion of electron flow from PSII to PSI.[171] Fig. 5(b) indicates that DCPIP reduction was faster in the g-$C_3N_4$ and chloroplast complex than in g-$C_3N_4$ and chloroplast alone, resulting in a higher ETR. In addition, 10 mg $L^{-1}$ g-$C_3N_4$ reduces DCPIP to the maximum level compared to other treatments and increases ETR up to 44.5%.[69] However, ferricyanide reduction and PL lifetime assays have not yet been explored for g-$C_3N_4$. Future studies incorporating both these techniques are essential to provide stronger validation and recommendations for the application of g-$C_3N_4$ in agricultural systems. NPs are crucial in the intricate photophosphorylation process, facilitating oxygen production in the chloroplast.[188]

The ferricyanide assay is based on the photophosphorylation activity in the chloroplast. In the presence of light and ferricyanide, isolated chloroplasts produce oxygen and transfer electrons from PSII to reduce ferricyanide to ferrocyanide. Thus, increased ferricyanide reduction indicates higher electron production. A mixture of chloroplast/CQD resulted in higher ferricyanide reduction compared to pure chloroplast. PL lifetime measurement is another method employed to evaluate electron transfer between mixtures. CQDs alone remain excited for a long time (4.16 ns), whereas when mixed with chloroplasts, their PL lifetime is drastically reduced (0.08 ns). The shortened lifetime indicates quick and efficient electron transfer from CQDs to the chloroplast.[183] The fluorescence properties of nanomaterials can substantially influence the photosynthetic responses in plants. Analysis of two g-$C_3N_4$ morphologies showed that the homogeneous lamellar structure exhibited broader emission peaks at 420–440 nm upon excitation at 285–365 nm, whereas the heterogeneous form showed a narrower 420–430 nm peak

 This journal is © The Royal Society of Chemistry 2026

Open Access Article. Published on 09 Nyenyankulu 2026. Downloaded on 2026-05-16 11:57:57.
This article is licensed under a Creative Commons Attribution 3.0 Unported Licence.

upon excitation in the range of 265–365 nm. Fluorescence lifetime measurements further indicated a longer lifetime for the lamellar structure ($\tau$ = 3.5603 ± 1.0269 μs) compared to the heterogeneous form ($\tau$ = 2.4970 ± 0.1390 μs). The longer lifetime and emission peaks suggest slower charge-carrier recombination and more efficient electron–hole separation, supporting its photophysical behaviour.[102] The foliar application of two different morphologies to lettuce plants results in enhanced overall growth and physiological responses, including photosynthetic efficiency and stronger antioxidant activity. Additionally, the UV-vis absorption spectra of both morphologies exhibited absorption in the visible light region,[102] which indicates their better utilisation of light. These improvements strongly correspond with the findings reported by Chandra *et al.*,[183] where the prolonged PL lifetime in chloroplast-CQD systems enhanced photosynthesis by improving charge carrier separation. The parallel trends suggest that the longer fluorescence lifetime of the lamellar g-$C_3N_4$ structure may similarly contribute to the observed enhancement in lettuce performance. The morphology-dependent metabolic enhancement correlates with improved plant growth by increasing antioxidant mechanisms and carbon utilisation. Moreover, the principal component analysis of the lettuce plant revealed clear separation of both homogeneous and heterogeneous forms of g-$C_3N_4$ from the control group. In the homogeneous g-$C_3N_4$ group, the level of caffeic acid increased from 13.26 to 111.21 μg $g^{-1}$ FW ($\log_2$ FC = 3.07) and neochlorogenic acid from 1.74 to 19.12 μg $g^{-1}$ FW ($\log_2$ FC = 3.46), reflecting enhanced antioxidant metabolism. In the heterogeneous g-$C_3N_4$ group, compounds such as apigenin-7-(4″,6″-diacetylglucoside)-4′-glucoside ($\log_2$ FC = 3.09) and cytisine B ($\log_2$ FC = 4.61) were markedly upregulated with the enrichment of carbon metabolism and glucogenesis pathways.[102] These findings substantiate that distinct morphologies of g-$C_3N_4$ nanomaterials drive divergent metabolic routes in lettuce, leading to pathway-specific adjustments.

NPs greatly enhance enzyme activities, such as phosphoenolpyruvate carboxylase (PEPC) and RuBisCO. These enzymes play a significant role in $CO_2$ fixation during light-independent reactions, affecting carbohydrate accumulation and photosynthesis.[189] Among the carbon nanomaterials explored in the literature,[171,190] 10 mg $L^{-1}$ g-$C_3N_4$ exposure significantly influenced PEPC and RuBisCO activity by 156% and 242%, respectively. The results indicate that g-$C_3N_4$ exposure remarkably increased the potential quantum efficiency of PSII ($F_v/F_m$ ratio).[69] The quantum efficiency is the photon absorption capacity to drive photochemical reactions within PSII. The quantum efficiency of PSII is expressed as $[F_v/F_m = (F_m - F_o)/F_m]$, where $F_m$ is the maximum fluorescence measured with an intense flash of light that closes all PSII reaction sites, exhibiting the maximum fluorescence yield. $F_o$ is the minimum fluorescence observed after dark adaptation of the leaf. The maximum $F_v/F_m$ ratio is between 0.75 and 0.85, which is proportional to the quantum yield of photochemistry.[191,192]

The expression of the *psaA* and *psbA* genes responsible for photosynthesis was upregulated in maize plants. The improved photosynthetic activity is directly proportional to the increase in ATP (32.3%) and NADPH (96.9%).[69] A similar study reported that nitrogen-doped carbon dots upregulate the *psbA* gene response up to 81.7-fold and stimulate the production of the D1 protein. The D1 protein repairs the damage to the PSII system that occurs during abiotic stress. Thus, nitrogen-doped carbon dots increase the net photosynthetic rate and repair light-harvesting pathways in the plant system.[38] These results strongly suggest future directions for applying g-$C_3N_4$ to promote photosynthesis in plant systems.

## 6. Uptake, translocation, and tracing of g-$C_3N_4$

The soil or foliar application of NPs is well known to be translocated from root to shoot (xylem to aerial parts) and shoot to root (phloem to root system).[193] In foliage application, the penetration of NPs relies on the organelles, such as stomata, cuticles, and trichomes, present in the leaves.[16] The stomatal opening size falls within the micrometre scale, and thus NPs enter the phloem cells. Notably, stomata occupy over 5% of the total leaf surface. However, the frequency of stomatal conductance depends on temperature coefficients like RH, $CO_2$ level, and light intensity.[194]

Conversely, the root system facilitates the uptake of NPs through the epidermis. The release of negatively charged mucus or organic acids from the root surface often attracts the positively charged NPs towards the roots.[195] Fig. 8 depicts a schematic representation of the uptake and translocation pathways of NPs in plants. The root anatomy is arranged in the order of epidermis, cortex, endodermis, pericycle, and vascular bundle. The compaction of cortex cells and Casparian strips restricts the apoplastic (intercellular movement) absorption of NPs.[194]

The symplastic (intracellular movement) or protoplast pathway relies on the size of plasmodesmata, which is restricted to 2–20 nm in diameter.[196] Furthermore, Sun *et al.* designed a protocol for imaging NPs within the plant system, especially in root tissues, using CLSM and TEM. The fluorescently labelled $Fe_3O_4$ NPs are internalised inside the *Arabidopsis thaliana* root epidermis.[197] The metal and metal-doped carbon NPs with sizes ranging from 5 to 200 nm were accurately imaged within the plant root tissues (xylem catheters, epidermal cells, and cell walls).[197]

Recent advances in microscopic techniques have eased the accurate tracking of NPs in plant tissues, including their presence in leaves, stems, and roots. Characteristics such as size, shape, and charge of NPs determine their uptake and mobility.[16] Wang *et al.* first reported the presence of g-$C_3N_4$ in the root, stem, and leaf of maize plants. However, to date,

Open Access Article. Published on 09 Nyenyankulu 2026. Downloaded on 2026-05-16 11:57:57.
This article is licensed under a Creative Commons Attribution 3.0 Unported Licence.

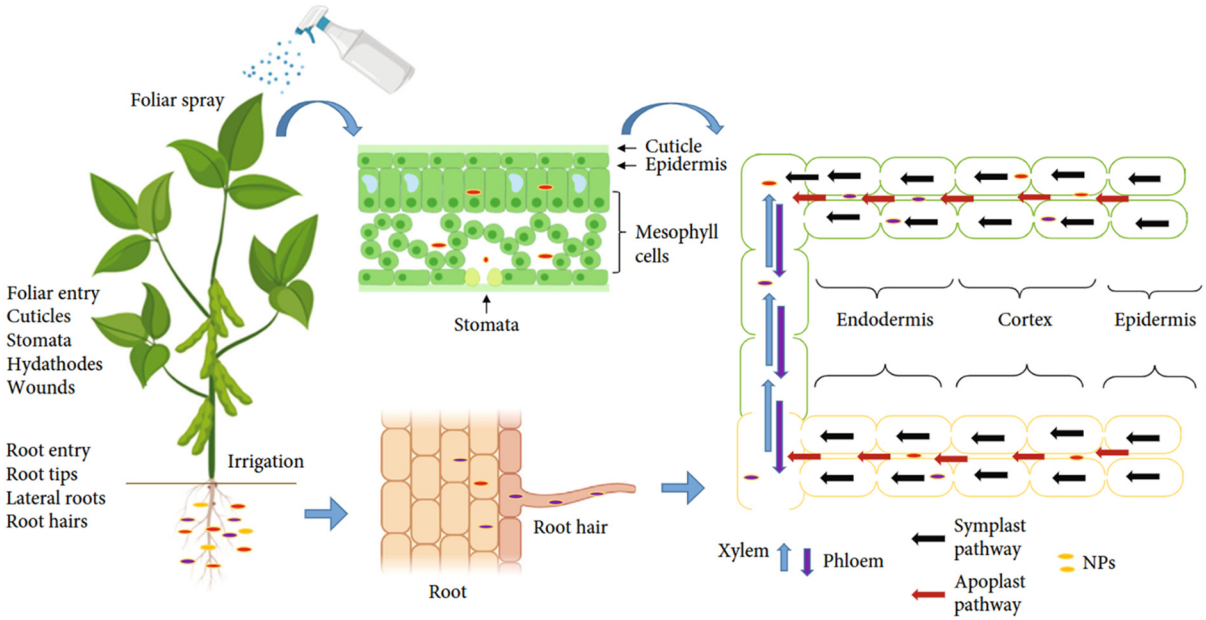


Fig. 8 Uptake and translocation pathway of NPs in the plant system.[318] Reproduced with permission from ref. 318.

no other studies have observed the *in situ* detection of g-$C_3N_4$ in the plant system. TEM images confirm that g-$C_3N_4$ was detected on the surface of maize root with a diameter of 56.5 nm, and its morphology was changed to a tube-like structure. In addition, the CLSM image exhibits blue fluorescence inside the root tips, validating the uptake of g-$C_3N_4$ by the maize plant. The fluorescence intensity was predominant in roots than in leaves, highlighting that g-$C_3N_4$ accumulates in roots and is translocated to other parts.[69]

NPs can accumulate in plants through the shoot or root systems and be transported to different parts *via* vascular tissues.[28] The fluorescent g-$C_3N_4$ was tracked using CLSM equipped with 405 nm laser excitation. Surface-sterilised root tips and leaves with a length of 0.5–1 cm and a breadth of ~1 mm were mounted on a glass slide, covered with a glass slip, and imperviously coated with nail oil. Fig. 7(c–f) confirm the uptake and translocation of g-$C_3N_4$ in the root, stem, and leaf veins of a maize plant, carried out in a hydroponic system. g-$C_3N_4$ exhibits blue fluorescent illumination at the wavelength of 405 nm, indicating its uptake and translocation in the maize plant.[69] The evidence from NP tracking and its impact on growth kinetics in plant systems suggests that g-$C_3N_4$ is a promising option for achieving higher agricultural productivity. These results substantiate its uptake and translocation in the plant system. However, comprehensive studies on its intracellular localisation are required to delineate its uptake and translocation routes. Heterogeneity in the size and morphology of NPs may lead to behavioural inconsistency in biological systems. NPs can be taken up by plants, particularly when their size falls within the nanoscale, ranging from 1–100 nm. This size dependency influences their effective translocation and accumulation within plants.[198] g-$C_3N_4$ is a 2D material with a size typically varying from 2–5 nm in thickness, with lateral dimensions of several hundreds of nanometres to micrometres.[199] To overcome this inconsistency, an alternative strategy to enhance the uptake and translocation of g-$C_3N_4$ in the plant system is the use of g-$C_3N_4$ carbon dots (g-$C_3N_4$/CD). Due to their tunable size and surface functionalities, they offer better interaction with the plant system.[200] Indeed, g-$C_3N_4$/CDs have a precise size, promising their efficient uptake and translocation in plants.[200] To get clarity on the synthesis and photocatalytic properties of g-$C_3N_4$/CDs, refer to the comprehensive study by Wang *et al.*[201] However, the optical and photocatalytic properties of g-$C_3N_4$/CDs remain untapped and require systematic evaluation within the plant system. In a comparative study on nucleic acid delivery in leaf cells of *Nicotiana benthamiana*, three different morphologies of g-$C_3N_4$, including nanosheets, nanoporous, and CDs, were applied as a foliar spray. The g-$C_3N_4$ morphologies were modified with exogenous nucleic acid (dsRNA). The main objective of this study was to silence the TMV coat protein gene (dsCP) through a biocompatible g-$C_3N_4$-based delivery vehicle. Notably, the TEM images of g-$C_3N_4$/CD exhibit a diameter of 2–4 nm and better penetration capacity than the nanoporous and nanosheet morphologies. Stomatal opening and closing play a significant role in the uptake and penetration of the three different morphologies. This phenomenon was compared with abscisic acid (ABA), an inducer of stomatal closing and an abundant water condition in the soil. The results disclose that a decreased stomatal aperture occurs upon ABA treatment and better stomatal opening upon water treatment. To test the uptake efficiency, dsGFP, which is an exogenous nucleic acid, was

 This journal is © The Royal Society of Chemistry 2026

Open Access Article. Published on 09 Nyenyankulu 2026. Downloaded on 2026-05-16 11:57:57.
This article is licensed under a Creative Commons Attribution 3.0 Unported Licence.

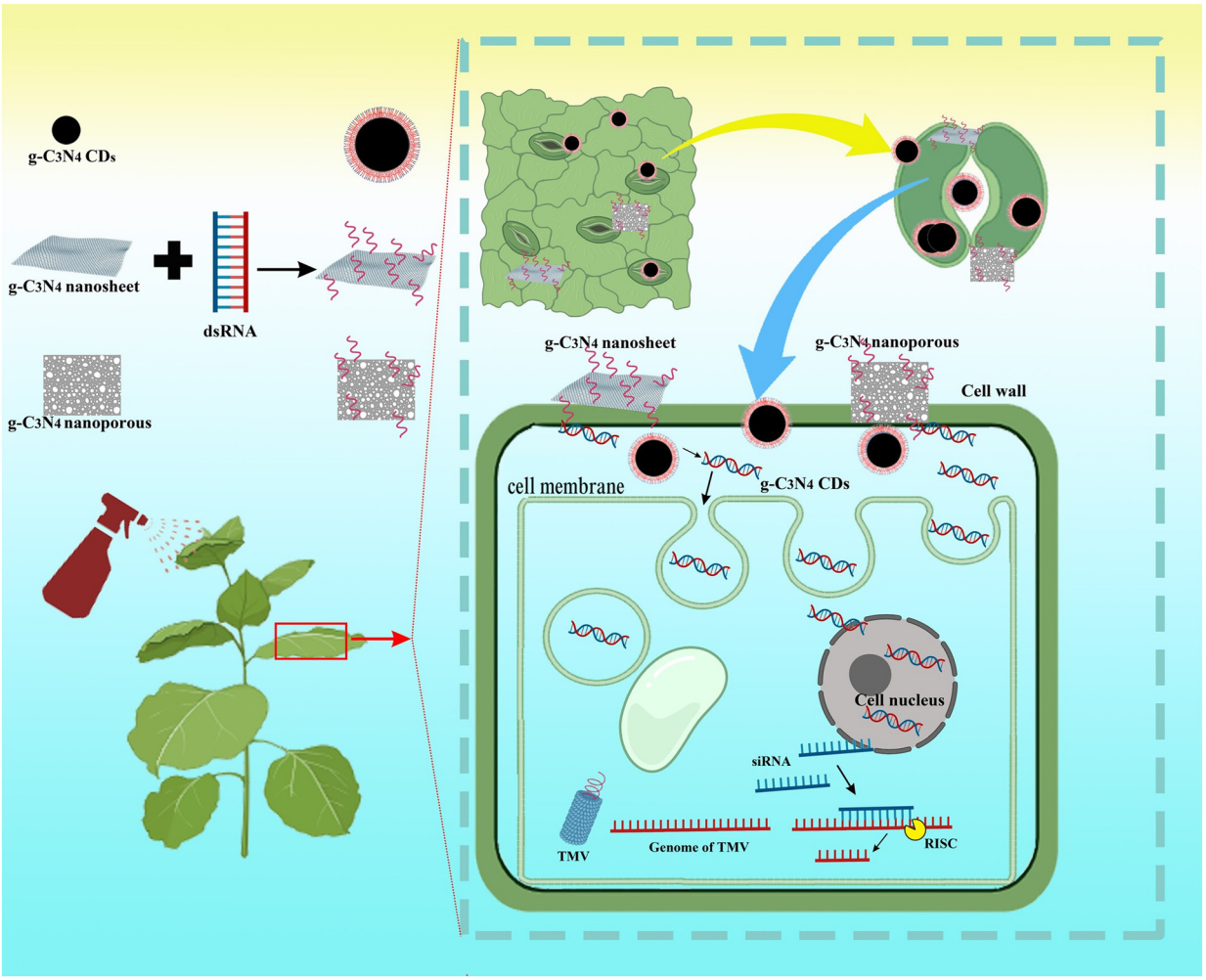


Fig. 9 Schematic representing the application of g-$C_3N_4$ morphologies, uptake, and targeted gene delivery system[202] (adapted from ref. 202, © 2025, Wiley. Published under the CC BY 4.0 licence).

modified with g-$C_3N_4$/CD@dsGFP for silencing the GFP gene. The results showed that the encapsulated g-$C_3N_4$/CD@dsGFP-induced GFP gene silencing was weaker in the ABA treatment group. As shown in Fig. 9, the delivery efficiency of exogenous nucleic acid is regulated by stomatal opening and the endocytosis pathway.[202] Endocytosis is the primary entry route for membrane lipids, proteins, and extracellular molecules into plant cells.[203] The uptake and translocation of NPs are highly dependent on stomatal aperture and the NP size. Similarly, g-$C_3N_4$/CD@dsCP successfully silenced the TMV coat protein in *Nicotiana benthamiana*. This is essential for TMV replication and systemic movement in plants. A single spray of g-$C_3N_4$/CD@dsCP conferred viral resistance for at least 5 days and was not observed to exhibit any adverse effects on plant growth and development.[202] Thus, we conclude that g-$C_3N_4$ exhibiting different morphologies can be used as a promising solution for gene editing technologies. Furthermore, to evaluate the performance of different g-$C_3N_4$ morphologies inside the plant system, more systematic studies have to be conducted.

## 7. g-$C_3N_4$-mediated pollutant remediation in agroecosystems

Soil and water are primary sources for crop production in agriculture. In recent decades, the accumulation of hazardous materials in the soil and water bodies has impeded sustainable food production.[204] To address pollution concerns, g-$C_3N_4$ has been effectively used to remove organic dyes,[205] pharmaceuticals,[206] heavy metals,[207] and for desalination.[118] This section describes the various pollutant degradation mediated by g-$C_3N_4$. Although the nanomaterial (g-$C_3N_4$) is the same, the mechanisms will differ for soil and water atmospheres, respectively.[208] Firstly, g-$C_3N_4$ is an ecologically sound semiconductor composed of carbon and nitrogen, which are abundant on Earth. Its excellent properties include metal-free and nontoxic nature, exceptional electronic band alignment, feasible synthesis procedure, and thermal and chemical stability.[209] Recent studies have confirmed the role of defect-active sites in the g-$C_3N_4$ moiety, which promises superior photocatalytic performance compared to other materials. Density functional

Open Access Article. Published on 09 Nyenyankulu 2026. Downloaded on 2026-05-16 11:57:57.
This article is licensed under a Creative Commons Attribution 3.0 Unported Licence.

theory (DFT) is a quantum mechanical modelling method that unveils how carbon and nitrogen vacancies in g-$C_3N_4$ alter its electronic structure.[210,211] The defects narrow the band gap energy from approximately 2.80 eV to 2.67 eV.[211] The intrinsic electronic feature and tunable defect surface chemistry enhance the charge separation efficiency and reactivity.[212] The band gap reduction drives the utilisation of broader wavelengths of light. Furthermore, intra-structural modifications play a crucial role in reducing charge recombination through charge localisation and better molecular adsorption.[213] DFT simulations predict that the lone-pair-rich nitrogen atoms (pyridinic N)[214] and triazine ring[215] defects are chemically active. In addition, DFT calculations predict the adsorption of the reaction intermediates ($O_2$, $H_2O_2$, *etc.*) at the N vacancies and edge sites. The projected density states indicate that the N 2p orbitals significantly absorb light in the valence band, promoting charge transfer.[210] Conversely, the DFT values for the $Ti^{4+}$ centres in titanium dioxide ($TiO_2$) in the anatase phase are coordinatively unsaturated due to the presence of oxygen vacancies. However, oxygen vacancies not only enhance the visible light activity but also act as a centre for electron–hole recombination. Owing to its wide band gap of ~3.2 eV, anatase-$TiO_2$ only absorbs UV light, making it unsuitable for visible light degradation.[216] In similar research, DFT simulations reveal that in ferric oxide ($Fe_2O_3$), the $Fe^{3+}$ electron occupies 3d orbitals, creating a sluggish surface. This results in poor electrical conductivity and limits its photoelectrochemical performance. Additionally, a high exciton binding energy is required to separate electrons and holes. A high binding energy reduces the charge separation and carrier mobility.[217] $TiO_2$ and $Fe_2O_3$ rely on defect engineering or band gap engineering for enhancing the active sites.[59,60] Overall, we reiterate that g-$C_3N_4$ offers exceptional structural stability compared to existing photocatalytic materials, making it a suitable choice for sustainable photocatalysis. Fig. 10(c) illustrates a schematic representation of g-$C_3N_4$ as a visible light photocatalyst with a band gap of 2.70 eV, promising effective pollutant degradation in water bodies.[208]

Spectroscopic insights underscore the intrinsic advantage of g-$C_3N_4$ for solar-driven applications, making it as a promising candidate for environmental remediation. The use of time-resolved fluorescence decay curves helps in understanding the charge carrier dynamics of nanomaterials.[218–220] The photoluminescence decay curve of g-$C_3N_4$ is biexponential, given that it is comprised of short-lived and long-lived components. In g-$C_3N_4$, its longer lifetime (20–40 ns) is attributed to trap-assisted recombination near N-rich defect sites or surface heterogeneities.[218,219] The interfacial electron movement in the 2D π-conjugated and planar structure extends the lifetime of excited electrons and holes without recombination.[221] The decay curve of other photocatalysts achieves only sub-nanosecond and picosecond lifetimes, which indicates electron recombination and poor charge retention. To match the performance of g-$C_3N_4$, materials such as $TiO_2$[222] and $Fe_2O_3$[223] require external modifications, like elemental/impurity doping and forming heterojunctions with other semiconductors. Pristine $Fe_2O_3$ suffers from inherent low electrical conductivity, which severely limits its photocatalytic ability.[60] In some cases, the pristine g-$C_3N_4$ poses limitations, including inadequate utilisation of visible light and recombination of photogenerated electrons and holes ($e^-$ and $h^+$). Modifying the structure of g-$C_3N_4$ through band gap engineering can enhance its photocatalytic performance, as shown in Fig. 10(a and b).[224]

Methods such as impurity doping with foreign atoms,[225] exfoliation of the 2D sheet into layers,[225] and heterojunction designs,[226] enhance the semiconducting property of g-$C_3N_4$. A study reported that the lamellar g-$C_3N_4$ structure exhibited superior photocatalytic activity, degrading 92% of methylene blue in 3 h compared with 76% for the aggregated structure. This enhancement was linked to its higher crystallinity, longer fluorescence lifetime, and narrower band gap (2.75 eV *vs.* 3.13 eV), which together promote efficient charge separation, reduced recombination, and improved light utilisation.[102] Thus, although both forms are chemically identical, the morphological shift significantly alters the photocatalytic performance.

For example, fabricating a heterojunction structure of ZnO and strontium with g-$C_3N_4$ (ZnO:Sr/g-$C_3N_4$) composite resulted in the reduced band gap of 1.9 eV rather than 3.5 eV of pure ZnO. In addition, this nanocomposite exhibits comparatively higher photocatalytic properties, degrading cationic and anionic dyes by up to 95–99%.[227] For instance, the synergetic effect of the rGO/$Fe_2O_3$/g-$C_3N_4$ nanocomposite enables rapid charge transfer in its nanochannels, degrading ciprofloxacin and tetracycline drugs with visible light intervention.[206] In another study, the heterojunction of g-$C_3N_4$/$FeTiO_3$/rGO promotes rapid photocatalytic charge separation and reduces the redox potential. rGO plays a crucial role in facilitating electron transfer without the recombination of $e^-$ and $h^+$. The reactive species, such as superoxide radicals ($^{\bullet}O_2^-$) and hydroxyl radicals ($^{\bullet}OH$), were generated from the valence and conduction bands, respectively. These oxidising species can transform hazardous organic pollutants to $CO_2$, $H_2O$, and less toxic inorganic ions.[228] Recently, the emergence of two-dimensional (2D) transition metal carbide and nitride materials has been recognised as a promising substitute for noble metal cocatalysts. These materials are termed MXenes, which exhibit higher conductivity, better hydrophilicity, plasmonic effect, more active sites, and a modifiable work function. MXenes are identified as potential cocatalysts with promising interfacial contact and charge extraction properties.[229] Although graphene-based 2D nanomaterials have received more attention in the field of materials science, their applicability is limited due to the weak van der Waals bonding between their layered structure. Thus, to overcome this shortfall, fabricating complex layered structures containing more than one element is required to obtain

 This journal is © The Royal Society of Chemistry 2026

Open Access Article. Published on 09 Nyenyankulu 2026. Downloaded on 2026-05-16 11:57:57.
This article is licensed under a Creative Commons Attribution 3.0 Unported Licence.

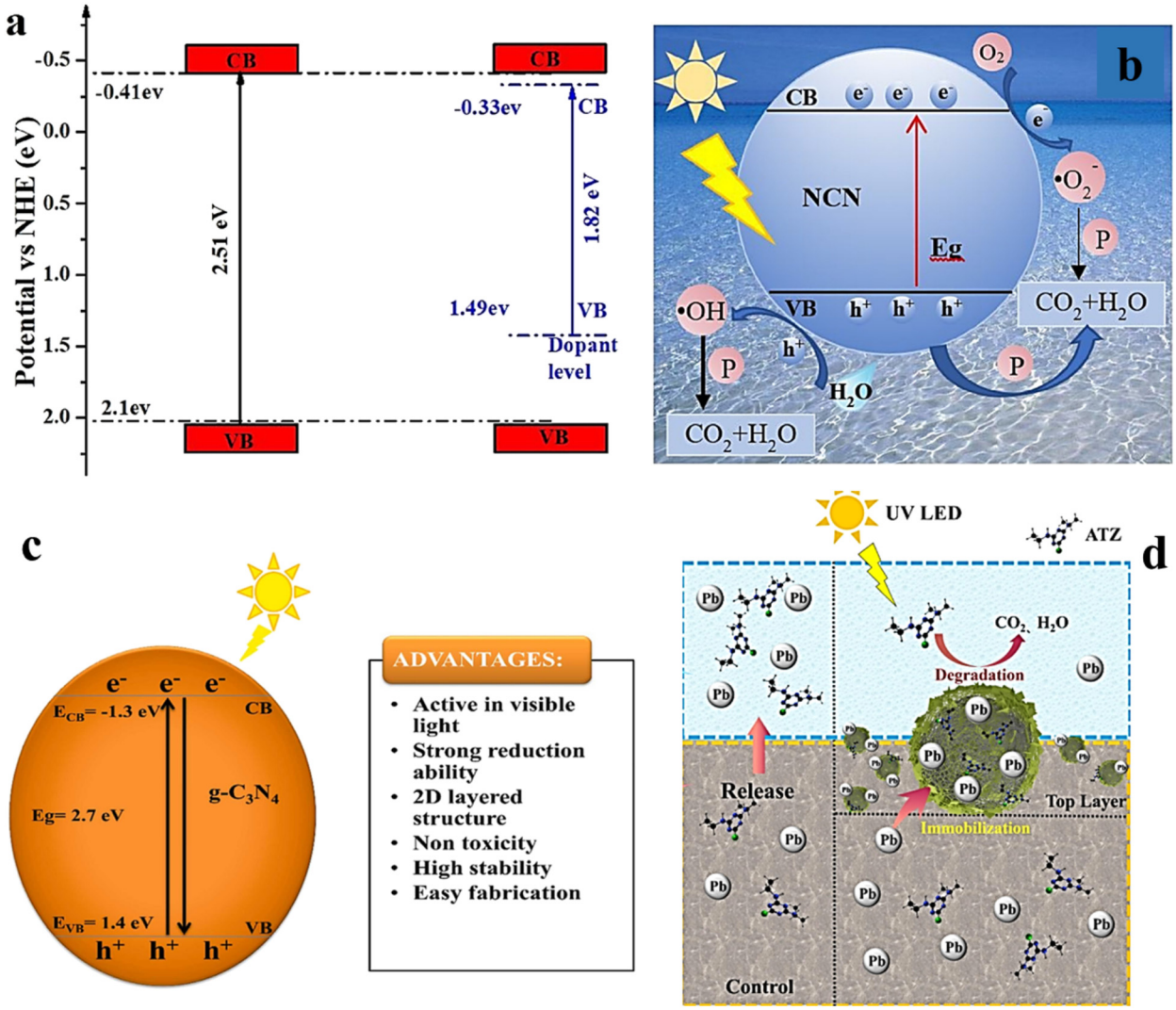


**Fig. 10** (a and b) Charge separation mechanism and transport of photogenerated electron–hole pairs at N-doped g-$C_3N_4$, respectively. Reproduced with permission from ref. 208 (adapted from ref. 208 with permission from Elsevier, Copyright 2021). (c) Advantages of g-$C_3N_4$ in photocatalysis. Reproduced with permission from ref. 209 (adapted from ref. 209 with permission from Elsevier, CC-BY-NY licence). (d) Decontamination of ATZ and Pb in paddy soil using alkalised biochar and g-$C_3N_4$ composite[234] (adapted from ref. 234 with permission from Elsevier, Copyright 2023).

compositional variables with tunable specific properties. MXenes have been identified as ideal alternatives to existing 2D nanomaterials due to their complex chemical properties. MXenes are established with the formula of $M_{n+1}AX_n$, where 'M' is an early transitional metal, $n$ is 1, 2, or 3, 'A' refers to A-group elements (group 13 and 14), and X is carbides and/or nitrides, forming a single laminated structure.[230] The combination of MXenes with narrow-bandgap semiconductors, such as metal oxides, sulfides, III–V, and II–VI group compounds, facilitates the development of a Z-scheme or type-II heterojunction photocatalysis system.[231] For example, a novel nanocomposite ternary heterojunction material was synthesised to improve the solar energy conservation efficiency. This study focused on utilising synergistic ternary composites by integrating 2D niobium carbide ($Nb_2C$) MXene with g-$C_3N_4$ and lead halide perovskite ($CsPbBr_3$) quantum dot interlayers. The addition of 2D $Nb_2C$ to the ternary heterojunction (g-$C_3N_4$/$Nb_2C$/$CsPbBr_3$) resulted in the maximum reduction of $CO_2$ to CO with a production rate of 53.07 μmol $g^{-1}$ $h^{-1}$. The activity of the ternary composite surpasses the rates of pure g-$C_3N_4$, $CsPbBr_3$ QDs, and the binary composite g-$C_3N_4$/$CsPbBr_3$ by approximately 8.4, 10, and 2 times, respectively. The simulations and theoretical results validate that the presence of $Nb_2C$ MXene promotes electron transfer, thereby enhancing the photocatalytic activity.[232]

Conversely, nanomaterials exhibiting quantum confinement due to their size possess unusual electronic and optical properties, leading to the phenomenon of quantum dots (QDs). QDs are known to be zero-dimensional (0D) and a maximum size of 10 nm. Since the identification of g-$C_3N_4$ QDs in 2014, numerous applications have been unveiled in

Open Access Article. Published on 09 Nyenyankulu 2026. Downloaded on 2026-05-16 11:57:57.
This article is licensed under a Creative Commons Attribution 3.0 Unported Licence.

various domains, including photocatalysis, biomedicine, optoelectronics, and sensing. Compared to other carbon-based QDs, such as carbon nanodots and graphene QDs, g-$C_3N_4$ QDs display higher photoluminescence quantum yields. Quantum confinement leads to distinct properties from bulk structures, including a high surface area, a non-zero band gap, enhanced dispersibility due to the significant edge effect, an amphiphilic nature, and highly adjustable physical and chemical properties.[233] This notable breakthrough on g-$C_3N_4$ QDs opens a broader array of applications. Rather than applying pure or pristine nanoparticles, insights into the incorporation of MXene and QD heterojunction structures can enhance the photocatalytic efficiency of g-$C_3N_4$. For example, Nie *et al.* developed MXene QDs (MQDs), decorated with a p–n heterojunction photocatalyst by introducing two different semiconductors, *viz.*, g-$C_3N_4$ and bismuth oxyiodide (BiOI). The synergistic effect of the ternary g-$C_3N_4$/MQDs/BiOI photocatalyst achieves higher removal of nitric oxide through deep oxidation of 42.23% and produces fewer nitrite intermediaries than individual and binary materials. In addition, the performance of the ternary nanocomposite significantly influences the photoreduction of $CO_2$ to CO, with a production rate of 57.8 μmol $g^{-1}$ $h^{-1}$ and a $CH_4$ production rate of 3.6 μmol $g^{-1}$ $h^{-1}$.[229] Here, we reiterate that the nanocomposite enhances the activity of the photocatalytic system's by reducing electron recombination and facilitating

**Table 3** Recent advances and applications of g-$C_3N_4$ in environmental remediation

| Composite materials | Application | Quantitative efficiency | References |
|---|---|---|---|
| Biosensor application | | | |
| Si/g-$C_3N_4$ | The composites act as biosensors to detect prochloraz and 2,4,6-trichlorophenol, which are widely used chemicals in the agroecosystem | pH = 7 to 8 enhances electrochemiluminescence sensing | 236 |
| ZIF6/CN | CN is the base framework of g-$C_3N_4$, while carbonyl has been functionalised by adding 2-thiouracil. The nanocomposite is a highly sensitive biosensor with more active sites to detect glyphosate contamination in environmental water samples | Detection limit 0.04 pg $L^{-1}$, linear range from $10^{-12}$ to $10^{-5}$ g $L^{-1}$ | 237 |
| Cu/Fe/g-$C_3N_4$ | The nanocomposites are used as biosensors under greenhouse conditions | 1. Gas sensing-90%<br>2. Humidity sensing-82%<br>3. Soil moisture sensing-72% (black soil) and 59% (red garden soil) | 238 |
| $Fe_3O_4$@MoC MFs/g-$C_3N_4$ | The nanosensor successfully detected the parathion pesticide in food samples | 1. Lowest detection limit-7.8 nM<br>2. Sensitivity-2.16 μA $μM^{-1}$ $cm^{-2}$ | 239 |
| Water treatment and disinfection | | | |
| Ag/$C_3N_4$–NiSe | The NPs efficiently degrade the RhB dye and inhibit the enzymes of harmful *Staphylococcus aureus* bacteria | 1. Catalytic degradation-69.58%<br>2. Antimicrobial activity-(1.75 and 3.90 mm) low and (3.35 and 4.55 mm) high concentration | 205 |
| AgNPs/g-$C_3N_4$ | The photocatalytic degradation of 2,4-D herbicide was better under visible light irradiation than when treated with Ag NPs alone (>420 nm) | 3% AgNPs/g-$C_3N_4$ degrade 2,4-D completely in 240 min with an absorption peak at 283 nm | 240 |
| PdNPs@g-$C_3N_4$-BLE | In addition to catalytic properties, the nanoparticles exhibit antimicrobial properties | 1. 72–98% in Suzuki–Miyaura cross-coupling (12 reuse)<br>2. 68–98% in cyanation reactions (6 reuse) | 55 |
| ZnO/CN | Nanocomposites remove cyanobacterial algal blooms by neutralising the charge of algal cells (negative) and NPs (positive) | Within 10 min at a dose of 4.0 g $L^{-1}$ (ZnO/CN – 2 : 1), it removes 93% of algal cells | 241 |
| CdO/$NiFe_2O_4$/g-$C_3N_4$ | Photocatalytic nanocomposites efficiently degrade the crystal violet dye and diclofenac sodium drug | 86% and 84% higher degradation of diclofenac sodium and crystal violet, when compared to pure NPs (CdO and $NiFe_2O_4$). | 242 |
| Ag@GCN | The photodegradation of rose Bengal and the composite application enhanced the removal of xylenol orange dye in wastewater | 1.5 mM concentration nanocomposite degrades 76% of rose Bengal and 15% to 36% of xylenol orange dye | 243 |
| Ag@AgCl/g-$C_3N_4$ | The nanomaterial degrades the new coccine food colourant under the visible light spectrum | 95.7% of degradation in 60 min | 244 |
| Pbi-Zno-g-$C_3N_4$ | The nanocomposite degrades persistent atrazine, slowly releases P fertiliser from biochar, and improves microbial growth on g-$C_3N_4$ treatment | 85.3% degradation after 260 min | 245 |
| Biomedical applications | | | |
| g-$C_3N_4$/CS/PAA/CUR | The nanocomposites are a carrier for curcumin drugs to inhibit cancer cells | Drug release (96 h) – ~98% and 69% in acidic and neutral pH, respectively | 246 |
| pCN/CNTs | In biomedical applications, the synthesized NPs promise wound healing and sterilizing pathogens | pCN/CNTs (5 : 1) at a concentration of ~$10^6$ CFU $mL^{-1}$ to (0–2 CFU $mL^{-1}$) inactivated pathogens within 2 h | 247 |

Note: CN – carbon nitride, GCN – graphitic carbon nitride (synonymous to g-$C_3N_4$), and pCN – polymeric carbon nitride have similar base composition, structural motif, and precursors.

 This journal is © The Royal Society of Chemistry 2026

Open Access Article. Published on 09 Nyenyankulu 2026. Downloaded on 2026-05-16 11:57:57.
This article is licensed under a Creative Commons Attribution 3.0 Unported Licence.

the faster migration of photogenerated electrons to the active sites.

The application of an alkalized nano-biochar (BC) and g-$C_3N_4$ (BCNaOH/g-$C_3N_4$) composite significantly removed lead (Pb) and atrazine (ATZ) from the rice ecosystem. The ATZ present in overburden water was degraded through photo-responsive electron generation and Pb sorption from contaminated paddy soil reached 94.70% and 47.75%, respectively.[234] Fig. 10(d) depicts the mechanism of action of nanomaterials on Pb sorption and photodecomposition of ATZ molecules. In modern agricultural practices, ATZ has been extensively used as a herbicide worldwide to control weed growth. However, despite its economic benefits, it presents hazardous concerns due to its long persistence in the soil ecosystem, lasting up to 57 weeks and exceeding the permissible limit in water bodies, which need to be addressed.[235] In Table 3, we present the utilisation of g-$C_3N_4$ for pollutant degradation under various circumstances. Cd-contaminated soils impede crop development and present a hazard to the ecosystem.[120] In this case, g-$C_3N_4$ can potentially remediate contaminated soils and transform Cd into immobile forms, improving soil fertility. In a greenhouse study, the addition of g-$C_3N_4$ to soil under Cd-contaminated conditions reduced the oxidative stress on soybean plants and converted Cd into low-toxic forms. Compared to non-treated plants, the application of g-$C_3N_4$ increased the dry weight of soybean plants and reduced the Cd content in shoots and roots by 35.7% and 54.1%, respectively.[119] Hastuti *et al.* demonstrated the composite application of rGO/g-$C_3N_4$ in hydroponic rice seedling growth under Pb-contaminated conditions. Co-exposure to the nanocomposite enhanced the seedling mass by alleviating Pb toxicity and fostered notable improvement in root and leaf length. rGO/g-$C_3N_4$ possesses a high surface area and active sites that adsorb Pb and convert it to an unavailable form. Therefore, the optimal doses combat heavy metal stress, whereas excessive doses or additional stressors may trigger oxidative stress and inhibit plant growth. The MDA content with the co-treatment of Pb and rGO/g-$C_3N_4$ yielded 0.48 ± 0.027 μM $mg^{-1}$ protein, which was higher than Pb treatment alone (0.48 ± 0.027 μM $mg^{-1}$).[123] Furthermore, the co-transport of g-$C_3N_4$ and adsorbed pollutants in water and soil must be studied to prevent water and soil contamination. The upcoming section deliberately discusses the g-$C_3N_4$-involved soil dynamics and microbial augmentation.

## 8. g-$C_3N_4$ improved the soil dynamics and microbial interaction

Recent findings underscore the potential of g-$C_3N_4$ in modulating soil microbial communities and nutrient dynamics in plants. In cadmium (Cd)-contaminated soils, exposure to g-$C_3N_4$ significantly reduced the Cd accumulation in soybean plants. Notably, soil treatment with g-$C_3N_4$ at a concentration of 0.8% by weight led to a 49.7% reduction in Cd content in soybean roots, a phenomenon strongly associated with elevated nitrogen levels in the rhizosphere.[207] Nitrogen (N) application promotes the physiological activities and reduces pollutant accumulation by inducing a dilution effect in the plant system.[248] Researchers identified that different forms of N impart varying results in the accumulation and uptake of heavy metals in plants. It should be noted that several studies indicate that nitrate ($NO_3^-$) supply enhanced the uptake and accumulation of Zn and Cd in crops, including rice, wheat, cabbage, and tomato.[248]

Researchers found that the influence of the nitrate transporter gene (*NRT1.1*) mediated nitrate uptake or sensing, and it conferred resistance to lead ($Pb^{2+}$) uptake in *Arabidopsis* plants. The co-supply of $NO_3^-$ and $NH_4^+$ ensures the induction of *NRT1.1*, which influences the uptake of $Pb^{2+}$. The sole $NO_3^-$ supply results in the consumption of $H^+$ ions by roots, causing alkalization in the rhizosphere, and impeding the uptake and bioavailability of $Pb^{2+}$.[249] In a contrasting result, ammonium ($NH_4^+$) releases more $H^+$ ions, leading to lower pH in the rhizosphere, causing solubility and enhancing Cd uptake by plants.[250] Here, we conclude that a change in the soil rhizosphere pH associated with N supply provides varying outcomes in heavy metal accumulation in the plant system. The availability of rhizosphere N in the forms of $NO_3^-$ and $NH_4^+$ increased by 41.9% and 26.1% in the Cd + g-$C_3N_4$-treated groups. Conversely, soybean roots absorb more $NH_4^+$ as a defence mechanism under Cd stress conditions.[207] There could be two reasons for $NH_4^+$ mediating stress mitigation in soybean plant, *viz.*, 1) cell membrane depolarisation in the root cells, leading $NH_4^+$ influx into the cytoplasm, which reduces Cd uptake and 2) higher $NH_4^+$ content in *Oryza sativa* L roots inhibits pectin methylesterase activity, causing a negative charge in the cell wall, which significantly reduces Cd uptake in the roots.[249,250] Notable nutrient enrichment was negatively correlated with Cd accumulation in the plant system, highlighting the protective mechanism mediated by the nutrient-ion-metal interactions.[207]

Thus, this indicates two critical findings: 1) the enhancement of N content in the soil rhizosphere has substantial potential to reduce pollutant bioavailability and 2) g-$C_3N_4$ could supply available N in the form of $NO_3^-$ and $NH_4^+$ for plant growth and development. A comparative study on tetracycline (TC) remediation in pig farm soil and riverbed soil was demonstrated; g-$C_3N_4$ treatment significantly removed TC in both soil groups compared to the nontreated group. According to the treatment design, samples with different concentrations of TC, g-$C_3N_4$, and co-application were placed in a homeothermic incubator at the optimum temperature of 30 °C and 2000 lux illumination, with a light–dark period of 12:12 h for 30 days. However, the TC residue in the pig farm soil remains higher than in the riverbed soil. A noticeable shift occurred in the microbial community of riverbed soil, particularly in Acidobacteriota, Actinobacteriota, and Desulfobacterota. The microbiota of pig farm soil remained stable due to their stable microbial network. g-$C_3N_4$ significantly minimises the tetracycline-

Open Access Article. Published on 09 Nyenyankulu 2026. Downloaded on 2026-05-16 11:57:57.
This article is licensed under a Creative Commons Attribution 3.0 Unported Licence.

resistant genes and other antibiotic-resistant genes by restricting resistant bacterial species. Overall, g-$C_3N_4$ influences bacterial metabolism associated with the removal of resistant genes.[251] This study concluded that g-$C_3N_4$ is an eco-friendly photocatalyst and has no adverse effect on the soil microbiota.

From a microbial ecology perspective, g-$C_3N_4$ influenced the composition and function of soil microbial communities. The alterations in rhizosphere functional genes reflect the forms of N content in the soil. The available N content was estimated by adopting three microbial-driven N transformations, including nitrification, denitrification, and N fixation.[252] The relative abundance of N-fixing bacteria increased significantly, supported by the upregulation of the nitrogenase iron protein (*nifH* gene), which encodes the biological nitrogen fixation. Concurrently, g-$C_3N_4$-treatment resulted in the suppression of the nitrifying genes ammonium mono-oxygenase subunit (*amoA*) and nitrite oxidoreductase subunit A (*nxrA*) over the control group. Taxa such as *Flavisolibacter*, *Niastella*, *Pirellula*, and *Opitutus* were enriched under g-$C_3N_4$ exposure, as confirmed with analysis based on Spearman correlation. The genus is positively correlated ($p < 0.05$) with the *nifH* gene, which promotes the N-fixing and retention process, especially ammoniacal-N ($NH_4^+$-N) in the roots of the soybean plant.[207] At the molecular level, g-$C_3N_4$ treatment downregulated the expression of transporter genes such as *OsIRT1* (rice iron-regulated transporter 1) and *OsNIP1;1* (rice nodulin 26-like intrinsic proteins). However, in the case of metal exposure, both genes were upregulated in the rice plant.[253]

An enhanced N content in the rhizosphere region of the soybean plant leads to a larger microbial population, particularly in Cd-exposed groups. Compared to the control group, there is an increase in microbial classes, such as Nitrososphaeria (70%) and Actinobacteria (226%), particularly in the genera *Sphingomonas* (24%) and *Bradyrhizobium* (122%), associated with Cd uptake resistance.[120] The strong correlation between N enrichment and rhizosphere microbial abundance indicates that g-$C_3N_4$ treatment can augment plant growth by shifting microbial communities. In addition, g-$C_3N_4$ treatments influenced the activity of the urease enzyme (UE) compared to the control group. These alterations created a more favourable nitrogen-rich soil microenvironment. The application of g-$C_3N_4$ in agricultural soil greatly influences the N cycling in the rhizosphere, promotes N-fixation, and reduces nitrification. We elucidate this phenomenon, which provides insights into N sources for plant growth and development. Notably, the higher accumulation of readily available $NH_4^+$ can minimise energy consumption through the breakdown of carbohydrates owing to nitrate reduction activity.[121]

Beyond soybeans, the application of g-$C_3N_4$ has addressed Cd and arsenate (As) toxicity, as demonstrated in rice cultivation. When applied at a concentration of 250 mg $kg^{-1}$ in metal-contaminated soils, g-$C_3N_4$ significantly improved plant biomass and reduced Cd and As accumulation in plant tissue. A key mechanism underlying this effect is that the alteration of endophytic bacterial communities in rice roots can restrict metal toxicity by conferring metalloid resistance and participating in bioremediation. In particular, the suppression of the *Deinococcus* (72.3%) population plays a crucial role in reducing As(v) to the more mobile and toxic As(iii), contributing to limiting the As uptake in plants.[118] Building on these findings, we propose two refined directions to tap into the application of g-$C_3N_4$ in the agricultural field. Firstly, designing pH-responsive g-$C_3N_4$ nanomaterials to reduce the risk of solubility and bioavailability of heavy metals. Additionally, pH buffering in the soil rhizosphere with $NH_4^+$ and $NO_3^-$ induces metal passivation. Secondly, harnessing a bio-nano hybrid system in the context of stress tolerance, nutrient cycling and pollutant resistance. Based on literature evidence, g-$C_3N_4$ intervention reshapes the soil microbiota, upregulates nitrogen-fixing genes, and downregulates metal transporter genes. This dual strategy of pH responsiveness and tailored microbial consortia makes g-$C_3N_4$ a versatile tool for agricultural applicability. This integrated approach enhances the relevance of g-$C_3N_4$ in this field, promoting crop resilience by improving soil fertility. Taken together, these findings demonstrate that g-$C_3N_4$ not only reduces the bioavailability of heavy metals but also validates that they are a potential option for mediating soil–plant–micro–metal interactions at the transcriptional and community level. Beyond their photocatalytic functions, g-$C_3N_4$ acts as an excellent nutritional source, supplying N in multiple bioavailable forms and enhancing soil properties by modulating the microbial dynamics. The multidimensionality of $C_3N_4$, such as nutrient enrichment and microbial regulation, positions it as an asset in sustainable agriculture. To date, studies have not flagged any toxicity concerns associated with g-$C_3N_4$. However, to ensure its safe and effective integration in the vast agricultural horizons, it is imperative to understand its long-term behaviour and environmental impact in open agricultural fields. Expanding research focusing on the forefront could unlock substantial opportunities for deploying g-$C_3N_4$ applications under real-world field conditions.

## 9. Toxicity and biocompatibility of g-$C_3N_4$

Studies have highlighted that carbon-based nanomaterials are naturally present in food items. Standard food preparation techniques, such as heating, roasting, and grilling, can manipulate carbon-based nanomaterials. Consequently, human exposure to carbon materials through dietary intake is frequent, and to date, has not been associated with a significant health risk.[3] Numerous studies have investigated the biocompatibility of g-$C_3N_4$ to validate its potential for ecosystem sustainability. These studies rely heavily on cytotoxicity, genotoxicity, antimicrobial, and biomedical tests involving living systems, which are essential for thoroughly assessing the safety of nanomaterials.

 This journal is © The Royal Society of Chemistry 2026

Open Access Article. Published on 09 Nyenyankulu 2026. Downloaded on 2026-05-16 11:57:57.
This article is licensed under a Creative Commons Attribution 3.0 Unported Licence.

Freshwater zebrafish, an aquatic model organism with more than 1000 genes homologous to humans,[3,254] has become a valuable tool in toxicity studies. Its features, transparent embryos, small size, rapid development, and well-characterised genetic background, making it ideal as a model organism for toxicity assessments.[255]

For instance, an investigation revealed the efficacy of a ternary nanocomposite (g-$C_3N_4$/$Nb_2O_5$/Ag) in degrading environmental pollutants, norfloxacin (NRF) and methylene blue (MB). Upon treatment with the nanocomposite under polluted conditions (NRF and MB) at pH 9, zebrafish embryos and larvae exhibited high mortality rates (80–90%) within 48 h post-fertilisation. Along with that, severe malformations appeared in the eye, tail, brain, and spine, with overall growth retardation. In contrast, 72 h post-fertilisation, water treated with the nanocomposite exhibited efficient photocatalytic pollutant degradation, achieving 83% and 92% for NRF and MB, respectively, and no toxic effects on zebrafish embryos.[256] This demonstrates that g-$C_3N_4$-based nanocomposites offer a sustainable approach to mitigate environmental degradation.

To assess cell viability and cytotoxicity effects, scientists widely use assays, most notably the MTT assay, a calorimetric test that quantifies cell viability.[257] Dong *et al.* investigated the photocatalytic degradation potential of g-$C_3N_4$ on the paraquat (PQ) herbicide, accompanied by toxicity studies using human lung (A549) cells, zebrafish models, and mice tissue analysis (lung and stomach). The A549 cells were employed in an MTT assay, where treatment with 10 mg $L^{-1}$ of g-$C_3N_4$ increased the cell viability from 54% to 91.4% in PQ-damaged cells. In addition, the PQ group and the g-$C_3N_4$ + PQ group were observed with SEM. The results demonstrate that the PQ group showed a malformed cell morphology. In the g-$C_3N_4$ + PQ group, the NPs shield the cells from PQ, and there was no significant difference in morphology with the control group. Furthermore, the $IC_{50}$ of PQ and g-$C_3N_4$ at 24 h was observed to be 400 μm $L^{-1}$ and 1250 mg $L^{-1}$. In the survival analysis, the zebrafish were exposed to PQ and g-$C_3N_4$ at 100 mg $L^{-1}$ and 500 mg $L^{-1}$, respectively. Accordingly, the g-$C_3N_4$ has no significant impact on zebra fish survival rate. After 7 days, PQ detoxification with g-$C_3N_4$ increased the survival by 70% compared with 30% in the PQ group. This study confirmed that g-$C_3N_4$ significantly reduced PQ accumulation and its associated toxicity across all models. Real-time fluorescence imaging of the paraquat distribution in mice and zebrafish, as shown in Fig. 11(a and b), supports

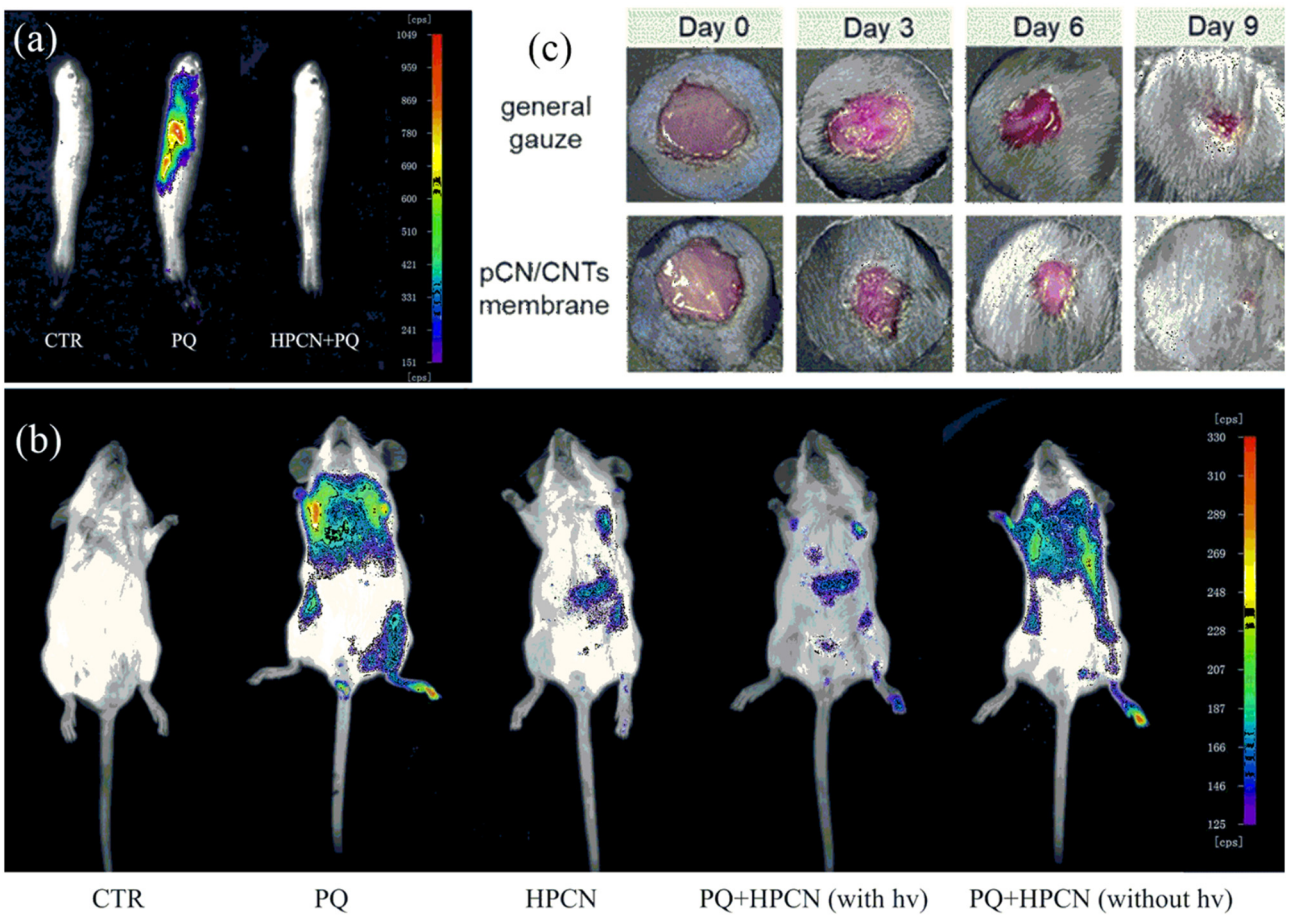


**Fig. 11** (a and b) Animal images recorded for g-$C_3N_4$ (HPCN) accumulation in zebrafish and mice, respectively[258] (adapted from ref. 258 with permission from Elsevier, Copyright 2023). (c) Photograph of *S. aureus*-infested wound healing in laboratory mice treated with polymeric carbon nitride (pCN)[247] (adapted from ref. 247, © 2023, RSC. Published under the CC BY-NC 3.0 licence).

Open Access Article. Published on 09 Nyenyankulu 2026. Downloaded on 2026-05-16 11:57:57.
This article is licensed under a Creative Commons Attribution 3.0 Unported Licence.

this finding. Furthermore, pristine g-$C_3N_4$ did not cause significant apoptosis or mortality in either zebrafish or mice.[258]

Cytotoxicity assessment using HepG2 cells (human liver cancer cells) revealed distinct responses between the two g-$C_3N_4$ morphologies. The homogeneous lamellar form at 300 mg $L^{-1}$ exhibited markedly lower toxicity, maintaining approximately 80% cell viability, whereas the heterogeneous structure resulted in only 20% viability. The higher viability of the homogeneous lamellar form is attributed to its structural uniformity, while the heterogeneous form contains more defects and reactive sites within its nanostructure.[102] These findings reveal contrasting perspectives on the suitability of g-$C_3N_4$ materials for biomedical applications, demonstrating that morphological variations in g-$C_3N_4$ can lead to markedly different biological responses and must be carefully evaluated under varying conditions.

In terms of antibacterial properties, a study investigated the incubation of bacterial strains, along with an rGO/g-$C_3N_4$/$FeTiO_3$ nanocomposite at concentrations of 50 μg $mL^{-1}$ and 75 μg $mL^{-1}$ for 24 h at 37 °C. The results indicated that the g-$C_3N_4$-based nanocomposite exhibited higher inhibition of both Gram-positive (*Staphylococcus aureus*) and Gram-negative (*Escherichia coli*) bacterial species. Furthermore, the nanocomposite at different dosages (6.25, 12.5, 25, 50, and 100 mg $L^{-1}$) were tested on zebrafish embryos. Post 48 h exposure to the nanocomposite, the $LC_{50}$ value was determined as 20.79 μm $L^{-1}$. After 48 h of exposure to different doses, higher concentrations cause embryonic toxicity, including decreased egg hatching rate, overall mortality and other abnormalities.[228] In a similar study, the minimum inhibitory concentration (MIC) method was adopted to evaluate the antimicrobial effects of a nanocomposite (g-$C_3N_4$/Ca/*Aloe vera*) against the same Gram-positive and Gram-negative bacteria. Likewise, the nanocomposite hade an MIC value for both *S. aureus* and *E. coli* strains of 1 mg $mL^{-1}$. The reason for this may be that upon exposure to light, g-$C_3N_4$ generates ROS, which disrupts the bacterial membranes and inhibits their growth.[259] One of the critical advantages of g-$C_3N_4$ lies in its simple chemical composition, consisting solely of carbon and nitrogen atoms, which might be metabolizable by living organisms.

Sen and Perveen used g-$C_3N_4$ for biomedical applications in their respective studies, especially for drug release and bioimaging of cancer cells.[260,261] In fabricating a drug delivery system, g-$C_3N_4$ was used as a carrier for cisplatin, an anticancer drug. The complex has an adsorption energy ($E_{ad}$) of −1.25 eV. The N–H non-bonding interactions ensure better interaction between the carrier and the drug. Further, the complex exhibits a higher dipole moment (12.79 Å) than g-$C_3N_4$, which improves its solubility in polar solvents. These weak interactions between the carrier and drug enables drug release from the carrier matrix.[261]

Alipournazari *et al.* confirmed the successful delivery of doxorubicin (DOX) drug from the pH-sensitive starch/PVA/g-$C_3N_4$ hydrogel for inhibiting the proliferation of breast cancer cells (MCF-7). The nanocarrier achieved a loading efficiency of 44.75% and entrapment efficiency of 88%. According to the results, it was concluded that the cells treated with starch/PVA/g-$C_3N_4$ have higher viability (94.8%) than the control group (93.9%). Contrastingly, the cells treated with starch/PVA/g-$C_3N_4$/DOX showed 36.4% survival. In addition, the results demonstrate that the DOX release kinetics is faster at acidic pH (5.4), which is pertinent to tumour cells *versus* healthy tissues having a pH 7.4.[262]

Due to its low biological toxicity and high surface area, g-$C_3N_4$ is widely utilised in biomedical research, particularly as a carrier matrix in targeted drug delivery systems for cancer treatment. It can transport therapeutic agents without mobilising the active molecule. However, limitations in the shape and structure of g-$C_3N_4$ prevent its direct use in the biomedical field, as it lacks features such as slow-release capability and specific drug-molecule interaction. Therefore, integrating g-$C_3N_4$ with nano-hybrid structures has become promising for overcoming these shortcomings, thereby enhancing its utility in biomedical applications.

Sabzini *et al.* prepared a hybrid nanoformulation (chitosan/halloysite/g-$C_3N_4$) loaded with quercetin (QC) drug using a water-in-oil-in-water emulsion, which acts as a slow-release anticancer drug delivery system. The nanovehicle enhanced the entrapment effectiveness of QC by 86%. The targeted pH-responsive sustained release of QC was confirmed by 96 h extended release under pH 5.4, and holding the antitumor agent within the nanovehicle under neutral conditions (pH 7.4) limits its side effects by avoiding burst release. Furthermore, subjecting MCF-7 cells for 24 h to chitosan/halloysite/g-$C_3N_4$/QC resulted in the lowest cell viability and lower vitality than the cells treated with free QC.[263]

Khamene and coworkers fabricated a nanocomposite comprising polyvinyl alcohol, bacterial cellulose, calcium, *aloe vera* fibres, and g-$C_3N_4$ in a single structure. In this study, each material was selected based on its wound-healing properties. The composite dressing materials were tested against diabetic wounds in an animal model (mice). They significantly influenced tissue regeneration and accelerated wound healing, achieving a 95% healing rate in 3 weeks, compared with the 57% healing capacity of the curcumin/lignin dressing.[259] Fig. 11(c) illustrates the wound healing property of g-$C_3N_4$, a similar carbon nitride group having the same composition as g-$C_3N_4$. The possible mechanism of the synergistic effect of g-$C_3N_4$ on photocatalytic wound healing involves its light-induced generation of ROS, which helps to sterilise the wound by killing bacteria.[264] Mild ROS levels modulate inflammation by activating signalling pathways. This balanced inflammatory response supports tissue reconstruction. Additionally, ROS promotes the proliferation of fibroblasts and the production of collagen, thereby aiding in regeneration and wound closure.[259] Furthermore, studies suggest that g-$C_3N_4$ exhibits good biocompatibility and does not cause any adverse effects in humans.[265]

 This journal is © The Royal Society of Chemistry 2026

Open Access Article. Published on 09 Nyenyankulu 2026. Downloaded on 2026-05-16 11:57:57.
This article is licensed under a Creative Commons Attribution 3.0 Unported Licence.

Moreover, an *in silico* study on g-$C_3N_3$, a carbon nitride analogue, utilised molecular dynamics (MD) simulations to assess its interaction with model lipid membranes. This study concluded that g-$C_3N$ does not penetrate the cytoplasm unless subjected to external stimuli. Due to its low likelihood of causing membrane damage, g-$C_3N_3$ is predicted to be biocompatible, similar to g-$C_3N_4$.[266] For clarity and reference, we include the biocompatibility studies on g-$C_3N_4$ (Table S1). Collectively, these research findings strongly suggest that g-$C_3N_4$ exhibits minimal or no toxic effects and holds considerable promise for eco-friendly and biomedical applications.

## 10. Persistence, migration and physicochemical transformation of g-$C_3N_4$ in the ecosystem

The anthropogenic application of nanomaterials to soil and water bodies is intricately linked to the ecosystem. However, their deliberate use in agriculture and environmental systems necessitates a thorough understanding of their biocompatibility and potential ecological impacts. The key concern in applying nanomaterials in the agroecosystem is their potential for bioaccumulation. NPs can readily accumulate in plant tissues, infiltrate the food web, and exert toxic effects on both terrestrial and aquatic organisms. The accumulation of NPs in the food chain raises high toxicity concerns for the ecosystem.[267]

Although g-$C_3N_4$ is often considered a biocompatible material, its long-term effects, including degradation byproducts and bioaccumulation, are poorly understood. Current evidence from acute ecotoxicity tests in zebrafish, microbial toxicity and animal models is insufficient for widespread agricultural implications. The transformation of g-$C_3N_4$ under hydrolysis, oxidation, or microbial breakdown may fragment the polymer into low-molecular N-containing species in soil-water media. The breakdown of g-$C_3N_4$ under environmental conditions may lead to an increase in N species, such as ammonia and nitrate, in the soil and water.[120,207] Tackling nitrate pollution in the ecosystem is becoming difficult these days. The degradation products could alter soil properties and lead to chronic ecotoxicity, such as eutrophication. Nitrate ($NO_3$) is an inorganic source of N ions, which is prone to leaching and bioaccumulation. Anthropogenic activities lead to nitrate pollution, destroy water quality, and cause health complications in living organisms, especially blue baby syndrome in human infants.[268,269]

In addition, the soil column experiment is used to determine the mobility, transformation, and soil interaction of $C_3N_4$ through leachate collection.[121,270–272] Cheng and coworkers conducted a soil column experiment simulating a realistic rice agroecosystem for four months from planting to harvest. g-$C_3N_4$ and Fe–$C_3N_4$ were added to the soil, each at concentrations of 0.5 g $kg^{-1}$ and 2 g $kg^{-1}$, which influence the chemical oxygen demand (COD) and $NH_4^+$ and $NO_3^-$ release in the surface water. After each fertilisation with NPK at various growth stages, g-$C_3N_4$ and Fe-$C_3N_4$ exposure decreased the COD and $NH_4^+$ and $NO_3^-$ levels compared to the control group. Overall, the g-$C_3N_4$ and Fe-$C_3N_4$ treatments generate oxygen species in soil, which is related to their catalytic-oxidative properties, making them beneficial for pollution reduction in agriculture.[121] This study highlights that the addition of g-$C_3N_4$ and its composite reduced N species, but treated soils increased the total nitrogen and phosphorus levels. If unregulated, their elevated levels can contribute to eutrophication, plant nutrient imbalance, and microbial disruption, which can have long-term environmental consequences.

If prioritising the application of g-$C_3N_4$, plenty of issues remain unaddressed regarding safety aspects. Also, the studies have not described the migration and transformation behaviour of g-$C_3N_4$ in the soil ecosystem. These validations are highly anticipated to determine the environmental hazards and food chain accumulation posed by the application of g-$C_3N_4$. The multifunctional capabilities of g-$C_3N_4$ include photocatalytic $O_2$ evolution, $H_2$ evolution, water splitting, $H_2O_2$ production, $CO_2$ reduction, $N_2$ fixation, electrochemical sensing, pollutant removal and organic synthesis.[273–276] All these applications are involved in ecosystem sustainability, which comprises soil and water systems. With the extensive use and increased production of g-$C_3N_4$, it is inevitably released into the environment. Although the biocompatibility of g-$C_3N_4$ has garnered attention, a holistic evaluation of its transformation and migration behaviour within soil matrices is yet to be investigated. Recent environmental studies mainly focused on the degradation or removal of pollutants using g-$C_3N_4$. Nonetheless, many disinfection studies using g-$C_3N_4$ have shown antimicrobial properties in wastewater treatment.[277–279] The persistence of g-$C_3N_4$ after targeted execution towards environmental remediation threatens nontargeted organisms present in the natural environment. In short, addressing one problem should not create another. Generally, carbon materials such as biochar and graphene oxide exhibit better dispersion in the aqueous phase due to the presence of hydrophilic functional groups on their surface. Often, the transport and fate of the particles in porous media are decided by their physicochemical properties, the media, hydraulic flow, soil colloids and solution chemistry.[280,281]

In the case of g-$C_3N_4$, it is hydrophobic in nature, but its triazine and tri-s-triazine structural building blocks are rich in hydrophilic amine groups (–$NH_2$, –NH–, and =N–). Rather than being a true solution, the amino groups in g-$C_3N_4$ exhibit better dispersibility and adsorption capacity in aqueous and porous media.[282,283] The deposition and migration of carbon nanomaterials, including g-$C_3N_4$, nano biochar and graphene oxide, were tested in packed columns that resemble the actual mechanism in the soil system. Studies have concluded that the presence of heavy metals

Open Access Article. Published on 09 Nyenyankulu 2026. Downloaded on 2026-05-16 11:57:57.
This article is licensed under a Creative Commons Attribution 3.0 Unported Licence.

and organic pollutants inhibited the migration of g-$C_3N_4$ in the porous media. Simultaneously, g-$C_3N_4$ acts as a transporter of adsorbed pollutants in a small fraction, discharging out of the saturated column media.[271,284,285] Furthermore, the promotion or inhibition of deposition in a saturated medium is influenced by the soil components, such as limestone,[286] humus,[287] clay minerals[284] and hydrated iron oxides.[288] We speculate that the dispersibility of g-$C_3N_4$ and its mobility under different conditions could cause accumulation in the tropic levels.

For example, Dong and Jian demonstrated the migration behaviour of g-$C_3N_4$ under various conditions, including water flow rate, pH, multivalent cation solution, ionic strength (IS), humic acid incorporation, and particle size of quartz sand media.[271,272] The mobility of graphene oxide in a porous medium was high under low IS (1 mM), but highly inhibited under higher IS (10 mM).[289] At the same time, humic acid is rich in negative charges, and its higher levels improve the electronegativity for both g-$C_3N_4$ and sand media. As a result of the high electrostatic repulsion and negative zeta potential of g-$C_3N_4$ and sand media, increased mobility was observed in the saturated media.[286,290,291] Based on the above-mentioned results, Dong *et al.* investigated the transport and migration of g-$C_3N_4$ under the combined effect of IS (0.1, 1 and 10 mM) and other factors, including quartz sand grain size (0.70–0.85, 0.35–0.45 and 0.15–0.20 mm), humic acid concentration (0, 1 and 5 mg), and solution pH (4.0, 6.0, and 8.5). In this study, the one-site kinetic model was used to simulate the retention and transport of g-$C_3N_4$ in porous media, with very well-fitted breakthrough curves. Overall, the mobility of g-$C_3N_4$ in porous media was enhanced by an increase in sand grain size, solution pH, and humic acid concentration. Following the same trend, lower IS levels result in higher mobility of g-$C_3N_4$ in porous media.[272]

A similar study demonstrated the transport behaviour of g-$C_3N_4$ in quartz sand porous media in a packed column experiment under various factors, including flow rates (0.5, 1.0 and 2.0 mL $min^{-1}$), IS (0.1, 0.01, 0.001, 0.0001 M KCl, pH = 7), pH (4, 7 and 9 using 0.001 M NaOH or 0.001 M HCl) and multivalent cations (KCl–$K^+$, $CaCl_2$–$Ca^{2+}$, $MgCl_2$–$Mg^{2+}$, and $AlCl_3$–$Al^{3+}$, IS = 0.0001 M, pH = 7). It differs from the previous study, which integrates factors like flow rates and multivalent cations. The breakthrough curves are constructed as a function of the injection concentration ratios to the effluent rate. Based on the mass balance calculation, the recoveries of g-$C_3N_4$ at 0.1, 0.01, 0.001, 0.0001 M IS and DI water are 2.36%, 1.96%, 14.52%, 60.46% and 88.46%, respectively. g-$C_3N_4$ was retained in the sand column with a maximum amount at IS greater than 0.01 M. The nitrogen lone pair electrons on the surface of g-$C_3N_4$ easily bonded with the Si–OH group on the quartz sand surface. This phenomenon was confirmed by the FTIR spectrum, with the peak at around 970 $cm^{-1}$ corresponding to the stretching vibration of Si–OH. As the electric double layer of the g-$C_3N_4$ colloid was compressed with an increase in IS, there is a high probability of forming hydrogen bonds between g-$C_3N_4$ and the media. Conversely, the first layer of g-$C_3N_4$ was hydrogen-bonded to the surface of quartz sand, creating new adsorption sites through π–π conjugation. The reduced recovery of g-$C_3N_4$ under high IS conditions is attributed to the enhanced self-adsorption of g-$C_3N_4$. The migration efficiency was greatly inhibited under acidic conditions (6.99%), followed by basic (88.46%) and alkaline (93.14%) conditions. Lowering the pH results in excess $H^+$ ions, with a less negative zeta potential, weakening the electrostatic repulsion and colloidal stability, and thereby promoting stronger adsorption and aggregation. The flow rates (0.5 to 2 mL $min^{-1}$) have a weak effect on transporting g-$C_3N_4$ in the porous media, yielding recoveries of 86.63%, 88.46% and 91.61%.[271] According to the Schulze–Hardy rule, cations possess higher colloidal coagulation properties. Subsequently, compared to monovalent cations, multivalent cations significantly hinder the mobility of NPs in porous media.[292] Consistent with this trend, the g-$C_3N_4$ retention effect in porous media follows the order of $Al^{3+}$ (98.49%) > $Ca^{2+}$ (69.67%) > $Mg^{2+}$ (65.09%) > $K^+$ (39.54%). The multivalent cation crosslinks with g-$C_3N_4$, especially $Al^{3+}$ ions, forming flocculation precipitation at pH > 4.3 to produce aluminium hydroxide. Thus, $AlCl_3$ treatment at 0.1 mM exhibits the strongest aggregation and deposition of g-$C_3N_4$ in the soil porous media.[271] In the case of divalent cations ($Ca^{2+}$ > $Mg^{2+}$) with similar charge, the flocculation effect is closely related to the hydrated shell thickness of metal cations.[293]

Adding more complexity by incorporating heavy metals and diverse soil components to the experimental setup provided insights into the transport behaviour of g-$C_3N_4$. Zhou *et al.* demonstrated the impact of water flow rate, ionic strength, and presence of heavy metal (Pb) on the migration behaviour of g-$C_3N_4$. The above-mentioned factors were tested in complex soil components, including quartz sand, montmorillonite and humic acid-coated quartz sand in a packed column experiment. The results indicated that the water flow rate (2 mL $min^{-1}$) and IS (0.0001 mol $L^{-1}$) substantially increased the recovery of g-$C_3N_4$ by up to 79.81%, 73.01% and 71.74%. In contrast, a lower flow rate (0.5 ml $min^{-1}$) and higher IS greatly inhibited the recovery of g-$C_3N_4$ in all media. The incorporation of Pb modulates the transport behaviour, decreasing the g-$C_3N_4$ recovery in quartz sand, montmorillonite, and humic acid-coated sand media by up to 0.34%, 5.86% and 15.34%, respectively, compared to the media not contaminated with Pb. The C and N functional groups and π-conjugated structures present in g-$C_3N_4$ mediate Pb adsorption onto g-$C_3N_4$. The Pb adsorption data for g-$C_3N_4$ fitted the Langmuir model, indicating monolayer adsorption on the surface rather than interaction between adsorbates, with a maximum capacity of 61.86 mg $g^{-1}$. A cotransport experiment on quartz sand, montmorillonite and humic acid-coated sand revealed that the recovery of g-$C_3N_4$ was substantially reduced from 79.81%, 73.01% and 71.74% to 17.57%, 21.72%, and 21.47%, respectively, in the case of mixed liquid of Pb and g-$C_3N_4$. The possible mechanisms for

 This journal is © The Royal Society of Chemistry 2026

Open Access Article. Published on 09 Nyenyankulu 2026. Downloaded on 2026-05-16 11:57:57.
This article is licensed under a Creative Commons Attribution 3.0 Unported Licence.

the reduction in the recovery of g-$C_3N_4$ could be: 1) Pb adsorption in the media decreases the zeta potential and reduces the electrostatic repulsion between g-$C_3N_4$ and media, 2) the Pb and g-$C_3N_4$ mixed solution increases the ionic strength, enabling easier agglomeration within the media, and 3) the initially deposited g-$C_3N_4$ in the media provides new sites for free Pb adsorption.[270]

According to the above-mentioned experimental results, there is a high chance of transporting g-$C_3N_4$ from surface soil to deeper soil and underground water. Varying physicochemical factors should be considered for evaluating the potential transport behaviour of g-$C_3N_4$ under soil conditions. In addition, the immobile stable heavy metal compounds were enhanced in cotransport with g-$C_3N_4$. Linking the above-mentioned findings together on the reported transport behaviour, more factors that are prevalent under natural conditions still need to be tested. In addition, the reported results were obtained under controlled circumstances, whereas the natural ecosystem possesses diverse factors, which include 1) soil structure, 2) texture, 3) porosity, 4) permeability, 5) organic matter, 6) pH, 7) cation exchange capacity, and 8) biological activity. Certainly, it is inevitable to balance the reports on g-$C_3N_4$ transport under controlled circumstances. The application of g-$C_3N_4$ in the agroecosystem focuses on plant growth and development through varying interventions such as direct plant physiological development, altering soil properties by augmenting microbes and metal passivation. We present the discussion not based on the fate of g-$C_3N_4$ in relation to its transport behaviour. It is case-specific that applying dosages and permissible limits has been less explored in real-time applications. Under natural conditions, g-$C_3N_4$ can be degraded or broken down with exposure to light, temperature and microorganisms. This situation should be considered in the transport behaviour of g-$C_3N_4$ at different levels, where it may not persist or accumulate at any trophic levels. The outcomes on the biocompatibility of g-$C_3N_4$ with various organisms, as well as a cohort study on persistent or breakdown byproducts, could strengthen its utility. Concurrently, regardless of the breakdown process, the degraded products must not compromise the integrity of the ecosystem.

To address this, we propose X-ray absorption spectroscopy (XAS) analysis for the chemical modification of g-$C_3N_4$.[294] XAS has the potential to unravel the degradation routes upon exposure to light and soil circumstances. Alongside its application, structural transformations occur, such as the cleavage of its C–N bonds and the formation of N-rich intermediates, including imide, nitrile, and amine groups. The structural changes are sensitively detected *via* N and C K-edge, which refers to the energy required to eject an electron from the core K-shell of an atom. It indicates a shift in $\pi^*$ and $\sigma^*$ conjugated systems, as reflected in the hybridisation and bonding environments.[295] The imide, nitrile, and amine derivatives, namely phthalimide, acrylonitrile, and nitrosamines, are reported to be highly carcinogenic and mutagenic to living organisms. The release of these contaminants may have long-term negative impacts by persisting in soil and water, causing hazards to multiple trophic levels.[296–298]

The fate of g-$C_3N_4$ in the soil ecosystem is site-specific, which depends on the soil properties. Among the nanomaterials with similar properties that exist in the present era, there has been a rise in their negative impact on society. Thus, the multidimensional properties of g-$C_3N_4$ have positive outcomes that play a significant role in improving the ecosystem. Rather than researchers focusing only on applications, proportionate consideration should be given to its degradation, biocompatibility, and fate. It is essential to establish a framework for addressing the limitations to ensure clarity and applicability.

## 11. Scalability proposal for agricultural application

Conventional fertiliser production is an industrialised process that turns out nitrogen, phosphorus, and potassium in the forms of ammonia, phosphoric acid, and potassium chloride, respectively. Among these vital nutrients, nitrogen is an indispensable source for plants to complete their lifecycle. Thus, the nitrogen demand is rectified by applying various nitrogenous fertilisers. For instance, ammonia is produced through the Haber–Bosch process, which involves expensive machinery for fertiliser processing. The Haber–Bosch process involves a large-scale sour gas unit, an air separation unit, an acid-gas separation unit, and an ammonia production unit.[3,299] Since 1909, the invention of artificial nitrogen fixation by Fritz Haber and Carl Bosch has revolutionised large-scale fertiliser production through industrial ammonia synthesis.[299] Here, ammonia production proceeds through a multi-step catalytic process operating at high temperatures (400 °C to 650 °C) and pressure ranging from 200 to 400 atmosphere.[300] Within a decade after the development of ammonia production, industrial urea production was started by adopting the Bosch–Meiser process in 1922. The process involves temperatures above 180 °C and a pressure of 150 atmosphere.[301] Despite using expensive machinery and an energy-intensive process, the feasibility of fertilisers is due to the large-scale manufacturing industries. Fortunately, over 80% of global ammonia is used in the form of fertiliser-grade urea, which supplements the nitrogen needs of plants.[302] In addition to fertiliser, urea has been widely used in the synthesis of plastics, animal feeds, urea-formaldehyde-based resins, and adhesives.[301]

It is known that g-$C_3N_4$ is synthesised using nitrogen-rich precursors, including melamine, urea, thiourea, cyanamide, dicyanamide, and ammonium thiocyanate.[303] g-$C_3N_4$ has been proposed as an eco-friendly photocatalyst due to its attractive properties, including metal-free precursors, chemical stability, and less toxic to humans.[218] Among the existing precursors for the synthesis of g-$C_3N_4$, urea has

Open Access Article. Published on 09 Nyenyankulu 2026. Downloaded on 2026-05-16 11:57:57.
This article is licensed under a Creative Commons Attribution 3.0 Unported Licence.

outperformed all other sources in terms of quality[304] and compatibility.

In a life cycle assessment study, eight synthesis methodologies were considered for g-$C_3N_4$ production, among which thermal etching has the lowest global warming potential (in kg $CO_2$ eq.) to produce 1 g of g-$C_3N_4$. Optimising the calcination procedure, including shorter heating periods and faster ramp rates, reduces the electricity demand. Considering sustainability, the precursor production of 1 kg each of melamine, urea, and cyanamide was compared with the benchmark $TiO_2$ (titanium isopropoxide and titanium tetrabutoxide) precursors. The environmental impact assessment indicates that urea production has the lowest impact, followed by melamine. In comparison, the two $TiO_2$ NP precursors exhibit a greater environmental impact than urea and melamine but are less harmful than cyanamide. This study highlights that urea-based g-$C_3N_4$ production has the lowest cumulative environmental impact and demonstrates good scalability among the existing precursors and synthesis methods.[52] This study indicates that process optimisation and renewable energy sources are key to overcoming the scalability burdens.

In contrast to conventional nanomaterials such as $TiO_2$, ZnO, and Ag, which require high calcination temperature, hydrothermal reactors, chemical vapour deposition,[305–307] these multistep processes are energy-intensive and demand high input costs. For example, synthesising Ag NPs necessitates regulations for using reducing agents and stabilisers.[307] Although the synthesis of $TiO_2$ typically involves multistep hydrothermal or sol–gel processes,[306,308,309] it raises concerns about scalability and toxicity. Conversely, g-$C_3N_4$ is a low-cost, metal-free replacement, synthesised *via* one-step thermal polymerisation of precursors without demanding more complex reactors or toxic reagents.

When considering cost-effectiveness, producing g-$C_3N_4$ with precursors such as urea and melamine is economical *via* a simple thermal condensation technique.[310] Numerous studies have reported the efficiency of g-$C_3N_4$ produced using different precursor sources. Meanwhile, in a comparative study among nitrogen-rich precursors, g-$C_3N_4$ produced from the urea precursor resulted in a better nanostructure, specific surface area, and electron–hole separation.[304] Although promising, current synthesis techniques are optimised for laboratory-scale protocols, yet are highly anticipated to achieve cost-efficient industrial-scale synthesis.

Long ago, the synthesis of ammonia and urea was considered emerging technology, but rapidly scaled in response to global demand. Analogously, at present, g-$C_3N_4$ is limited to lab-scale production, but exhibits strong potential in various sectors, including agriculture, making it an ideal candidate for large-scale synthesis. Based on the compatibility of urea as a precursor, urea manufacturing industries can render a feasible platform for integrated g-$C_3N_4$ production. However, transitioning g-$C_3N_4$ synthesis from batch-based laboratory protocols to industrial-scale continuous processing is still in the early stage. This mass production further needs optimisation of uniformity in yield, which has not been reported in the published research findings. Additionally, there are technical challenges in governing high temperatures (~450–600 °C)[311] for controlling the uniformity in large reactors, and their impact on photocatalytic stability aspects. However, with targeted research strategies, pilot-scale validation, and interdisciplinary efforts, robust and industrial-scale models for g-$C_3N_4$ production will be attainable shortly. In the case of large-scale applications, techno-economic analysis can help break down the barriers to accepting the potential of g-$C_3N_4$ for farmers and other stakeholders.

## 12. Techno-economic assessment and adoption potential of farmers

A rigorous examination of g-$C_3N_4$ for agricultural deployment must integrate production energetics/costs with beneficial functions and regulatory guidelines for consideration.[124] Life-cycle analysis (LCA)[312] and techno-economic analysis (TEA)[313] with respect to g-$C_3N_4$ are highly recommended for laboratory proof of concept to agricultural relevance. LCA and TEA studies are the principal determinants of cost and environmental burdens.[313] The two main factors involved in LCA and TEA are (i) the energy utilisation for thermal polymerisation and (ii) the environmental and monetary cost of precursor production. A comparative LCA analysis shows that producing less expensive routes for g-$C_3N_4$ with widely available nitrogen-rich precursors, particularly urea, tends to achieve the lowest cradle-to-gate impacts among the synthesis routes.[52] The provided insights on electricity demand for thermal energy management through process optimisation and upstream feedstock selection are the primary contributors to improving the techno-economic profile of g-$C_3N_4$. For instance, thermal decomposition offers a scalable and economical pathway to produce an abundance of g-$C_3N_4$.[101]

In contrast, the well-established industrial process for nitrogen fertiliser production, the Haber–Bosch route for ammonia production, followed by urea synthesis, is an energy-intensive process.[314,315] However, decades-long optimisation processes, including heat integration and production scale-up, enable a significant reduction in unit production costs.[316] Recent LCA and TEA assessments of ammonia and urea industries indicate that significant production gains are closely linked to integrated utilities such as heat recovery and shared feedstock logistics. It helps in lowering the capital expenditure (CAPEX) and operating expenditure (OPEX) on a unit basis.[314] Likewise, the low cost of urea, with its scalability and simple chemical composition (C, N, O, and H), has made it the most commonly adopted precursor.[97]

We propose that co-locating g-$C_3N_4$ production with urea production facilities can be a strategy for process heat integration, sourcing bulk urea as a precursor, and opportunities for shared logistics could reduce CAPEX and OPEX for g-$C_3N_4$ manufacture. Despite this, current g-$C_3N_4$ production methods are optimised at the bench level, and

 This journal is © The Royal Society of Chemistry 2026

Open Access Article. Published on 09 Nyenyankulu 2026. Downloaded on 2026-05-16 11:57:57.
This article is licensed under a Creative Commons Attribution 3.0 Unported Licence.

there is a scarcity in pilot reports or scale-up demonstrations. Thus, reliance on critical engineering pathways enables facilities to operate with continuous furnaces, a faster ramp rate and improved product quality.

From an agronomic and economic perspective, it is essential to evaluate benefits in terms of services delivered per hectare or per cropping season, not as a raw mass. Thus far, no field investigations, either at the pilot scale or full scale, have been conducted to evaluate the application of g-$C_3N_4$ in the agroecosystem context. However, g-$C_3N_4$ in the proposed agriculture utility offers multiple functions by improving soil microbial growth,[120] enhancing nutrient use efficiency,[121] directly augmenting photosynthesis,[69] increasing seed germination, passivating heavy metals[119] and serving as a photocatalyst to break down pollutants.[303,317] Conventional fertilisers have a foreseeable future, being a cheap source of plant nutrients available on a mass basis. When the multidimensional g-$C_3N_4$ can replace many inputs, the net economic balance can shift in favour of adopting g-$C_3N_4$ despite the higher per-kg material cost.

Pilot studies focusing on the amount of energy required to produce a unit mass of g-$C_3N_4$ (kilowatt-hours per kilogram) and quantifiable agronomic effectiveness (for example, the percentage of conventional input that is replaced or percentage reduction per unit). To ensure a robust TEA, future pilot studies should provide clear data on energy utilisation and the actual agronomic benefits deliverable in real farming scenarios.

Its acceptance by farmers will be contingent on a clear demonstration of economic benefits, ease of handling or application and integration into existing input supply chains. g-$C_3N_4$ can be applied in the form of a seed coating, seed priming, foliar spray, or soil amendment, depending on the specific endeavour pursued. Additionally, the role of extension services in demonstrating pilot field studies by accommodating public and private stakeholders can play a decisive role. Coordinated efforts among farmers, scientists, policymakers and other stakeholders could facilitate the adoption of g-$C_3N_4$ in real-time agriculture, thereby addressing the persisting limitations. The initial costs of adopting nanotechnology in agriculture are expensive at this stage due to the less developed infrastructure. Capacity building and awareness programs are essential for introducing innovations or practices that are less prevalent among the farming community. The government should establish participatory training with community engagement for knowledge sharing. As a whole, a holistic approach by all stakeholders can ensure long-term benefits, including higher yield and lower input costs.

## 13. Conclusion and future perspective

In conclusion, g-$C_3N_4$ is the most promising metal-free nanomaterial, providing numerous benefits for agricultural improvement. The g-$C_3N_4$ aids plant growth and development by augmenting artificial photosynthesis and improving the antibiotic mechanism. The photosynthetic rate increased remarkably in association with enhanced stomatal conductance, $CO_2$ concentration, chlorophyll content, oxygen evolution, ATP/NADPH formation, DCPIP reduction and increased activities of key enzymes such as RuBisCO and PEPC. Further, g-$C_3N_4$ increases the electron transfer rate through higher photon absorption from the visible light region. The above-mentioned factors collectively increase photosynthate accumulation, which ultimately promotes plant growth and yield. The metabolic pathways of g-$C_3N_4$ interaction in the plant system confirmed that it can mitigate abiotic stress in crops by improving antioxidant metabolism. A reduction in ROS levels is achieved by producing antioxidants such as POD, SOD, and CAT. g-$C_3N_4$ exhibits superior photocatalytic degradation and biocompatibility, making it an alternative to existing materials with similar applications. In terms of the soil ecosystem, g-$C_3N_4$ alters the soil microbial community, nutrient use efficiency and heavy metal passivation. The enhanced photocatalytic activity of g-$C_3N_4$ facilitates the degradation of organic pollutants and promotes the transformation of heavy metals into a biologically non-assimilable form.

In this context, several key technical bottlenecks must be addressed to accelerate future research with the practical deployment of g-$C_3N_4$ in crop improvement. (1) Considering the contrasting photosynthesis pathways and physiological behaviours of $C_3$ and $C_4$ plants, targeted studies across diverse crop groups are essential to understand differential responses. (2) The compatibility of g-$C_3N_4$ with other nanomaterials and agricultural inputs, and assurance of their nontoxic interaction with organisms, must be systematically investigated. (3) Although the g-$C_3N_4$ precursors are relatively inexpensive compared with other nanomaterials offering similar functionalities, their synthesis remains energy-intensive. Optimisation of scalable energy-efficient production methods is therefore critical for real-world agricultural applications. (4) All existing studies have been conducted under controlled laboratory or greenhouse conditions. Field environments exhibit heterogeneous soil, fluctuating light intensity, and uncertain weather, which pose unique challenges that will determine the practical feasibility of g-$C_3N_4$ application. In addition, designing field trials prioritising the above-mentioned external circumstances is needed to validate laboratory outcomes and identify real-world limitations. (5) There is limited information on degradation pathways, long-term decomposition products, and their ecological impacts in soil and water, which are still unexplored, posing uncertainty in sustainable application. Cohort studies and life cycle assessment studies focusing on the cradle-to-grave stage of the application of g-$C_3N_4$ in the agroecosystem need to be performed. (6) Mechanistic studies focusing on *in situ* characterisations, molecular docking and multi-omics (transcriptomics, proteomics, and metabolomics) to track the translocation pathway, localisation, biochemical effects and to predict and visualise the interaction of g-$C_3N_4$ within the plant system. (7) Formulating agriculturally

Open Access Article. Published on 09 Nyenyankulu 2026. Downloaded on 2026-05-16 11:57:57.
This article is licensed under a Creative Commons Attribution 3.0 Unported Licence.

relevant forms such as granules, urea-g-$C_3N_4$ hybrid forms, slow-release agents, and seed coatings. These co-application strategies with other inputs may enhance stakeholder interest by reducing application costs and improving ease of handling. (8) A comprehensive techno-economic analysis is also warranted to evaluate the potential cost savings achieved by reducing conventional agricultural inputs when g-$C_3N_4$ is applied. These assessments can offset the high input cost associated with intensive farming practices.

This review provides the first comprehensive insights into the potential of g-$C_3N_4$ nanomaterials in agroecosystems and outlines the scientific and industrial opportunities for their application. It offers guidance to researchers, students, agricultural practitioners and chemical industries on the emerging role of g-$C_3N_4$ in enhancing crop performance. While synthetic nitrogen fertilisers have remained largely irreplaceable for nearly a century, the current global push for sustainable agriculture demands innovative alternatives. Addressing the above-mentioned challenges through coordinated and interdisciplinary efforts may open a new horizon in nutrient management, ultimately enabling the responsible and effective use of g-$C_3N_4$ in crop production systems.

## Author contributions

Conceptualisation: T. P. K., R. J., and S. M. R.; investigation: T. P. K., and S. M. R.; formal analysis: T. P. K.; writing – original draft preparation, R. J.; and supervision: T. P. K.

## Conflicts of interest

There are no conflicts to declare.

## Abbreviation

| | |
|---|---|
| NPs | Nanoparticles |
| $Fe_3O_4$ | Ferric oxide |
| CD | Carbon dots |
| CQD | Carbon quantum dot |
| CNT | Carbon nanotubes |
| $TiO_2$ | Titanium dioxide |
| LED | Light emitting diode |
| ATP | Adenosine triphosphate |
| $O_2$ | Oxygen |
| NADPH | Nicotinamide adenine dinucleotide phosphate |
| ETR | Electron transfer rate |
| Cd | Cadmium |
| POD | Peroxidase |
| CAT | Catalase |
| SOD | Superoxide dismutase |
| MDA | Malondialdehyde |
| ROS | Reactive oxygen species |
| RNS | Reactive nitrogen species |
| $CeO_2$ | Cerium dioxide |
| $FeO_2$ | Iron dioxide |
| TEM | Transmission electron microscopy |
| FESEM | Field emission scanning electron microscopy |
| ZnO | Zinc oxide |
| NiO | Nickel(II) oxide |
| GO | Graphene oxide |
| MWCNT | Multi-walled carbon nanotube |
| PL | Photoluminescence |
| CLSM | Confocal laser scanning microscopy |
| $NO_3$ | Nitrate |
| $NH_4$ | Ammonium |
| dsRNA | Double-stranded RNA |
| GFP | Green fluorescent protein |
| TMV | Tobacco mosaic virus |
| CP | Coat protein gene |
| ABA | Abscisic acid |
| DFT | Density functional theory |
| rGO | Reduced graphene oxide |
| SPAD | Soil plant analysis development |
| RuBisCO | Ribulose-1,5-bisphosphate carboxylase/oxygenase |
| SOM | Soil organic matter |
| TOC | Total organic carbon |
| XPS | X-ray photoelectron spectroscopy |
| BET | Brunauer–Emmett–Teller |
| ORR | Oxygen reduction rate |
| OER | Oxygen evolution rate |
| PEPC | Phosphoenolpyruvate carboxykinase |
| KCl | Potassium chloride |
| HCl | Hydrogen chloride |
| NaOH | Sodium hydroxide |
| LC50 | Lethal concentration 50 |
| $CaCl_2$ | Calcium chloride |
| $MgCl_2$ | Magnesium chloride |
| FTIR | Fourier transform infrared spectroscopy |
| $Al^{3+}$ | Aluminium ion |
| $Ca^{2+}$ | Calcium ion |
| $Mg^{2+}$ | Magnesium ion |
| TEA | Techno-economic analysis |
| CAPEX | Capital expenditure |
| OPEX | Operating expenses |

## Data availability

No primary research results, software or code have been included, and no new data were generated or analysed as part of this review.

Supplementary information (SI): for Supplementary Table 1 (g-$C_3N_4$-based nanocomposites and their biomedical and antimicrobial applications. The table outlines assay models, and major biological or functional outcomes). See DOI: https://doi.org/10.1039/d5en00446b.

## Acknowledgements

The author(s) declare that financial support was received for the publication of this article. This research was funded by Vellore Institute of Technology, Vellore, India. We thank VIT University for providing technical support throughout the

 This journal is © The Royal Society of Chemistry 2026

Open Access Article. Published on 09 Nyenyankulu 2026. Downloaded on 2026-05-16 11:57:57.
This article is licensed under a Creative Commons Attribution 3.0 Unported Licence.

manuscript preparation. TPK acknowledges VIT for providing VIT SEED GRANT (RGEMS) – Sanction Order No.: SG20230059 for the seed germination work.

## References

1 R. R. Timilsina, S. Khosla, D. B. Rahut, P. R. Jena and T. Sonobe, A comprehensive review of the soil health status for enhancing agricultural sustainability, *Front. Environ. Sci.*, 2025, **13**, 1548095.
2 P. Sharma, P. Sharma and N. Thakur, Sustainable farming practices and soil health: a pathway to achieving SDGs and future prospects, *Discov. Sustain.*, 2024, **5**(1), 250.
3 Y. A. P. Chowmasundaram, T. L. Tan, R. Nulit, M. Jusoh and S. A. Rashid, Recent developments, applications and challenges for carbon quantum dots as a photosynthesis enhancer in agriculture, *RSC Adv.*, 2023, **13**, 25093–25117.
4 R. J. Yates, E. J. Steel, T. J. Edwards, R. J. Harrison, B. F. Hackney and J. G. Howieson, Adverse consequences of herbicide residues on legumes in dryland agriculture, *Field Crop Res.*, 2024, **308**, 109271.
5 S. Vaidya, C. Deng, Y. Wang, N. Zuverza-Mena, C. Dimkpa and J. C. White, Nanotechnology in agriculture: A solution to global food insecurity in a changing climate?, *NanoImpact*, 2024, **34**, 100502.
6 N. Thakur and A. N. Yadav, Nanotechnology in Agriculture: A Review on Precision Farming and Sustainable Crop Production, *BioNanoScience*, 2025, **15**(2), 243.
7 F. T. Maestre, E. Guirado, D. Armenteras, H. E. Beck, M. S. AlShalan and N. T. Al-Saud, *et al.*, Bending the curve of land degradation to achieve global environmental goals, *Nature*, 2025, **644**, 347–355.
8 A. Rodríguez-Seijo, V. Santás-Miguel, D. Arenas-Lago, M. Arias-Estévez and P. Pérez-Rodríguez, Use of nanotechnology for safe agriculture and food production: Challenges and limitations, *Pedosphere*, 2025, **35**(1), 20–32.
9 M. Y. Alzate Zuluaga, R. Fattorini, S. Cesco and Y. Pii, Plant-microbe interactions in the rhizosphere for smarter and more sustainable crop fertilization: the case of PGPR-based biofertilizers, *Front. Microbiol.*, 2024, **15**, 1440978.
10 J. Poore and T. Nemecek, Reducing food's environmental impacts through producers and consumers, *Science*, 2018, **360**(6392), 987–992.
11 J. Tomalka, C. Hunecke, L. Murken, T. Heckmann, C. Cronauer and R. Becker, *et al.*, *Stepping back from the precipice: Transforming land management to stay within planetary boundaries [Internet]*, Potsdam, Germany, 2024, DOI: 10.48485/pik.2024.018.
12 United Nations Convention to Combat Desertification, *The Global Land Outlook*, Bonn, 2022.
13 M. T. Khan, S. Supronienė, R. Žvirdauskienė and J. Aleinikovienė, Climate, Soil, and Microbes: Interactions Shaping Organic Matter Decomposition in Croplands, *Agronomy*, 2025, **17**(8), 1928.
14 K. Kiprotich, E. Muema, C. Wekesa, T. Ndombi, J. Muoma and D. Omayio, *et al.*, Unveiling the roles, mechanisms and prospects of soil microbial communities in sustainable agriculture, *Discov. Soil*, 2025, **2**(1), 10.
15 M. Kah, C. Sabliov, Y. Wang and J. C. White, Nanotechnology as a foundational tool to combat global food insecurity, *One Earth*, 2023, **6**, 772–775.
16 A. Singh, V. D. Rajput, A. Varshney, K. Ghazaryan and T. Minkina, Small Tech, Big Impact: Agri-nanotechnology Journey to Optimize Crop Protection and Production for Sustainable Agriculture, *Plant Stress*, 2023, **10**, 100253.
17 Q. Wang, C. Shan, P. Zhang, W. Zhao, G. Zhu and Y. Sun, *et al.*, The combination of nanotechnology and potassium: applications in agriculture, *Environ. Sci. Pollut. Res.*, 2024, **31**, 1890–1906.
18 S. Chen, H. Liu, Z. Yangzong, J. L. Gardea-Torresdey, J. C. White and L. Zhao, Seed Priming with Reactive Oxygen Species-Generating Nanoparticles Enhanced Maize Tolerance to Multiple Abiotic Stresses, *Environ. Sci. Technol.*, 2023, **57**(48), 19932–19941.
19 G. V. Lowry, A. Avellan and L. M. Gilbertson, Opportunities and challenges for nanotechnology in the agri-tech revolution, *Nat. Nanotechnol.*, 2019, **14**(6), 517–522.
20 D. Kour, S. S. Khan, S. Kumari, S. Singh, R. T. Khan and C. Kumari, *et al.*, Microbial nanotechnology for agriculture, food, and environmental sustainability: Current status and future perspective, *Folia Microbiol.*, 2024, **69**, 491–520.
21 N. A. H. Abdelfattah, M. A. Yousef, A. A. Badawy and S. S. Salem, Influence of biosynthesized magnesium oxide nanoparticles on growth and physiological aspects of cowpea (Vigna unguiculata L.) plant, cowpea beetle, and cytotoxicity, *Biotechnol. J.*, 2023, **18**(12), 2300301.
22 H. Onyeaka, S. Ghosh, K. Obileke, T. Miri, O. A. Odeyemi and O. Nwaiwu, *et al.*, Preventing chemical contaminants in food: Challenges and prospects for safe and sustainable food production, *Food Control*, 2024, **155**, 110040.
23 A. Singh, V. Rajput, A. Varshney, R. Sharma, K. Ghazaryan and T. Minkina, *et al.*, Revolutionizing Crop Production: Nanoscale Wonders - Current Applications, Advances, and Future Frontiers, *Egypt. J. Soil Sci.*, 2024, **64**(1), 221–258.
24 E. V. R. Campos, J. Ratko, N. Bidyarani, V. Takeshita and L. F. Fraceto, Nature-Based Herbicides and Micro-/Nanotechnology Fostering Sustainable Agriculture, *ACS Sustainable Chem. Eng.*, 2023, **11**(27), 9900–9917.
25 M. F. Khalid, R. Iqbal Khan, M. Z. Jawaid, W. Shafqat, S. Hussain and T. Ahmed, *et al.*, Nanoparticles: The Plant Saviour under Abiotic Stresses, *Nanomaterials*, 2022, **12**(21), 3915.
26 A. Ahmad, S. S. Hashmi, J. M. Palma and F. J. Corpas, Influence of metallic, metallic oxide, and organic nanoparticles on plant physiology, *Chemosphere*, 2022, **290**, 133329.
27 G. Martí, L. Mallón, N. Romero, L. Francàs, R. Bofill and K. Philippot, *et al.*, Surface-Functionalized Nanoparticles as Catalysts for Artificial Photosynthesis, *Adv. Energy Mater.*, 2023, **13**(21), 2300282.

Open Access Article. Published on 09 Nyenyankulu 2026. Downloaded on 2026-05-16 11:57:57.
This article is licensed under a Creative Commons Attribution 3.0 Unported Licence.

28 J. R. Lead, G. E. Batley, P. J. J. Alvarez, M. N. Croteau, R. D. Handy and M. J. McLaughlin, *et al.*, Nanomaterials in the environment: Behavior, fate, bioavailability, and effects—An updated review, *Environ. Toxicol. Chem.*, 2018, **37**, 2029–2063.
29 R. Jayasoorya and P. Kumar, Utilization of biodegradable carrier-based nano herbicide formulations for sustainable weed management in agriculture, *Front. Agron.*, 2024, **6**, 1497041.
30 M. Li, P. Zhang, M. Adeel, Z. Guo, A. J. Chetwynd and C. Ma, *et al.*, Physiological impacts of zero valent iron, Fe3O4 and Fe2O3 nanoparticles in rice plants and their potential as Fe fertilizers, *Environ. Pollut.*, 2021, **269**, 116134.
31 Z. Tao, Q. Zhou, T. Zheng, F. Mo and S. Ouyang, Iron oxide nanoparticles in the soil environment: Adsorption, transformation, and environmental risk, *J. Hazard. Mater.*, 2023, **459**, 132107.
32 M. M. M. Sharma, D. Kapoor, A. Loyal, R. Kumar, P. Sharma and A. Husen, *Carbon-Based Nanomaterials*, 2024, pp. 337–353.
33 A. Hossain, R. G. Kerry, M. Farooq, N. Abdullah and M. Tofazzal Islam, *Nanotechnology in the Life Sciences*, Springer Science and Business Media B.V, 2020, pp. 135–159.
34 M. Safarkhani, M. R. Saeb, J. H. Lee, Y. S. Huh and N. Rabiee, Carbon-based nanomaterials for CRISPR/Cas delivery: a perspective on the design approach, *Carbon Lett.*, 2024, **34**, 387–397.
35 T. A. Swift, D. Fagan, D. Benito-Alifonso, S. A. Hill, M. L. Yallop and T. A. A. Oliver, *et al.*, Photosynthesis and crop productivity are enhanced by glucose-functionalised carbon dots, *New Phytol.*, 2021, **229**(2), 783–790.
36 K. Aggrawal, V. Dixit, A. K. Pal, K. K. Chaubey, S. Barman and S. Pandey, *et al.*, Recent Research on the Use of Carbon Nanomaterials in Plant Growth and Development, *Carbon-Based Nanomaterials*, 2024, pp. 123–144.
37 S. Z. Ahmadi, B. Zahedi, M. Ghorbanpour and H. Mumivand, Comparative morpho-physiological and biochemical responses of Capsicum annuum L. plants to multi-walled carbon nanotubes, fullerene C60 and graphene nanoplatelets exposure under water deficit stress, *BMC Plant Biol.*, 2024, **24**(1), 116.
38 C. Wang, Y. Yao, L. Yue, F. Chen, X. Cao and J. Li, *et al.*, Regulation Mechanisms of Nitrogen-Doped Carbon Dots in Enhanced Maize Photosynthesis under Drought Stress, *ACS Agric. Sci. Technol.*, 2023, **3**(2), 181–189.
39 R. Avanasi, W. A. Jackson, B. Sherwin, J. F. Mudge and T. A. Anderson, C60 fullerene soil sorption, biodegradation, and plant uptake, *Environ. Sci. Technol.*, 2014, **48**(5), 2792–2797.
40 A. Rahman, N. Jamil, M. Yasir, M. N. Aftab, Q. Kanwal and M. Z. Kamran, *et al.*, Toxicity of nanomaterials in the environment: a critical review of current understanding and future directions, *J. Nanopart. Res.*, 2025, **27**(6), 147.
41 M. Shirvani, T. Zhang, Y. Gu and M. Hosseini-Sarvari, Sorghum grain as a bio-template: emerging, cost-effective, and metal-free synthesis of C-doped g-C3N4 for photo-degradation of antibiotic, bisphenol A (BPA), and phenol under solar light irradiation, *Environ. Sci. Pollut. Res.*, 2025, **32**(4), 2036–2054.
42 P. Molaei and F. Rahimi-Moghadam, Porous g-C3N4 nanosheets through facile thermal polymerization of melamine in the air for photocatalyst application, *J. Mater. Sci.: Mater. Electron.*, 2021, **32**(14), 19655–19666.
43 R. Das, Z. Shahnavaz, M. E. Ali, M. M. Islam and S. B. Abd Hamid, Can We Optimize Arc Discharge and Laser Ablation for Well-Controlled Carbon Nanotube Synthesis?, *Nanoscale Res. Lett.*, 2016, **11**(1), 510.
44 A. Yahyazadeh, S. Nanda and A. K. Dalai, Carbon Nanotubes: A Review of Synthesis Methods and Applications, *Reactions*, 2024, **5**, 429–451.
45 L. Sousa Lobo and S. A. C. Carabineiro, Carbon formation at high temperatures (550–1400 °C): Kinetics, alternative mechanisms and growth modes, *Catalysts*, 2020, **10**(5), 465.
46 M. E. Khan, State-of-the-art developments in carbon-based metal nanocomposites as a catalyst: photocatalysis, *Nanoscale Adv.*, 2021, **3**, 1887–1900.
47 M. I. Nabeel, T. Gulzar, S. Kiran, N. Ahmad, S. A. Raza and U. Batool, *et al.*, Tailoring Graphitic Carbon Nitride (g-C3N4) for Multifunctional Applications: Strategies for Overcoming Challenges in Catalysis and Energy Conversion, *Int. J. Energy Res.*, 2025, **2025**(1), 5599894.
48 B. He, M. Feng, X. Chen and J. Sun, Multidimensional (0D-3D) functional nanocarbon: Promising material to strengthen the photocatalytic activity of graphitic carbon nitride, *Green Energy Environ.*, 2021, **6**, 823–845.
49 T. Narkbuakaew and P. Sujaridworakun, Synthesis of Tri-S-Triazine Based g-C3N4 Photocatalyst for Cationic Rhodamine B Degradation under Visible Light, *Top. Catal.*, 2020, **63**(11–14), 1086–1096.
50 G. Liao, Y. Gong, L. Zhang, H. Gao, G. J. Yang and B. Fang, Semiconductor polymeric graphitic carbon nitride photocatalysts: The "holy grail" for the photocatalytic hydrogen evolution reaction under visible light, *Energy Environ. Sci.*, 2019, **12**(7), 2080–2147.
51 X. Qian, W. Li, X. Wang, H. Guan, Q. Bao and B. Zhao, *et al.*, Multifunctional Roles of Ionic Microenvironments in the Preparation, Modification, and Application of g-C3N4, *Adv. Funct. Mater.*, 2025, **35**(11), 2416946.
52 N. Aquino de Carvalho and L. M. Gilbertson, Comparative life cycle assessment of graphitic carbon nitride synthesis routes, *J. Ind. Ecol.*, 2023, **27**(3), 1008–1020.
53 M. Selase Akple, C. Atombo, G. K. Sipi Takyi and A. Dumenya, Scientometric Assessment and Mini Review of Graphitic Carbon Nitride (g-C3N4) for Photocatalytic CO2 Reduction: An Evidence of Progress, *J. Data Sci. Info. Citation Studies*, 2022, **1**(1), 22–34.
54 S. Dhiman, N. Debnath, K. Bandyopadhyay and S. Das, Novel Approach of Nanophotonic Electron Transfer for Augmenting Photosynthesis in Arachis hypogaea: A Biophysical Rationale behind the Plasmonic Enhancement of Chemical Energy Transfer, *ACS Omega*, 2024, **9**(33), 35332–35347.

 This journal is © The Royal Society of Chemistry 2026

Open Access Article. Published on 09 Nyenyankulu 2026. Downloaded on 2026-05-16 11:57:57.
This article is licensed under a Creative Commons Attribution 3.0 Unported Licence.

55 H. G. Sampatkumar, A. M. Antony, M. Trivedi, M. Sharma, M. Ghate and M. Baidya, *et al.*, In situ biosynthesis of palladium nanoparticles on banana leaves extract-coated graphitic carbon nitride: An efficient and reusable heterogeneous catalyst for organic transformations and antimicrobial agent, *Biomass Convers. Biorefin.*, 2024, **14**(9), 10045–10066.

56 H. J. Kang, T. G. Lee, G. A. K. M. R. Bari, H. W. Seo, J. W. Park and H. J. Hwang, *et al.*, Sulfuric acid treated G-CN as a precursor to generate high-efficient G-CN for hydrogen evolution from water under visible light irradiation, *Catalysts*, 2021, **11**(1), 1–13.

57 P. Dash, A. K. Kar, R. Srivastava and K. Parida, Harnessing mesoporous g-C3N4-based photocatalytic materials for sustainable fuel production via solar energy conversion: a review, *Mater. Horiz.*, 2025, **12**(17), 6485–6557.

58 W. Li, X. Wang, Y. Chen, P. Wu, Z. Li and Z. Wang, *et al.*, Non-metal cocatalyst CNT-modified emerging g-C 3 N 4 for enhanced treatment of waste drilling fluid filtrate, *RSC Adv.*, 2025, **15**(2), 1311–1322.

59 I. H. Ifijen, U. U. Akobundu, J. U. Chukwu, S. E. Obuba, S. E. Edem and E. C. Solomon, *et al.*, Titanium-based nanoparticles: innovations in energy applications, wastewater treatment, and tissue engineering for cardiac regeneration, *Discov. Chem.*, 2025, **2**(1), 1–58.

60 A. A. Mamun and M. A. Talukder, Improved photocatalytic activity of α-Fe2O3 by introducing B, Y, and Nb dopants for solar-driven water splitting: a first-principles study, *Adv. Mater.*, 2025, **6**, 4755–4767.

61 J. Jiang, Y. Chen, S. Zhou, H. Xie, C. Li and Z. Wei, *et al.*, Dual defect sites at g-C3N4 synergistically induce the electron localization effect for boosting photocatalytic H2O2 production, *Catal. Sci. Technol.*, 2024, **14**(22), 6701–6709.

62 V. Thiagarajan and S. Ramasubbu, Fate and Behaviour of TiO2 Nanoparticles in the Soil: Their Impact on Staple Food Crops, *Water, Air, Soil Pollut.*, 2021, **232**(7), 274.

63 M. Šebesta, M. Kolenčík, B. Ratna Sunil, R. Illa, J. Mosnáček and A. P. Ingle, *et al.*, Field application of zno and tio2 nanoparticles on agricultural plants, *Agronomy.*, 2021, **11**(11), 2281.

64 M. S. Nasir, G. Yang, I. Ayub, S. Wang, L. Wang and X. Wang, *et al.*, Recent development in graphitic carbon nitride based photocatalysis for hydrogen generation, *Appl. Catal., B*, 2019, **257**, 117855.

65 Y. Zhao, J. Zhang and L. Qu, Graphitic Carbon Nitride/Graphene Hybrids as New Active Materials for Energy Conversion and Storage, *ChemNanoMat*, 2015, **1**, 298–318.

66 H. Yang, Z. Wang, S. Liu, Y. Shen and Y. Zhang, Molecular engineering of CxNy: Topologies, electronic structures and multidisciplinary applications, *Chin. Chem. Lett.*, 2020, **31**(12), 3047–3054.

67 S. Bhowmik, S. J. Phukan, N. K. Sah, M. Roy, S. Garai and P. K. Iyer, Review of Graphitic Carbon Nitride and Its Composite Catalysts for Selective Reduction of CO2, *ACS Appl. Nano Mater.*, 2021, **4**, 12845–12890.

68 X. Cao, L. Yue, F. Lian, C. Wang, B. Cheng and J. Lv, *et al.*, CuO nanoparticles doping recovered the photocatalytic antialgal activity of graphitic carbon nitride, *J. Hazard. Mater.*, 2021, **403**, 123621.

69 C. Wang, B. Cheng, L. Yue, F. Chen, X. Cao and Y. Liu, *et al.*, Fluorescent g-C3N4 nanosheets enhanced photosynthetic efficiency in maize, *NanoImpact*, 2021, **24**, 100363.

70 M. S. Akple, G. K. S. Takyi and S. P. Chimmikuttanda, Graphitic carbon nitride (g-C3N4) based materials: current application trends in health and other multidisciplinary fields, *Int. Nano Lett.*, 2023, **13**, 223–234.

71 H. Liu, S. Ma, L. Shao, H. Liu, Q. Gao and B. Li, *et al.*, Defective engineering in graphitic carbon nitride nanosheet for efficient photocatalytic pathogenic bacteria disinfection, *Appl. Catal., B*, 2020, **261**, 118201.

72 G. Zhang, J. Zhang, M. Zhang and X. Wang, Polycondensation of thiourea into carbon nitride semiconductors as visible light photocatalysts, *J. Mater. Chem.*, 2012, **22**(16), 8083–8091.

73 Z. Li, D. Huang, C. Zhou, W. Xue, L. Lei and R. Deng, *et al.*, Metal-free carbon nitride with boosting photo-redox ability realized by the controlled carbon dopants, *Chem. Eng. J.*, 2020, **382**, 122657.

74 Z. Chen, T. T. Fan, X. Yu, Q. L. Wu, Q. H. Zhu and L. Z. Zhang, *et al.*, Gradual carbon doping of graphitic carbon nitride towards metal-free visible light photocatalytic hydrogen evolution, *J. Mater. Chem. A*, 2018, **6**(31), 15310–15319.

75 P. Panchal, P. Rauwel, S. Sharma, S. P. Nehra, E. Estephan, K. Praakle and E. Rauwel, Ocimum tenuiflorum leaf-mediated graphitic carbon nitride and ZnO/GCN nanohybrid: a sustainable approach for environmental applications, *Environ. Sci. Pollut. Res.*, 2025, **32**, 113692.

76 S. Khan, K. Qi, I. Khan, A. Wang, J. Liu and M. Humayun, *et al.*, Eco-friendly graphitic carbon nitride nanomaterials for the development of innovative biomaterials: Preparation, properties, opportunities, current trends, and future outlook, *J. Saudi Chem. Soc.*, 2023, **27**, 101753.

77 W. Zhu, Y. Yue, H. Wang, B. Zhang, R. Hou and J. Xiao, *et al.*, Recent advances on energy and environmental application of graphitic carbon nitride (g-C3N4)-based photocatalysts: A review, *J. Environ. Chem. Eng.*, 2023, **11**, 110164.

78 M. Ismael, A review on graphitic carbon nitride (g-C3N4) based nanocomposites: Synthesis, categories, and their application in photocatalysis, *J. Alloys Compd.*, 2020, **846**, 156446.

79 H. S. Zhai, L. Cao and X. H. Xia, Synthesis of graphitic carbon nitride through pyrolysis of melamine and its electrocatalysis for oxygen reduction reaction, *Chin. Chem. Lett.*, 2013, **24**(2), 103–106.

80 A. Raza, H. Shen, A. A. Haidry and S. Cui, Hydrothermal synthesis of Fe3O4/TiO2/g-C3N4: Advanced photocatalytic application, *Appl. Surf. Sci.*, 2019, **488**, 887–895.

Open Access Article. Published on 09 Nyenyankulu 2026. Downloaded on 2026-05-16 11:57:57.
This article is licensed under a Creative Commons Attribution 3.0 Unported Licence.

81 A. R. Kuldeep, R. S. Dhabbe and K. M. Garadkar, Development of g-C3N4-TiO2 visible active hybrid photocatalyst for the photodegradation of methyl orange, *Res. Chem. Intermed.*, 2021, **47**(12), 5155–5174.
82 B. Yuan, Y. Wang, A. Y. Elnaggar, I. H. E. Azab, M. Huang and M. H. H. Mahmoud, *et al.*, Physical vapor deposition of graphitic carbon nitride (g-C3N4) films on biomass substrate: optoelectronic performance evaluation and life cycle assessment, *Adv. Compos. Hybrid Mater.*, 2022, **5**(2), 813–822.
83 M. I. Chebanenko, L. A. Lebedev, V. L. Ugolkov, N. D. Prasolov, V. N. Nevedomskiy and V. I. Popkov, Chemical and structural changes of g-C3N4 through oxidative physical vapor deposition, *Appl. Surf. Sci.*, 2022, **600**, 154079.
84 X. Gao, Q. Y. Li, Y. L. Wang, Q. Wei, S. P. Cui and Z. R. Nie, A facile soft-hard template cooperative organization approach for mesoporous g-C3N4 with high photocatalytic performance, *Appl. Surf. Sci.*, 2024, **657**, 159574.
85 J. Liu, J. Yan, H. Ji, Y. Xu, L. Huang and Y. Li, *et al.*, Controlled synthesis of ordered mesoporous g-C3N4 with a confined space effect on its photocatalytic activity, *Mater. Sci. Semicond. Process.*, 2016, **46**, 59–68.
86 F. Saman, C. H. Se Ling, A. Ayub, N. H. B. Rafeny, A. H. Mahadi and R. Subagyo, *et al.*, Review on synthesis and modification of g-C3N4 for photocatalytic H2 production, *Int. J. Hydrogen Energy*, 2024, **77**, 1090–1116.
87 D. R. Paul, R. Sharma, S. P. Nehra and A. Sharma, Effect of calcination temperature, pH and catalyst loading on photodegradation efficiency of urea derived graphitic carbon nitride towards methylene blue dye solution, *RSC Adv.*, 2019, **9**(27), 15381–15391.
88 S. Wang, C. Li, T. Wang, P. Zhang, A. Li and J. Gong, Controllable synthesis of nanotube-type graphitic C3N 4 and their visible-light photocatalytic and fluorescent properties, *J. Mater. Chem. A*, 2014, **2**(9), 2885–2890.
89 M. Ismael, Y. Wu, D. H. Taffa, P. Bottke and M. Wark, Graphitic carbon nitride synthesized by simple pyrolysis: Role of precursor in photocatalytic hydrogen production, *New J. Chem.*, 2019, **43**(18), 6909–6920.
90 W. Iqbal, B. Yang, X. Zhao, M. Rauf, M. Waqas and Y. Gong, *et al.*, Controllable synthesis of graphitic carbon nitride nanomaterials for solar energy conversion and environmental remediation: The road travelled and the way forward, *Catal. Sci. Technol.*, 2018, **8**(18), 4576–4599.
91 F. Safari, R. Poursalehi and H. Delavari, Urea-driven g-C3N4 nanostructures for highly efficient photoreduction of Cr(vi) under visible LED light: effects of calcination temperature, *RSC Adv.*, 2024, **14**(37), 26943–26953.
92 N. Memarian, E. Farahi, N. Tobeiha, S. You and I. Concina, Understanding Graphitic Carbon Nitride as Photocatalyst: A Case Study on Thermal Engineering of Physical and Chemical Features, *Phys. Status Solidi A*, 2024, **221**(7), 2300844.
93 M. D. Capobianco, J. A. Jayworth, B. Shang, N. J. Harmon, H. Wang and G. W. Brudvig, Effect of Synthesis Temperature on Transient Photoconductivity of g-C3N4 from Urea, *Chem. Mater.*, 2023, **35**(22), 9747–9755.
94 P. Wang, L. Wang, L. Rao, J. Shao, Q. Yuan and S. Shan, Simple and low-cost synthesis of g-C3N4 for efficient sunlight photocatalytic degradation of antibiotics in biogas slurry, *J. Environ. Manage.*, 2025, **360**, 124692.
95 N. Wang, L. Cheng, Y. Liao and Q. Xiang, Effect of Functional Group Modifications on the Photocatalytic Performance of g-C3N4, *Small*, 2023, **19**, 2300109.
96 Y. Bai, H. Zheng, X. Shen, K. Hu, W. Huang and J. Liu, g-C3N4 Based Composite Materials for Photo-Fenton Reaction in Water Remediation: A Review of Synthesis Methods, Mechanism and Applications, *ChemCatChem*, 2024, **16**, e202400802.
97 E. E. Elemike, I. C. Onunkwo, O. E. Ididama, O. E. Okorodudu, I. P. Okogbenin and O. R. Egbele, *et al.*, Exploring the production and storage of hydrogen energy using graphitic carbon nitride (g-C3N4), *Int. J. Hydrogen Energy*, 2024, **70**, 212–232.
98 Q. Hao, G. Jia, W. Wei, A. Vinu, Y. Wang and H. Arandiyan, *et al.*, Graphitic carbon nitride with different dimensionalities for energy and environmental applications, *Nano Res.*, 2020, **13**, 18–37.
99 S. Cao, J. Low, J. Yu and M. Jaroniec, Polymeric Photocatalysts Based on Graphitic Carbon Nitride, *Adv. Mater.*, 2015, **27**(13), 2150–2176.
100 J. Fu, J. Yu, C. Jiang and B. Cheng, g-C3N4-Based Heterostructured Photocatalysts, *Adv. Energy Mater.*, 2018, **8**, 1701503.
101 A. Hayat, M. Sohail, A. El Jery, K. M. Al-Zaydi, K. F. Alshammari and J. Khan, *et al.*, Different Dimensionalities, Morphological Advancements and Engineering of g-C3N4-Based Nanomaterials for Energy Conversion and Storage, *Chem. Rec.*, 2023, **23**, e202200171.
102 X. Bi, Y. Fang, S. Zhang, T. Jiang, J. Xing and H. Xu, *et al.*, Plant–Nanoparticle Interactions with g-C3N4: Regulator Development, Metabolic Responses, and Physiological Mechanisms, *ACS Appl. Mater. Interfaces*, 2025, **17**(46), 63322–63333.
103 X. Zhang, X. Xie, H. Wang, J. Zhang, B. Pan and Y. Xie, Enhanced photoresponsive ultrathin graphitic-phase C3N 4 nanosheets for bioimaging, *J. Am. Chem. Soc.*, 2013, **135**(1), 18–21.
104 N. A. de Carvalho, Y. Wang, N. Morales-Soto, D. Waldeck, K. Bibby and K. Doudrick, *et al.*, Using C-Doping to Identify Photocatalytic Properties of Graphitic Carbon Nitride That Govern Antibacterial Efficacy, *ACS ES&T Water*, 2021, **1**(2), 269–280.
105 S. Kang, W. Huang, L. Zhang, M. He, S. Xu and D. Sun, *et al.*, Moderate Bacterial Etching Allows Scalable and Clean Delamination of g-C3N4 with Enriched Unpaired Electrons for Highly Improved Photocatalytic Water Disinfection, *ACS Appl. Mater. Interfaces*, 2018, **10**(16), 13796–13804.
106 D. Peng, W. Jiang, F. F. Li, L. Zhang, R. P. Liang and J. D. Qiu, One-Pot Synthesis of Boron Carbon Nitride Nanosheets for Facile and Efficient Heavy Metal Ions Removal, *ACS Sustainable Chem. Eng.*, 2018, **6**(9), 11685–11694.

 This journal is © The Royal Society of Chemistry 2026

Open Access Article. Published on 09 Nyenyankulu 2026. Downloaded on 2026-05-16 11:57:57.
This article is licensed under a Creative Commons Attribution 3.0 Unported Licence.

107 Q. Yan, G. F. Huang, D. F. Li, M. Zhang, A. L. Pan and W. Q. Huang, Facile synthesis and superior photocatalytic and electrocatalytic performances of porous B-doped g-C3N4 nanosheets, *J. Mater. Sci. Technol.*, 2018, **34**(12), 2515–2520.
108 P. Xiao, D. Jiang, T. Liu, D. Li and M. Chen, Facile synthesis of carbon-doped g-C3N4 for enhanced photocatalytic hydrogen evolution under visible light, *Mater. Lett.*, 2018, **212**, 111–113.
109 Z. F. Huang, J. Song, L. Pan, Z. Wang, X. Zhang and J. J. Zou, *et al.*, Carbon nitride with simultaneous porous network and O-doping for efficient solar-energy-driven hydrogen evolution, *Nano Energy*, 2015, **12**, 646–656.
110 H. Zhao, H. Yu, X. Quan, S. Chen, Y. Zhang and H. Zhao, *et al.*, Fabrication of atomic single layer graphitic-C3N4 and its high performance of photocatalytic disinfection under visible light irradiation, *Appl. Catal., B*, 2014, **152–153**, 46–50.
111 F. Dilnawaz, M. H. Kalaji and A. N. Misra, Nanotechnology in improving photosynthesis under adverse climatic conditions: Cell to Canopy action, *Plant Nano Biol.*, 2023, **3**, 100035.
112 M. Thiruvengadam, H. Y. Chi and S. H. Kim, Impact of nanopollution on plant growth, photosynthesis, toxicity, and metabolism in the agricultural sector: An updated review, *Plant Physiol. Biochem.*, 2024, **206**, 108370.
113 F. Gao, G. Liu, A. Chen, Y. Hu, H. Wang and J. Pan, *et al.*, Artificial photosynthetic cells with biotic–abiotic hybrid energy modules for customized CO2 conversion, *Nat. Commun.*, 2023, **14**(1), 6783.
114 J. Lv, J. Xie, A. G. A. Mohamed, X. Zhang, Y. Feng and L. Jiao, *et al.*, Solar utilization beyond photosynthesis, *Nat. Rev. Chem.*, 2023, **7**, 91–105.
115 R. Duan, Y. Shi, H. Xie, L. Li, B. Zhang and J. Li, The effects and mechanisms of g-C3N4 on the growth and photosynthetic efficiency of wheat seedlings, *S. Afr. J. Bot.*, 2025, **185**, 32–40.
116 N. Zhao, C. Liu, C. Ji, X. Jiang, J. Zhao and L. Qiang, *et al.*, A multi-omics approach reveals differences in toxicity and mechanisms in rice (Oryza sativa L.) exposed to anatase or rutile TiO2 nanoparticles, *NanoImpact*, 2024, **36**, 100530.
117 J. S. Rana and M. Chitkara, Kumar A. Importance of Manganese-Based Advanced Nanomaterial for Foliar Application, *J. Cluster Sci.*, 2024, **35**, 391–403.
118 Y. Hao, Z. Cai, C. Ma, J. C. White, Y. Cao and Z. Chang, *et al.*, Root Exposure of Graphitic Carbon Nitride (g-C3N4) Modulates Metabolite Profile and Endophytic Bacterial Community to Alleviate Cadmium- and Arsenate-Induced Phytotoxicity to Rice (Oryza sativa L.), *ACS Nano*, 2023, **17**(20), 19724–19739.
119 K. Xu, L. Zheng, K. Chu, C. Xing, J. Shu and K. Fang, *et al.*, Soil application of graphitic carbon nitride nanosheets alleviate cadmium toxicity by altering subcellular distribution, chemical forms of cadmium and improving nitrogen availability in soybean (Glycine max L.), *J. Environ. Manage.*, 2024, **368**, 122204.
120 J. Yan, L. Wang, C. Xing, S. Ma, J. Xu and B. Shou, *et al.*, Graphitic carbon nitride alleviates cadmium toxicity to microbial communities in soybean rhizosphere, *Environ. Sci. Pollut. Res.*, 2023, **30**(41), 94988–95001.
121 J. Cheng, X. Li, C. Ding, Y. Feng, P. Hou and L. Xue, *et al.*, g-C3N4 promotes agro-ecosystem productivity: a case study for rice, *Environ. Sci.: Nano*, 2023, **10**(8), 2132–2140.
122 A. Batista, V. C. Mai, K. Sadowska, M. Labudda, P. Jeandet and I. Morkunas, Application of silver and selenium nanoparticles to enhance plant-defense response against biotic stressors, *Acta Physiol. Plant.*, 2025, **47**, 21.
123 L. P. Hastuti, D. D. Ristiana, I. Tryawan, O. P. Arjasa and A. H. Budiman, Leveraging rGO/g-C3N4 composite for enhanced rice plant (Oryza sativa) tolerance to lead phytotoxicity and photocatalytic dye degradation, *Results Eng.*, 2025, **27**, 105862.
124 D. Moulick, A. Majumdar, A. Choudhury, A. Das, B. Chowardhara and B. K. Pattnaik, *et al.*, Emerging concern of nano-pollution in agro-ecosystem: Flip side of nanotechnology, *Plant Physiol. Biochem.*, 2024, **211**, 108704.
125 K. K. Rai, Revisiting the Critical Role of ROS and RNS in Plant Defense, *J. Plant Growth Regul.*, 2023, **42**, 6202–6227.
126 M. K. Mazumder, P. Sharma, D. Moulick, S. K. Tata and S. Choudhury, Salicylic acid ameliorates zinc and chromium-induced stress responses in wheat seedlings: a biochemical and computational analysis, *Cereal Res. Commun.*, 2022, **50**(3), 407–418.
127 S. Choudhury, D. Moulick, D. Ghosh, M. Soliman, A. Alkhedaide and A. Gaber, *et al.*, Drought-Induced Oxidative Stress in Pearl Millet (Cenchrus americanus L.) at Seedling Stage: Survival Mechanisms through Alteration of Morphophysiological and Antioxidants Activity, *Life*, 2022, **12**(8), 1171.
128 D. Kapoor, S. Singh, V. Kumar, R. Romero, R. Prasad and J. Singh, Antioxidant enzymes regulation in plants in reference to reactive oxygen species (ROS) and reactive nitrogen species (RNS), *Plant Gene*, 2019, **19**, 100182.
129 J. T. Hancock, Oxygen Is Instrumental for Biological Signaling: An Overview, *Oxygen*, 2021, **1**, 3–15, DOI: 10.3390/oxygen.
130 J. Fang, L. Liu, H. Yang and H. Du, Applications of Fenton/Fenton-like photocatalytic degradation in g-C3N4 based composite materials, *J. Environ. Chem. Eng.*, 2024, **12**, 114153.
131 Q. Niu, H. Yan, Q. Meng, S. Wang, G. Li and Q. Zhu, *et al.*, Hydrogen peroxide plus ascorbic acid enhanced organic matter deconstructions and composting performances via changing microbial communities, *J. Environ. Manage.*, 2021, **295**, 113126.
132 C. Mony, D. L. Callahan, J. E. Rookes, S. V. Eswaran, M. Wang and W. Yang, *et al.*, Molybdenum Disulfide Nanoparticle Enhancing Photosynthesis in Solanum Lycopersicum, *ChemistrySelect*, 2024, **9**(32), e202400977.
133 Y. Hao, Y. Yu, G. Sun, X. Gong, Y. Jiang and G. Lv, *et al.*, Effects of Multi-Walled Carbon Nanotubes and Nano-Silica on Root Development, Leaf Photosynthesis, Active Oxygen and Nitrogen Metabolism in Maize, *Plants*, 2023, **12**(8), 1604.

Open Access Article. Published on 09 Nyenyankulu 2026. Downloaded on 2026-05-16 11:57:57.
This article is licensed under a Creative Commons Attribution 3.0 Unported Licence.

134 N. Kamali-Andani, S. Fallah, J. R. Peralta-Videa and P. Golkar, A comprehensive study of selenium and cerium oxide nanoparticles on mung bean: Individual and synergistic effect on photosynthesis pigments, antioxidants, and dry matter accumulation, *Sci. Total Environ.*, 2022, **830**, 154837.

135 T. Noji, C. Kamidaki, K. Kawakami, J. R. Shen, T. Kajino and Y. Fukushima, *et al.*, Photosynthetic oxygen evolution in mesoporous silica material: Adsorption of photosystem II reaction center complex into 23 nm nanopores in SBA, *Langmuir*, 2011, **27**(2), 705–713.

136 J. P. Giraldo, M. P. Landry, S. M. Faltermeier, T. P. McNicholas, N. M. Iverson and A. A. Boghossian, *et al.*, Plant nanobionics approach to augment photosynthesis and biochemical sensing, *Nat. Mater.*, 2014, **13**(4), 400–408.

137 M. Chaudhary, P. Singh, G. P. Singh and B. Rathi, Structural Features of Carbon Dots and Their Agricultural Potential, *ACS Omega*, 2024, **9**, 4166–4185.

138 B. Bakbolat, C. Daulbayev, F. Sultanov, R. Beissenov, A. Umirzakov and A. Mereke, *et al.*, Recent developments of TiO2-based photocatalysis in the hydrogen evolution and photodegradation: A review, *Nanomaterials*, 2020, **10**, 1–16.

139 H. Yoshida, R. Yamada and T. Yoshida, Platinum cocatalyst loaded on calcium titanate photocatalyst for water splitting in a flow of water vapor, *ChemSusChem*, 2019, **12**(9), 1958–1965.

140 S. Liu, J. Han, X. Ma, X. Zhu, H. Qu and G. Xin, *et al.*, Repeated release of cerium oxide nanoparticles altered algal responses: Growth, photosynthesis, and photosynthetic gene expression, *Eco Environ. Health.*, 2024, **3**(3), 290–299.

141 M. H. Ghafariyan, M. J. Malakouti, M. R. Dadpour, P. Stroeve and M. Mahmoudi, Effects of magnetite nanoparticles on soybean chlorophyll, *Environ. Sci. Technol.*, 2013, **47**(18), 10645–10652.

142 S. Pradhan, P. Patra, S. Das, S. Chandra, S. Mitra and K. K. Dey, *et al.*, Photochemical modulation of biosafe manganese nanoparticles on vigna radiata: A detailed molecular, biochemical, and biophysical study, *Environ. Sci. Technol.*, 2013, **47**(22), 13122–13131.

143 M. A. Kekeli, Q. Wang and Y. Rui, The Role of Nano-Fertilizers in Sustainable Agriculture: Boosting Crop Yields and Enhancing Quality, *Plants*, 2025, **14**(4), 554.

144 S. Ahmad, N. Ahmad, M. S. Islam, M. A. Ahmad, S. Ercisli and R. Ullah, *et al.*, Rice seeds biofortification using biogenic ıron oxide nanoparticles synthesized by using Glycyrrhiza glabra: a study on growth and yield ımprovement, *Sci. Rep.*, 2024, **14**(1), 12368.

145 M. W. Mazhar, M. Ishtiaq, I. Hussain, A. Parveen, K. H. Bhatti and M. Azeem, *et al.*, Seed nano-priming with Zinc Oxide nanoparticles in rice mitigates drought and enhances agronomic profile, *PLoS One*, 2022, **17**(3), e0264967.

146 M. Mustafa, M. Azam, H. Nawaz Bhatti, A. Khan, L. Zafar and A. M. Rehan Abbasi, Green fabrication of copper nano-fertilizer for enhanced crop yield in cowpea cultivar: A sustainable approach, *Biocatal. Agric. Biotechnol.*, 2024, **56**, 102994.

147 M. Li, P. Zhang, Z. Guo, W. Cao, L. Gao and Y. Li, *et al.*, Molybdenum Nanofertilizer Boosts Biological Nitrogen Fixation and Yield of Soybean through Delaying Nodule Senescence and Nutrition Enhancement, *ACS Nano*, 2023, **17**(15), 14761–14774.

148 M. Iqbal, N. I. Raja, Z. U. R. Mashwani, M. Hussain, M. Ejaz and F. Yasmeen, Effect of Silver Nanoparticles on Growth of Wheat Under Heat Stress, *Iran. J. Sci. Technol.*, 2019, **43**(2), 387–395.

149 S. Gupta, G. S. Gupta, P. Madheshiya, A. K. Mishra and S. Tiwari, Nano fertilizers for sustaining future farming: A review, *Biocatal. Agric. Biotechnol.*, 2024, **56**, 103446.

150 J. J. Mim, S. M. M. Rahman, F. Khan, D. Paul, S. Sikder and H. P. Das, *et al.*, Towards smart agriculture through nano-fertilizer-A review, *Mater. Today Sustain.*, 2025, **30**, 101100.

151 Z. Iqbal, A. Sarkhosh, R. M. Balal, S. Rauf, N. Khan and M. A. Altaf, *et al.*, Silicon nanoparticles mitigate hypoxia-induced oxidative damage by improving antioxidants activities and concentration of osmolytes in southern highbush blueberry plants, *Agronomy*, 2021, **11**(11), 2143.

152 A. Emamverdian, Y. Ding, F. Mokhberdoran, Y. Xie, X. Zheng and Y. Wang, Silicon dioxide nanoparticles improve plant growth by enhancing antioxidant enzyme capacity in bamboo (Pleioblastus pygmaeus) under lead toxicity, *Tree Struct. Funct.*, 2020, **34**(2), 469–481.

153 A. Carrapiço, M. R. Martins, A. T. Caldeira, J. Mirão and L. Dias, Biosynthesis of Metal and Metal Oxide Nanoparticles Using Microbial Cultures: Mechanisms, Antimicrobial Activity and Applications to Cultural Heritage, *Microorganisms*, 2023, **11**(2), 378.

154 Y. Li, P. Zhang, M. Li, N. Shakoor, M. Adeel and P. Zhou, *et al.*, Application and mechanisms of metal-based nanoparticles in the control of bacterial and fungal crop diseases, *Pest Manage. Sci.*, 2023, **79**, 21–36.

155 J. K. Biswas and D. Sarkar, Nanopollution in the Aquatic Environment and Ecotoxicity: No Nano Issue!, *Curr. Pollut. Rep.*, 2019, **5**, 4–7.

156 M. Nekoukhou, S. Fallah, A. Abbasi-Surki, L. R. Pokhrel and A. Rostamnejadi, Improved efficacy of foliar application of zinc oxide nanoparticles on zinc biofortification, primary productivity and secondary metabolite production in dragonhead, *J. Cleaner Prod.*, 2022, **379**, 134803.

157 Z. A. Ganie, S. Guchhait, M. Talib, A. Choudhary and G. K. Darbha, Investigating the sorption of Zinc-Oxide nanoparticles on Tire-wear particles and their toxic effects on Chlorella vulgaris: Insights from toxicological models and physiological analysis, *J. Hazard. Mater.*, 2025, **483**, 136648.

158 A. Janova, M. Kolackova, Z. Bytesnikova, P. Capal, P. Chaloupsky and P. Svec, *et al.*, New insights into mechanisms of copper nanoparticle toxicity in freshwater algae Chlamydomonas reinhardtii: Effects on the pathways of secondary metabolites, *Algal Res.*, 2021, **60**, 102476.

159 A. Noori, T. Donnelly, J. Colbert, W. Cai, L. A. Newman and J. C. White, Exposure of tomato (Lycopersicon esculentum) to silver nanoparticles and silver nitrate: physiological and molecular response, *Int. J. Phytorem.*, 2020, **22**(1), 40–51.

 This journal is © The Royal Society of Chemistry 2026

Open Access Article. Published on 09 Nyenyankulu 2026. Downloaded on 2026-05-16 11:57:57.
This article is licensed under a Creative Commons Attribution 3.0 Unported Licence.

160 T. Mirmoeini, L. Pishkar, D. Kahrizi, G. Barzin and N. Karimi, Phytotoxicity of green synthesized silver nanoparticles on Camelina sativa L, *Physiol. Mol. Biol. Plants*, 2021, **27**(2), 417–427.

161 S. Lala, Enhancement of secondary metabolites in Bacopa monnieri (L.) Pennell plants treated with copper-based nanoparticles in vivo, *IET Nanobiotechnol.*, 2020, **14**(1), 78–85.

162 J. Sun, W. Yang, M. Li, S. Zhang, Y. Sun and F. Wang, Metagenomic analysis reveals soil microbiome responses to microplastics and ZnO nanoparticles in an agricultural soil, *J. Hazard. Mater.*, 2025, **492**, 138164.

163 C. Adiguzel and H. Karaboduk, Biochemical, Immunohistochemical, Histopathological, and Apoptotic Evaluation of Nickel Oxide Nanoparticle- and Microparticle-Induced Testicular Toxicity in Male Rats, *ACS Omega*, 2024, **9**(52), 50910–50921.

164 H. P. Borase, R. S. Singhal and S. V. Patil, Copper oxide nanoparticles exhibit variable response against enzymatic toxicity biomarkers of Moina macrocopa, *Environ. Sci. Pollut. Res.*, 2024, **31**(41), 54325–54337.

165 S. Durán-Fernández, O. D. Bermudez-Zambrano and J. E. Rodríguez-Páez, Synthesis of ZnO nanoparticles using a modified polymer complex method and evaluation of their biological effect on Capsicum annuum L. Nanotechnology for, *Environ. Eng.*, 2025, **10**(1), 18.

166 S. Gurunathan, Cytotoxicity of graphene oxide nanoparticles on plant growth promoting rhizobacteria, *J. Ind. Eng. Chem.*, 2015, **32**, 282–291.

167 M. Ghosh, A. Chakraborty, M. Bandyopadhyay and A. Mukherjee, Multi-walled carbon nanotubes (MWCNT): Induction of DNA damage in plant and mammalian cells, *J. Hazard. Mater.*, 2011, **197**, 327–336.

168 M. Ghosh, S. Bhadra, A. Adegoke, M. Bandyopadhyay and A. Mukherjee, MWCNT uptake in Allium cepa root cells induces cytotoxic and genotoxic responses and results in DNA hyper-methylation, *Mutat. Res., Fundam. Mol. Mech. Mutagen.*, 2015, **774**, 49–58.

169 H. Fan, Q. Sun, K. Dukenbayev, E. Benassi, L. Manarbek and A. A. Nurkesh, *et al.*, Carbon nanoparticles induce DNA repair and PARP inhibitor resistance associated with nanozyme activity in cancer cells, *Cancer Nanotechnol.*, 2022, **13**(1), 39.

170 S. Li, W. Su, H. Wu, T. Yuan, C. Yuan and J. Liu, *et al.*, Targeted tumour theranostics in mice via carbon quantum dots structurally mimicking large amino acids, *Nat. Biomed. Eng.*, 2020, **4**(7), 704–716.

171 H. Wang, M. Zhang, Y. Song, H. Li, H. Huang and M. Shao, *et al.*, Carbon dots promote the growth and photosynthesis of mung bean sprouts, *Carbon*, 2018, **136**, 94–102.

172 Y. Wang, S. Li, L. Liu, F. Lv and S. Wang, Conjugated Polymer Nanoparticles to Augment Photosynthesis of Chloroplasts, *Angew. Chem., Int. Ed.*, 2017, **56**(19), 5308–5311.

173 G. D. Scholes, G. R. Fleming, A. Olaya-Castro and R. Van Grondelle, Lessons from nature about solar light harvesting, *Nat. Chem.*, 2011, **3**, 763–774.

174 S. Mingyu, W. Xiao, L. Chao, Q. Chunxiang, L. Xiaoqing and C. Liang, *et al.*, Promotion of energy transfer and oxygen evolution in spinach photosystem ii by nano-anatase TiO2, *Biol. Trace Elem. Res.*, 2007, **119**(2), 183–192.

175 P. Sétif, G. Shimakawa, A. Krieger-Liszkay and C. Miyake, Identification of the electron donor to flavodiiron proteins in Synechocystis sp. PCC 6803 by in vivo spectroscopy, *Biochim. Biophys. Acta, Bioenerg.*, 2020, **1861**(10), 148256.

176 R. Höhner, A. Aboukila, H. H. Kunz and K. Venema, Proton gradients and proton-dependent transport processes in the chloroplast, *Front. Plant Sci.*, 2016, **7**, 218.

177 X. G. Zhu, S. P. Long and D. R. Ort, Improving photosynthetic efficiency for greater yield, *Annu. Rev. Plant Biol.*, 2010, **61**, 235–261.

178 M. Zhang, L. Hu, H. Wang, Y. Song, Y. Liu and H. Li, *et al.*, One-step hydrothermal synthesis of chiral carbon dots and their effects on mung bean plant growth, *Nanoscale*, 2018, **10**(26), 12734–12742.

179 M. Ge, Y. Yuan, S. Liu, J. Li, C. Yang and B. Du, *et al.*, Enhancing plant photosynthesis with dual light conversion films incorporating biomass-derived carbon dots, *Carbon Capture Sci. Technol.*, 2024, **13**, 100253.

180 F. Yi, L. Yang, L. Zhang, B. y. Peng, X. Tan and Y. Hong, *et al.*, Enhanced photosynthetic carbon fixation in microalgae through tandem synergies in electron transport flows, *Chem. Eng. J.*, 2025, **512**, 162505.

181 Q. Xu, J. Han, D. Wang, J. Zhuang, C. Hu and H. Dong, *et al.*, Unlocking Photosynthetic Potential: Harnessing Rosa roxburghii Derived Carbon Dots as Nanofertilizers for Enhanced Plant Growth, *ACS Appl. Bio Mater.*, 2024, **8**(1), 774–783.

182 H. Mattila, S. Khorobrykh, M. Hakala-Yatkin, V. Havurinne, I. Kuusisto and T. Antal, *et al.*, Action spectrum of the redox state of the plastoquinone pool defines its function in plant acclimation, *Plant J.*, 2020, **104**(4), 1088–1104.

183 S. Chandra, S. Pradhan, S. Mitra, P. Patra, A. Bhattacharya and P. Pramanik, *et al.*, High throughput electron transfer from carbon dots to chloroplast: A rationale of enhanced photosynthesis, *Nanoscale*, 2014, **6**(7), 3647–3655.

184 M. J. Wu, H. H. Hu, C. Z. Siao, Y. M. Liao, J. H. Chen and M. Y. Li, *et al.*, All Organic Label-like Copper(II) Ions Fluorescent Film Sensors with High Sensitivity and Stretchability, *ACS Sens.*, 2018, **3**(1), 99–105.

185 C. W. A. Do Nascimento and M. C. Marques, Metabolic alterations and X-ray chlorophyll fluorescence for the early detection of lead stress in castor bean (Ricinus communis) plants, *Acta Sci., Agron.*, 2018, **40**, e39392.

186 S. S. Suner, M. Sahiner, S. Demirci, E. Umut and N. Sahiner, Fluorescent Graphitic Carbon Nitride (g-C3N4)-Embedded Hyaluronic Acid Microgel Composites for Bioimaging and Cancer-Cell Targetability as Viable Theragnostic, *Pharmaceuticals*, 2024, **17**(2), 160.

187 F. Kopnov, I. Cohen-Ofri and D. Noy, Electron transport between photosystem ii and photosystem i encapsulated in sol-gel glasses, *Angew. Chem., Int. Ed.*, 2011, **50**(51), 12347–12350.

Open Access Article. Published on 09 Nyenyankulu 2026. Downloaded on 2026-05-16 11:57:57.
This article is licensed under a Creative Commons Attribution 3.0 Unported Licence.

188 S. Pradhan and D. R. Mailapalli, Interaction of Engineered Nanoparticles with the Agri-environment, *J. Agric. Food Chem.*, 2017, **65**(38), 8279–8294.
189 T. A. Swift, T. A. A. Oliver, M. Carmen Galan and H. M. Whitney, Functional nanomaterials to augment photosynthesis: Evidence and considerations for their responsible use in agricultural applications, *Interface Focus*, 2019, **9**(1), 20180048.
190 H. Li, J. Huang, Y. Liu, F. Lu, J. Zhong and Y. Wang, *et al.*, Enhanced RuBisCO activity and promoted dicotyledons growth with degradable carbon dots, *Nano Res.*, 2019, **12**(7), 1585–1593.
191 X. L. Yang, T. An, Z. W. Y. Ye, H. J. Kang, P. Robakowski and Z. P. Ye, *et al.*, Modeling light response of effective quantum efficiency of photosystem II for C3 and C4 crops, *Front. Plant Sci.*, 2025, **16**, 1478346.
192 L. Guidi, E. Lo Piccolo and M. Landi, Chlorophyll fluorescence, photoinhibition and abiotic stress: Does it make any difference the fact to be a C3 or C4 species?, *Front. Plant Sci.*, 2019, **10**, 174.
193 V. Rajput, T. Minkina, M. Mazarji, S. Shende, S. Sushkova and S. Mandzhieva, *et al.*, Accumulation of nanoparticles in the soil-plant systems and their effects on human health, *Ann. Agric. Sci.*, 2020, **65**, 137–143.
194 Y. Su, V. Ashworth, C. Kim, A. S. Adeleye, P. Rolshausen and C. Roper, *et al.*, Delivery, uptake, fate, and transport of engineered nanoparticles in plants: A critical review and data analysis, *Environ. Sci.: Nano*, 2019, **6**, 2311–2331.
195 J. Lv, P. Christie and S. Zhang, Uptake, translocation, and transformation of metal-based nanoparticles in plants: recent advances and methodological challenges, *Environ. Sci.: Nano*, 2019, **6**, 41–59.
196 A. Kaphle, P. N. Navya, A. Umapathi and H. K. Daima, Nanomaterials for agriculture, food and environment: applications, toxicity and regulation, *Environ. Chem. Lett.*, 2018, **16**, 43–58.
197 X. D. Sun, J. Y. Ma, L. J. Feng, J. L. Duan and X. Z. Yuan, Precise tracking of nanoparticles in plant roots, *Nat. Protoc.*, 2024, **20**(1), 48–271.
198 M. Djanaguiraman, V. Anbazhagan, O. P. Dhankher and P. V. V. Prasad, Uptake, Translocation, Toxicity, and Impact of Nanoparticles on Plant Physiological Processes, *Plants*, 2024, **13**(22), 3137.
199 M. Pourmadadi, M. Rajabzadeh-Khosroshahi, F. Saeidi Tabar, N. Ajalli, A. Samadi and M. Yazdani, *et al.*, Two-Dimensional Graphitic Carbon Nitride (g-C3N4) Nanosheets and Their Derivatives for Diagnosis and Detection Applications, *J. Funct. Biomater.*, 2022, **13**(4), 204.
200 G. Li, J. Xu and K. Xu, Physiological Functions of Carbon Dots and Their Applications in Agriculture: A Review, *Nanomaterials*, 2023, **13**(19), 2684.
201 W. Wang, J. C. Yu, Z. Shen, D. K. L. Chan and T. Gu, G-C3N4 quantum dots: Direct synthesis, upconversion properties and photocatalytic application, *Chem. Commun.*, 2014, **50**(70), 10148–10150.
202 X. Wei, G. Fan, S. Yang, X. Sun and L. Cai, Morphology effect of a novel biocompatible nucleic acid delivery nanosystem of g-C3N4@dsRNA for application in plant gene expression and plant virus disease protection, *Plant Biotechnol. J.*, 2025, 70189.
203 L. Fan, R. Li, J. Pan, Z. Ding and J. Lin, Endocytosis and its regulation in plants, *Trends Plant Sci.*, 2015, **20**, 388–397.
204 F. Xia, Z. Zhao, X. Niu and Z. Wang, Integrated pollution analysis, pollution area identification and source apportionment of heavy metal contamination in agricultural soil, *J. Hazard. Mater.*, 2024, **465**, 133215.
205 M. Imran, A. Haider, A. Shahzadi, M. Mustajab, A. Ul-Hamid and H. Ullah, *et al.*, Silver and carbon nitride-doped nickel selenide for effective dye decolorization and bactericidal activity: in silico docking study, *RSC Adv.*, 2024, **14**(28), 20004–20019.
206 S. Shanavas, S. Mohana Roopan, A. Priyadharsan, D. Devipriya, S. Jayapandi and R. Acevedo, *et al.*, Computationally guided synthesis of (2D/3D/2D) rGO/Fe2O3/g-C3N4 nanostructure with improved charge separation and transportation efficiency for degradation of pharmaceutical molecules, *Appl. Catal., B*, 2019, **255**, 117758.
207 X. Hu, N. Min, K. Xu, J. Wu, Y. Wang and J. Yan, *et al.*, Graphitic carbon nitride alleviates cadmium toxicity to soybeans through nitrogen supply, *Plant Physiol. Biochem.*, 2024, **211**, 108701.
208 D. Zhu and Q. Zhou, Nitrogen doped g-C3N4 with the extremely narrow band gap for excellent photocatalytic activities under visible light, *Appl. Catal., B*, 2021, **281**, 119474.
209 M. Surana, D. S. Pattanayak, V. K. Singh and D. Pal, g-C3N4 based Z-scheme photocatalysts for tetracycline degradation: A comprehensive review, *J. Hazard. Mater. Lett.*, 2024, **5**, 100116.
210 B. Zhu, L. Zhang, D. Xu, B. Cheng and J. Yu, Adsorption investigation of CO2 on g-C3N4 surface by DFT calculation, *J. CO2 Util.*, 2017, **21**, 327–335.
211 J. Han, M. Song, Y. Li, Y. Yao, S. Lu and X. Liao, Carbon-vacancy engineering approach to g-C3N4 for selective 5-hydroxymethylfurfural oxidation coupled with H2O2 production, *React. Chem. Eng.*, 2023, **9**(1), 148–159.
212 J. Xu, Y. Teng and F. Teng, Effect of Surface Defect States on Valence Band and Charge Separation and Transfer Efficiency, *Sci. Rep.*, 2016, **6**(1), 32457.
213 X. Wei, Y. Pan, M. Li, W. Linghu and X. Guo, Mechanism of Eu(III), La(III), Nd(III), and Th(IV) removal by g-C3N4 based on spectroscopic analyses and DFT theoretical calculations, *Res. Chem. Intermed.*, 2023, **49**(6), 2691–2704.
214 S. Kabir, K. Artyushkova, A. Serov, B. Kiefer and P. Atanassov, Binding energy shifts for nitrogen-containing graphene-based electrocatalysts - Experiments and DFT calculations, *Surf. Interface Anal.*, 2016, **48**(5), 293–300.
215 X. Yuan, K. Luo, N. Liu, X. Ji, C. Liu and J. He, *et al.*, Cluster-model DFT simulations of the infrared spectra of triazine-based molecular crystals, *Phys. Chem. Chem. Phys.*, 2018, **20**(32), 20779–20784.


This journal is © The Royal Society of Chemistry 2026

Open Access Article. Published on 09 Nyenyankulu 2026. Downloaded on 2026-05-16 11:57:57.
This article is licensed under a Creative Commons Attribution 3.0 Unported Licence.

216 S. Jia, J. Gao, Q. Shen, J. Xue, Z. Zhang and X. Liu, *et al.*, Effect of oxygen vacancy concentration on the photocatalytic hydrogen evolution performance of anatase TiO2: DFT and experimental studies, *J. Mater. Sci.: Mater. Electron.*, 2021, **32**(10), 13369–13381.

217 N. Naveas, R. Pulido, C. Marini, J. Hernández-Montelongo and M. M. Silván, First-principles calculations of hematite (α-Fe2O3) by self-consistent DFT+U+V, *iScience*, 2023, **26**(2), 106033.

218 D. Bhanderi, P. Lakhani and C. K. Modi, Graphitic carbon nitride (g-C3N4) as an emerging photocatalyst for sustainable environmental applications: a comprehensive review, *RSC Sustainability*, 2023, **2**, 265–287.

219 S. Kumar, S. Karthikeyan and A. F. Lee, g-C3N4-based nanomaterials for visible light-driven photocatalysis, *Catalysts*, 2018, **8**(2), 74.

220 H. Lemmetyinen, N. V. Tkachenko, B. Valeur, J. I. Hotta, M. Ameloot and N. P. Ernsting, *et al.*, Time-resolved fluorescence methods (IUPAC technical report), *Pure Appl. Chem.*, 2014, **86**(12), 1969–1998.

221 J. Dong, Y. Zhang, M. I. Hussain, W. Zhou, Y. Chen and L. N. Wang, G-c3 n4: Properties, pore modifications, and photocatalytic applications, *Nanomaterials*, 2022, **12**(1), 121.

222 N. Harada, M. Goto, K. Iijima, H. Sakama, N. Ichikawa and H. Kunugita, *et al.*, Time-resolved luminescence of TiO2 powders with different crystal structures, *Jpn. J. Appl. Phys., Part 1*, 2007, **46**(7 A), 4170–4171.

223 M. Qasim, M. A. Ghanem, X. Cao and X. Li, Modification of α-Fe2O3 Nanoparticles with Carbon Layer for Robust Photo-Fenton Catalytic Degradation of Methyl Orange, *Catalysts*, 2024, **14**(6), 393.

224 L. Mohanty, D. Sundar Pattanayak, R. Singhal, D. Pradhan and S. Kumar Dash, Enhanced photocatalytic degradation of rhodamine B and malachite green employing BiFeO3/g-C3N4 nanocomposites: An efficient visible-light photocatalyst, *Inorg. Chem. Commun.*, 2022, **138**, 109286.

225 A. Iqbal, K. M. Altalhi, B. A. Samy, S. Bibi and K. Narasimharao, Photocatalytic H2 production over exfoliated g-C3N4 nanosheets prepared at different treatment conditions, *Int. J. Hydrogen Energy*, 2025, **127**, 666–677.

226 H. Shi, W. Wang, L. Mao, L. Zhang, L. Zhu and C. Wu, *et al.*, Visible light photocatalytic degradation of pesticides and antibiotics by H3PO4-activated biochar combined with g-C3N4: Effects, mechanism, degradation pathway, and toxicity assessment, *J. Environ. Manage.*, 2025, **380**, 124929.

227 A. Sudha, I. Manimehan, B. Sundaresan, R. Arivuselvi, S. Manimaran and M. Ayyanar, *et al.*, Eco-friendly photocatalytic dye detoxification and biomedical applications of ZnO:Sr/ g-C3N4 nanocomposite: reaping the benefit of band gap reduction, *Appl. Phys. A: Mater. Sci. Process.*, 2025, **131**(5), 393.

228 A. Priyadharsan, C. Kamaraj, R. Ranjith, S. Sivakumar, R. Y. Dewiani and R. Thammasak, *et al.*, Synthesis of multifunctional rGO/g-C3N4/FeTiO3 ternary nanocomposites for photocatalyst, antibacterial, and ecotoxicity assessment of zebrafish embryo model, *J. Alloys Compd.*, 2024, **1007**, 176256.

229 J. Nie, X. Zhang, M. Wang, Y. Ou, S. Li and P. Zhong, *et al.*, MXene quantum dots decorated g-C3N4/BiOI heterojunction photocatalyst for efficient NO deep oxidation and CO2 reduction, *Sep. Purif. Technol.*, 2025, **354**, 128961.

230 M. Naguib, M. Kurtoglu, V. Presser, J. Lu, J. Niu and M. Heon, *et al.*, Two-dimensional nanocrystals produced by exfoliation of Ti 3AlC 2, *Adv. Mater.*, 2011, **23**(37), 4248–4253.

231 K. T. Wong, S. C. Kim, K. Yun, C. E. Choong, I. W. Nah and B. H. Jeon, *et al.*, Understanding the potential band position and e–/h+ separation lifetime for Z-scheme and type-II heterojunction mechanisms for effective micropollutant mineralization: Comparative experimental and DFT studies, *Appl. Catal., B*, 2020, **273**, 119034.

232 S. Zhang, Y. Wang, G. A. M. Mersal, A. Alhadhrami, D. A. Alshammari and Y. Wang, *et al.*, Enhanced photocatalytic CO2 reduction via MXene synergism: constructing an efficient heterojunction structure of g-C3N4/Nb2C/CsPbBr3, *Adv. Compos. Hybrid Mater.*, 2024, **7**(6), 226.

233 M. Majdoub, D. Sengottuvelu, S. Nouranian and A. Al-Ostaz, Graphitic Carbon Nitride Quantum Dots (g-C3N4 QDs): From Chemistry to Applications, *ChemSusChem*, 2024, **17**(13), e202301462.

234 H. Qie, M. Ren, C. You, X. Cui, X. Tan and Y. Ning, *et al.*, High-efficiency control of pesticide and heavy metal combined pollution in paddy soil using biochar/g-C3N4 photoresponsive soil remediation agent, *Chem. Eng. J.*, 2023, **452**, 139579.

235 S. Singh, N. A. Khan, R. Ramadan, N. Shehata, D. Kapoor and D. S. Dhanjal, *et al.*, Environmental fate, toxicological impact, and advanced treatment approaches: Atrazine degradation and emphasises on circular economy strategy, *Desalin. Water Treat.*, 2024, **317**, 100201.

236 J. Feng, Y. Zheng, T. Luo, F. Xi and H. Lai, Graphitic carbon nitride nanosheet supported silica nanochannel film for enhanced electrochemiluminescence sensing of 2,4,6-trichlorophenol and prochloraz, *RSC Adv.*, 2024, **14**(39), 28976–28983.

237 Q. Wang, Y. Liu, A. L. Shu and X. Chen, The electrochemical detection of glyphosate in aqueous environments using modified carbon nitride/ZIF67 nanocomposites, *Electroanalysis*, 2024, **14**, 28976–28983.

238 S. Khasim, A. Pasha, S. G. Dastager, C. Panneerselvam, T. A. Hamdalla and S. A. Al-Ghamdi, *et al.*, Design and development of multi-functional graphitic carbon nitride heterostructures embedded with copper and iron oxide nanoparticles as versatile sensing platforms for environmental and agricultural applications, *Ceram. Int.*, 2023, **49**(12), 20688–20698.

239 R. Keerthika Devi, M. Ganesan, T. W. Chen, S. M. Chen, K. Y. Lin and M. Akilarasan, *et al.*, Tailored architecture of molybdenum carbide/iron oxide micro flowers with graphitic carbon nitride: An electrochemical platform for nano-level detection of organophosphate pesticide in food samples, *Food Chem.*, 2022, **397**, 133791.

Open Access Article. Published on 09 Nyenyankulu 2026. Downloaded on 2026-05-16 11:57:57.
This article is licensed under a Creative Commons Attribution 3.0 Unported Licence.

240 P. T. Lan, N. H. Hao, N. T. Hieu, N. T. T. Ha, C. T. Brown and L. M. Cam, Graphitic carbon nitride supported silver nanoparticles (AgNPs/g-C3N4): synthesis and photocatalytic behavior in the degradation of 2,4-dichlorophenoxyacetic acid, *RSC Adv.*, 2024, **14**(27), 19014–19028.

241 H. Zhang, X. Li, D. Wu, B. Yu, S. Lu and J. Wang, *et al.*, A novel strategy for efficient capture of intact harmful algal cells using Zinc oxide modified carbon nitride composites, *Algal Res.*, 2023, **69**, 102932.

242 K. M. Katubi, A. Aslam, S. Khalil, Z. A. Alrowaili, M. S. Al-Buriahi and M. Anwar, *et al.*, Synthesis and characterization of graphitic carbon nitride composite with NiFe2O4/CdO for photocatalytic treatment of diclofenac sodium and crystal violet, *Opt. Mater.*, 2023, **139**, 113721.

243 S. Dahiya, A. Sharma and S. Chaudhary, Synthesis of phytoextract-mediated Ag-doped graphitic carbon nitride (Ag@GCN) for photocatalytic degradation of dyes, *Environ. Sci. Pollut. Res.*, 2023, **30**(10), 25650–25662.

244 D. Gong, X. Li, X. Zhang, W. Zhang, T. Chen and X. Zhang, Green fabrication of citrus pectin-Ag@AgCl/g-C3N4 nanocomposites with enhanced photocatalytic activity for the degradation of new coccine, *Food Chem.*, 2022, **387**, 132928.

245 X. An, H. Wang, C. Dong, P. Jiang, Z. Wu and B. Yu, Core-shell P-laden biochar/ZnO/g-C3N4 composite for enhanced photocatalytic degradation of atrazine and improved P slow-release performance, *J. Colloid Interface Sci.*, 2022, **608**, 2539–2548.

246 H. Abdouss, M. Pourmadadi, P. Zahedi, M. Abdouss, F. Yazdian and A. Rahdar, *et al.*, Green synthesis of chitosan/polyacrylic acid/graphitic carbon nitride nanocarrier as a potential pH-sensitive system for curcumin delivery to MCF-7 breast cancer cells, *Int. J. Biol. Macromol.*, 2023, **242**, 125134.

247 X. Peng, J. Ma, Z. Zhou, H. Yang, J. Chen and R. Chen, *et al.*, Molecular assembly of carbon nitride-based composite membranes for photocatalytic sterilization and wound healing, *Chem. Sci.*, 2023, **14**(16), 4319–4327.

248 C. Meng, D. Huan, H. M. Zhao, S. Li, H. Li and Y. W. Li, *et al.*, Nitrate supply decreases uptake and accumulation of ciprofloxacin in Brassica parachinensis, *J. Hazard. Mater.*, 2021, **403**, 123803.

249 J. Zhu, X. Z. Fang, Y. J. Dai, Y. X. Zhu, H. S. Chen and X. Y. Lin, *et al.*, Nitrate transporter 1.1 alleviates lead toxicity in Arabidopsis by preventing rhizosphere acidification, *J. Exp. Bot.*, 2019, **70**(21), 6363–6374.

250 Y. Yang, J. Xiong, L. Tao, Z. Cao, W. Tang and J. Zhang, *et al.*, Regulatory mechanisms of nitrogen (N) on cadmium (Cd) uptake and accumulation in plants: A review, *Sci. Total Environ.*, 2020, **708**, 135186.

251 X. Hu, X. Chen, Y. Tang, Z. Xu, Y. Zeng and Y. Wang, *et al.*, Effects of g-C3N4 on bacterial community and tetracycline resistance genes in two typical sediments in tetracycline pollution remediation, *Front. Microbiol.*, 2022, **13**, 964401.

252 J. F. Yan, L. Xiang, B. Y. Zhang, C. Tang, Y. Q. Xie and Y. W. Li, *et al.*, Mechanism and Association between Microbial Nitrogen Transformation in Rhizosphere and Accumulation of Ciprofloxacin in Choysum (Brassica parachinensis), *Environ. Sci. Technol.*, 2023, **57**(42), 16053–16064.

253 C. Ma, Y. Hao, J. Zhao, N. Zuverza-Mena, A. G. Meselhy and O. P. Dhankher, *et al.*, Graphitic carbon nitride (C3N4) reduces cadmium and arsenic phytotoxicity and accumulation in rice (oryza sativa L.), *Nanomaterials*, 2021, **11**(4), 839.

254 K. Howe, M. D. Clark, C. F. Torroja, J. Torrance, C. Berthelot and M. Muffato, *et al.*, The zebrafish reference genome sequence and its relationship to the human genome, *Nature*, 2013, **496**(7446), 498–503.

255 K. Raguvaran, M. Kalpana, T. Manimegalai and R. Maheswaran, Bioefficacy of isolated compound l-isoleucine, N-allyloxycarbonyl-, and dodecyl ester from entomopathogenic actinobacteria Actinokineospora fastidiosa against agricultural insect pests, human vector mosquitoes, and antioxidant activities, *Environ. Sci. Pollut. Res.*, 2023, **30**(15), 42608–42628.

256 S. Ramar, P. Elango, A. Velusamy, B. Athinarayanan, V. K. Jothi and D. Pattappan, *et al.*, An eco-safety g-C3N4/Nb2O5/Ag ternary nanocomposite for photocatalytic degradation of pharmaceutical wastes and dyes in wastewater and zebrafish embryonic assessment, *J. Mol. Struct.*, 2024, **1317**, 139127.

257 S. D. Mahajan, W. C. Law, R. Aalinkeel, J. Reynolds, B. B. Nair and K. T. Yong, *et al.*, Nanoparticle-mediated targeted delivery of antiretrovirals to the brain, *Methods Enzymol.*, 2012, 41–60.

258 S. Dong, J. Han, X. y. Sun, B. Zhang and W. Wang, A novel 2D g-C3N4 material applied for Paraquat adsorbing and detoxifying in vitro and in vivo, *Ecotoxicol. Environ. Saf.*, 2023, **266**, 115594.

259 A. Jeirani Khamene, F. Yazdian, M. Pourmadadi, M. Ghobeh, K. Khoshmaram and S. Fathi-karkan, *et al.*, Fabrication and characterization of an innovative g-C3N4/calcium/aloe vera enriched PVA-bacterial cellulose wound dressing: A novel approach to diabetic wound management, *Inorg. Chem. Commun.*, 2024, **168**, 112879.

260 L. L. Sen, Z. X. Cong, J. Li, K. M. Ke, S. S. Guo and H. H. Yang, *et al.*, Graphitic-phase C3N4 nanosheets as efficient photosensitizers and pH-responsive drug nanocarriers for cancer imaging and therapy, *J. Mater. Chem. B*, 2014, **2**(8), 1031–1037.

261 M. Perveen, S. Nazir, A. W. Arshad, M. I. Khan, M. Shamim and K. Ayub, *et al.*, Therapeutic potential of graphitic carbon nitride as a drug delivery system for cisplatin (anticancer drug): A DFT approach, *Biophys. Chem.*, 2020, **267**, 106461.

262 P. Alipournazari, M. Pourmadadi, M. Abdouss, A. Rahdar and S. Pandey, Enhanced delivery of doxorubicin for breast cancer treatment using pH-sensitive starch/PVA/g-C3N4 hydrogel, *Int. J. Biol. Macromol.*, 2024, **265**, 130901.

263 M. Sabzini, M. Pourmadadi, F. Yazdian, P. Khadiv-Parsi and H. Rashedi, Development of chitosan/halloysite/graphitic-carbon nitride nanovehicle for targeted delivery of quercetin to enhance its limitation in cancer therapy: An in vitro cytotoxicity against MCF-7 cells, *Int. J. Biol. Macromol.*, 2023, **226**, 159–171.

 This journal is © The Royal Society of Chemistry 2026

Open Access Article. Published on 09 Nyenyankulu 2026. Downloaded on 2026-05-16 11:57:57.
This article is licensed under a Creative Commons Attribution 3.0 Unported Licence.

264 H. Cheng, Z. Shi, K. Yue, X. Huang, Y. Xu and C. Gao, *et al.*, Sprayable hydrogel dressing accelerates wound healing with combined reactive oxygen species-scavenging and antibacterial abilities, *Acta Biomater.*, 2021, **124**, 219–232.
265 M. Ismael, Environmental remediation and sustainable energy generation via photocatalytic technology using rare earth metals modified g-C3N4: A review, *J. Alloys Compd.*, 2023, **931**, 167469.
266 A. Ghosh, T. K. Mukhopadhyay and A. Datta, Computational Assessment of the Biocompatibility of Two-Dimensional g-C3N3 Toward Lipid Membranes, *ACS Appl. Mater. Interfaces*, 2024, **16**(7), 8213–8227.
267 S. A. Atanda, R. O. Shaibu and F. O. Agunbiade, Nanoparticles in agriculture: balancing food security and environmental sustainability, *Discov. Agric.*, 2025, **3**(1), 26, DOI: 10.1007/s44279-025-00159-x.
268 Bijay-Singh and E. Craswell, Fertilizers and nitrate pollution of surface and ground water: an increasingly pervasive global problem, *SN Appl. Sci.*, 2021, **3**(4), 518.
269 M. Choudhary, M. Muduli and S. Ray, A comprehensive review on nitrate pollution and its remediation: conventional and recent approaches, *Sustain. Water Resour. Manag.*, 2022, **8**(4), 113.
270 S. Zhou, T. Zhou, D. Guan, Y. Yao, H. Sun and A. Ali Mosa, *et al.*, Effect of montmorillonite and humic acid on cotransport of g-C3N4 and lead: The role of triazine ring in lead adsorption and deposition in soil components, *Gondwana Res.*, 2024, **125**, 59–69.
271 Y. Jiang, D. Guan, Y. Liu, X. Yin, S. Zhou and G. Zhang, *et al.*, The transport of graphitic carbon nitride in saturated porous media: Effect of hydrodynamic and solution chemistry, *Chemosphere*, 2020, **248**, 125973.
272 S. Dong, W. Cai, L. Sheng, W. Wang, H. Liu and J. Xia, Combined effect of physicochemical factors on the retention and transport of g-C3N4 in porous media, *Chemosphere*, 2020, **256**, 127100.
273 Y. Chen, F. Su, H. Xie, R. Wang, C. Ding and J. Huang, *et al.*, One-step construction of S-scheme heterojunctions of N-doped MoS2 and S-doped g-C3N4 for enhanced photocatalytic hydrogen evolution, *Chem. Eng. J.*, 2021, **404**, 126498.
274 B. Song, Z. Zeng, G. Zeng, J. Gong, R. Xiao and S. Ye, *et al.*, Powerful combination of g-C3N4 and LDHs for enhanced photocatalytic performance: A review of strategy, synthesis, and applications, *Adv. Colloid Interface Sci.*, 2019, **272**, 101999.
275 L. Cheng, H. Yin, C. Cai, J. Fan and Q. Xiang, Single Ni Atoms Anchored on Porous Few-Layer g-C3N4 for Photocatalytic CO2 Reduction: The Role of Edge Confinement, *Small*, 2020, **16**(28), 2002411.
276 L. Chen, M. A. Maigbay, M. Li and X. Qiu, Synthesis and modification strategies of g-C3N4 nanosheets for photocatalytic applications, *Adv. Powder Mater.*, 2024, **3**(1), 100150.
277 M. Ghanbari and M. Salavati-Niasari, Copper iodide decorated graphitic carbon nitride sheets with enhanced visible-light response for photocatalytic organic pollutant removal and antibacterial activities, *Ecotoxicol. Environ. Saf.*, 2021, **208**, 111712.
278 J. Zhong, Y. Ahmed, G. Carvalho, Z. Wang, L. Wang and J. F. Mueller, *et al.*, Simultaneous removal of micropollutants, antibiotic resistant bacteria, and antibiotic resistance genes using graphitic carbon nitride under simulated solar irradiation, *Chem. Eng. J.*, 2022, **433**, 133839.
279 S. N. Mousavi, H. Daneshvar, M. S. Seyed Dorraji, Z. Ghasempour, V. Panahi-Azar and A. Ehsani, Starch/alginate/Cu-g-C3N4 nanocomposite film for food packaging, *Mater. Chem. Phys.*, 2021, **267**, 124583.
280 G. Cao, J. Sun, M. Chen, H. Sun and G. Zhang, Co-transport of ball-milled biochar and Cd2+ in saturated porous media, *J. Hazard. Mater.*, 2021, **416**, 125725.
281 Y. Jiang, X. Yin, D. Guan, T. Jing, H. Sun and N. Wang, *et al.*, Co-transport of Pb(II)and oxygen-content-controllable graphene oxide from electron-beam-irradiated graphite in saturated porous media, *J. Hazard. Mater.*, 2019, **375**, 297–304.
282 X. Ding, J. Zhu, Y. Zhang, Q. Xia, W. Bi and X. Yang, *et al.*, Separation and concentration of natural products by fast forced adsorption using well-dispersed velvet-like graphitic carbon nitride with response surface methodology optimisation, *Talanta*, 2016, **154**, 119–126.
283 Y. Feng, G. Chen, Y. Zhang, D. Li, C. Ling and Q. Wang, *et al.*, Superhigh co-adsorption of tetracycline and copper by the ultrathin g-C3N4 modified graphene oxide hydrogels, *J. Hazard. Mater.*, 2022, **424**, 127362.
284 S. Zhou, X. Ni, H. Zhou, X. Meng, H. Sun and J. Wang, *et al.*, Effect of nZVI/biochar nanocomposites on Cd transport in clay mineral-coated quartz sand: Facilitation and rerelease, *Ecotoxicol. Environ. Saf.*, 2021, **228**, 112971.
285 X. Yin, Y. Jiang, Y. Tan, X. Meng, H. Sun and N. Wang, Co-transport of graphene oxide and heavy metal ions in surface-modified porous media, *Chemosphere*, 2019, **218**, 1–13.
286 S. Dong, Y. Sun, B. Gao, X. Shi, H. Xu and J. Wu, *et al.*, Retention and transport of graphene oxide in water-saturated limestone media, *Chemosphere*, 2017, **180**, 506–512.
287 W. Yang, S. A. Bradford, Y. Wang, P. Sharma, J. Shang and B. Li, Transport of biochar colloids in saturated porous media in the presence of humic substances or proteins, *Environ. Pollut.*, 2019, **246**, 855–863.
288 Z. Qi, T. Du, P. Ma, F. Liu and W. Chen, Transport of graphene oxide in saturated quartz sand containing iron oxides, *Sci. Total Environ.*, 2019, **657**, 1450–1459.
289 M. Wang, B. Gao, D. Tang, H. Sun, X. Yin and C. Yu, Effects of temperature on graphene oxide deposition and transport in saturated porous media, *J. Hazard. Mater.*, 2017, **331**, 28–35.
290 S. Dong, Z. Zeng, W. Cai, Z. Zhou, C. Dou and H. Liu, *et al.*, The zeta potentials of g-C3N4 nanoparticles: Effect of electrolyte, ionic strength, pH, and humic acid, *J. Nanopart. Res.*, 2019, **21**(11), 233.
291 X. Lv, B. Gao, Y. Sun, X. Shi, H. Xu and J. Wu, Effects of humic acid and solution chemistry on the retention and transport of cerium dioxide nanoparticles in saturated porous media, *Water, Air, Soil Pollut.*, 2014, **225**(10), 2167.

Open Access Article. Published on 09 Nyenyankulu 2026. Downloaded on 2026-05-16 11:57:57.
This article is licensed under a Creative Commons Attribution 3.0 Unported Licence.

292 M. Wang, B. Gao, D. Tang and C. Yu, Concurrent aggregation and transport of graphene oxide in saturated porous media: Roles of temperature, cation type, and electrolyte concentration, *Environ. Pollut.*, 2018, **235**, 350–357.
293 K. Yang, B. Chen, X. Zhu and B. Xing, Aggregation, Adsorption, and Morphological Transformation of Graphene Oxide in Aqueous Solutions Containing Different Metal Cations, *Environ. Sci. Technol.*, 2016, **50**(20), 11066–11075.
294 M. Shrivastava, A. Srivastav, S. Gandhi, S. Rao, A. Roychoudhury and A. Kumar, *et al.*, Monitoring of engineered nanoparticles in soil-plant system: A review, *Environ. Nanotechnol., Monit. Manage.*, 2019, **11**, 100218.
295 J. R. Zhang, S. Y. Wang, M. Wei, Q. Fu and W. Hua, Effects of Structural Variations to X-ray Absorption Spectra of g-$C_3N_4$: Insights from DFT and TDDFT Simulations, *Appl. Phys. Lett.*, 2024, **124**, 14.
296 J. K. Peter, R. Singh, A. K. Yadav, R. Kothari and P. K. Mehta, Toxicity of nitriles/amides-based products in the environment and their enzymatic bioremediation, *J. Hazard. Mater. Adv.*, 2024, **13**, 100389.
297 A. Ismagilova, V. Kisand and L. Vares, Ecotoxicity risk assessment of amines used in 'switchable water' and CO2-capturing processes, *Environ. Sci.: Processes Impacts*, 2025, **27**(4), 974–980.
298 NOAA, *CAMEO Chemicals Database (National Oceanic and Atmospheric Administration)*, 2025.
299 C. Smith, A. K. Hill and L. Torrente-Murciano, Current and future role of Haber-Bosch ammonia in a carbon-free energy landscape, *Energy Environ. Sci.*, 2020, **13**(2), 331–344.
300 S. S. S. Ganti, P. K. Roy, N. Wagh, K. N. S. Siva Sai and S. Kumar, Strategically designed catalysts for ammonia synthesis under mild conditions: recent advances and challenges, *J. Mater. Chem. A*, 2025, **13**, 15361–15426.
301 M. Xia, C. Mao, A. Gu, A. A. Tountas, C. Qiu and T. E. Wood, *et al.*, Solar Urea: Towards a Sustainable Fertilizer Industry, *Angew. Chem., Int. Ed.*, 2022, **61**(1), e202110158.
302 M. Muhyuddin, G. Zuccante, P. Mustarelli, J. Filippi, A. Lavacchi and L. Elbaz, *et al.*, Electrochemical urea production using carbon dioxide and nitrate: state of the art and perspectives, *Energy Environ. Sci.*, 2024, **17**, 3739–3752.
303 X. Li, J. Xiong, X. Gao, J. Huang, Z. Feng and Z. Chen, *et al.*, Recent advances in 3D g-C3N4 composite photocatalysts for photocatalytic water splitting, degradation of pollutants and CO2 reduction, *J. Alloys Compd.*, 2019, **802**, 196–209.
304 P. Xia, G. Li, X. Li, S. Yuan, K. Wang and D. Huang, *et al.*, Synthesis of g-C3N4 from Various Precursors for Photocatalytic H2 Evolution under the Visible Light, *Crystals*, 2022, **12**(12), 1719.
305 M. H. Jawad, A. A. Assi and A. M. Hameed, Hydrothermal Synthesis of Zinc Oxide Nanostructures Using Varied Reactor Designs: A Comparative Study, *Plasmonics*, 2025, 1–2.
306 H. Khan, Sol-Gel Synthesis of TiO2 from TiOSO4 (Part 2): Kinetics and Photocatalytic Efficiency of Methylene Blue Degradation Under UV Irradiation, *Catalysts*, 2025, **15**(1), 64.
307 R. Abbas, J. Luo, X. Qi, A. Naz, I. A. Khan and H. Liu, *et al.*, Silver Nanoparticles: Synthesis, Structure, Properties and Applications, *Nanomaterials*, 2024, **14**(17), 1425.
308 M. Mhadhbi, H. Abderazzak and B. Avar, *Updates on Titanium Dioxide*, IntechOpen, 2023.
309 J. Xi, Y. Zhang, X. Chen and Y. Hu, A simple sol–gel hydrothermal method for the synthesis of defective TiO2 nanocrystals with excellent visible-light photocatalytic activity, *Res. Chem. Intermed.*, 2020, **46**(4), 2205–2214.
310 H. Ali, Z. Ajmal, I. Boukhris, A. M. Alenad, M. S. Al-Buriahi and A. M. Abu-Dief, *et al.*, Recent advances, synthesis, modifications and photogenerated carrier dynamics of g-C3N4 for photocatalytic water splitting, *Int. J. Hydrogen Energy*, 2025, **100**, 79–128.
311 K. Alam, K. I. Khan, M. S. Mehdi, A. Wahab, S. Haider and M. Stoller, Advanced Synthesis of Ag-Doped g-C3N4/NiFe-LDH Photocatalyst via Spin Disc Reactor for Enhanced RhB Dye Degradation, *Catal. Lett.*, 2025, **155**(5), 1–6.
312 F. Wu, Z. Zhou and A. L. Hicks, Life Cycle Impact of Titanium Dioxide Nanoparticle Synthesis through Physical, Chemical, and Biological Routes, *Environ. Sci. Technol.*, 2019, **53**(8), 4078–4087.
313 B. Rezvani, Innovative approaches in adsorbent production through pyrolysis of waste biomass: Effective parameters, modifications, and techno-economic analysis, *Can. J. Chem. Eng.*, 2025, **103**, 5296–5320.
314 K. Awani, N. Khallaghi, V. Kumar and S. A. Nabavi, Techno-economic assessment of an integrated GTL facility for urea production, *J. CO2 Util.*, 2025, **99**, 103157.
315 J. Boyce, R. Sacchi, E. Goetheer and B. Steubing, A prospective life cycle assessment of global ammonia decarbonisation scenarios, *Heliyon*, 2024, **10**(6), e27547.
316 M. Appl, *The Haber-Bosch Heritage: The Ammonia Production Technology 50th Anniversary of the IFA Technical Conference*, Sevilla, Spain, 1997.
317 M. Zedan, A. F. Zedan, R. M. Amin and X. Li, Visible-light active metal nanoparticles@carbon nitride for enhanced removal of water organic pollutants, *J. Environ. Chem. Eng.*, 2022, **10**(3), 107780.
318 S. Ali, A. Mehmood and N. Khan, Uptake, Translocation, and Consequences of Nanomaterials on Plant Growth and Stress Adaptation, *J. Nanomater.*, 2021, **2021**(1), 6677616.

 This journal is © The Royal Society of Chemistry 2026